# Nanoscale Electrodes for Bionanosensing

**Dilu Mathew**

Cancer is globally the second most common cause of death. Cancer burden rises to about 10 million deaths and more than 18 million new cases in 2018. Cancers are often diagnosed at a later stage preventing curative treatment. This underscores the need for an early stage diagnosis of cancer. Consequently, screening methods that can test patients' samples taken by less invasive methods capable of early stage diagnosis are highly sought for. Based on this motivation, here we developed lab-on-a-chip diagnostic systems that can be used for early detection of cancer. Three different types of nanoscale electrodes were fabricated: (i) nanogap electrodes (ii) nano interdigitated electrodes and (iii) nanodisc electrodes and the possibility of using them for sensing and signal transduction were investigated.

***Dilu Mathew*** was born in Kerala, India and is a graduate from CUSAT, India and the University of Leeds, the UK. He is now pursuing his PhD at the University of Twente, the Netherlands. The work described here is based on his research during the PhD. He is highly motivated to save lives of cancer patients through his remarkable research. He also won the Metrohm Young Chemist Award in 2018 for his novel and ground breaking research.

Nanoscale Electrodes for Bionanosensing

Dilu Mathew

# NANOSCALE ELECTRODES FOR BIONANOSENSING

**Dilu George Mathew**

# NANOSCALE ELECTRODES
# FOR
# BIONANOSENSING

**DISSERTATION**

to obtain

the degree of doctor at the University of Twente,

on the authority of the rector magnificus,

prof. dr. T.T.M. Palstra

on account of the decision of the Doctorate Board

to be publically defended

on Thursday, 18 April 2019 at 14.45 hr

by

## DILU GEORGE MATHEW

born on 30 May 1983

in Adoor, Kerala, India

This dissertation has been approved by promotor:

Prof. dr. ir. W. G. van der Wiel

The research reported in this thesis was carried out at the NanoElectronics group with in the faculty of Electrical Engineering, Mathematics and Computer Science and the MESA+ Institute for Nanotechnology at the University of Twente, Enschede, the Netherlands.

UNIVERSITY OF TWENTE. NANOELECTRONICS. MESA+ INSTITUTE

## Graduation committee:

**Chairman & Secretary**

Prof. dr. J. N. Kok                      University of Twente, EEMCS

**Promotor**

Prof. dr. ir. W. G. van der Wiel           University of Twente, EEMCS

**Members**

Prof. dr. S. J. G. Lemay               University of Twente, TNW

Prof. dr. ir. J. Huskens                University of Twente, TNW

Prof. dr. A. Rentmeister               University of Münster, Germany

Prof. dr. A. G. J. M. van Leeuwen      Amsterdam UMC, Amsterdam

Dr. S. Le Gac                         University of Twente, EEMCS

*To my beloved family and all cancer survivors…*

# Table of contents

*"Cancer is a word, not a sentence."*

*John Diamond*

# 1

## General Introduction

### 1.1 Motivation

According to the World Health Organization, a staggering 9.6 million deaths were reported across the globe in 2018 due to cancer, accounting for 17% of the total deaths.[1] Also, about 17 million new cases were reported during the same year. Although, the survival rate of patients vary with the type of cancer, age, gender, and medical history of the patient, it depends highly on the stage at which the disease is diagnosed.[2] In general, when diagnosed at stage 1 or earlier, when tumor is small and remains within the organ it started to grow and not spread further,[3] the survival rate is ~90% for most type of cancers. However, if diagnosed at stage 4, the survival rate plummets to ~20%. Early diagnosis helps in providing effective treatment, resulting in high probability of survival, and less expensive treatment. When the patient is diagnosed with cancer at a later stage, curative treatment becomes challenging. This underscores the need for early diagnosis of cancer. The screening among a high-risk population can help in detecting cancer at early stages, which in turn facilitates in providing efficient and personalized treatment. In order to conduct screening of a vast population with a relatively high risk-factor, an inexpensive and accurate diagnostic tool is essential. However, for most of the cancer types, early-stage screening tests are not available yet or they involve more complex invasive methods. These techniques have high impact on the patient's comfort: increasing fear, uncertainty and doubt about entering elaborate diagnosis and treatment programs. Consequently, screening tools/devices that can test patients' samples taken by no-/less invasive methods are highly sought after. For that reason, the motivation behind the research work

described in this thesis lies in developing a lab-on-a-chip (LOC) diagnostic system for early detection of cancer (and other diseases) and for personalized treatment. We hope that millions of patients across the globe will potentially benefit from such a device that can be used for early-stage screening personalized treatment.

## 1.2 Cancer diagnosis: state-of-the-art

State-of-the-art cancer diagnosis involves laboratory and/or imaging tests. Collection of a sample through biopsy, and analyzing it in the laboratory for cancer-specific markers is the most used and efficient method for conclusively diagnosing cancer. However, most of the time, tumors are *hidden* within the patient's body and not easily accessible for biopsy. Consequently, sample collection is painful or requires a surgery, possibly involving a long procedure, which causes discomfort for the patients. Furthermore, this method is useful when the tumor is big enough to collect the sample and hence it is useful at the later stages of cancer and hence is out of the scope of screening tests. Computerized tomography, magnetic resonance imaging, positron emission tomography, ultrasound and X-ray are the common imaging tools available for cancer diagnostics.[4] However, these imaging methods also fail to identify cancer at early stages due to their resolution limit. Meanwhile, other laboratory tests involve *liquid* biopsies (urine, blood or other body fluids) aimed at finding abnormalities which might be of cancer origin. *E.g.* a white blood cell count in blood could reveal leukemia. Specifically, detecting tumor markers in body fluids is a promising diagnostic method. Tumor markers are substances present in a tissue or blood or other body fluids that are produced by cancer cells or other cells as a response to cancer. Some common examples of tumor markers are prostate-specific antigen (PSA) for prostate cancer,[5] cancer antigen 15-3 for breast cancer,[6] cancer antigen 125 for ovarian cancer,[7] human chorionic gonadotropin for germ cell tumours,[8] carcinoembryonic antigen for colon cancer,[9] etc. Most of these markers can be used for early-stage diagnosis and prognosis. Furthermore, there are also some methods available for cancer screening, like Pap test/ smear, which is an effective cancer screening procedure for cervical cancer. Although more of such screening methods are highly desired, these methods should be easy,

sensitive, specific and inexpensive in order to be useful for screening large populations.

Since the detection mechanism for different tumor markers involves different procedures, it is not easy to develop one single method for the detection or screening of different types and sub-types of cancer. Hence, biochemists are interested in finding similar types of markers, such that they can use one method with minimum modifications to detect different types of cancer. As a result, circulating tumor DNA (ctDNA), circulating tumor cells, tumor-derived extracellular vesicles (tdEVs) have gained lot of interest recently. These tumor markers which are available in blood and other body fluids make suitable candidates for *liquid* biopsies. Moreover, ctDNA and tdEVs are also available at early stages of cancer.[10-13] Although the concentration of ctDNA vary from sample to sample, the concentration of ctDNA in blood range from a few picomolar to a few nanomolar.[10, 14-15] Hence a sensor with a sensitivity of picomolar range should be appealing for early-stage cancer screening with ctDNA sensing. Similarly, clinically relevant concentration of tdEVs is $\sim 10^7$ EVs/ml.[16] However, detecting these markers in blood or serum is comparable to *looking for a needle in a haystack. E.g.,* ctDNA is immensely outnumbered by non-cancerous DNA molecules and other components in body fluids, demanding highly selective and sensitive detection methods. Combination of polymerase chain reaction (PCR) and fluorescent-based ctDNA analysis is used for research laboratory tests. Although PCR amplifies ctDNA, it also amplifies the non-cancerous DNA molecules increasing the *noise* background level. Also for tdEV analysis, optical methods like fluorescence microscopy, Raman spectroscopy, surface resonance plasmon are used. Nevertheless, Optical methods suffer from resolution limitation, preventing them from detecting smaller molecules/ particles.

LOC devices are integrated sensors that perform one or more laboratory testing functions without the need of expert technicians and expensive equipment. LOC-based devices have been reported for detecting DNA, tdEV with electrochemical, electrical, optical, and mass-sensing methods. In their work on electrical detection of DNA, Roy and co-workers, trapped DNA in nanogaps and metallized DNA to make DNA- templated metal nanowires and measured the conductance change[17].

Tang *et al.*[18] described their work on DNA detection using a carbon nanotube field-effect sensor. George *et al.* reported LOC-based PCR amplification of DNA and detection using an acoustic mass-sensing method.[19] In their review describing the advances in piezoelectric acoustic biosensors, Fu *et al.*[20] explained the different piezoelectric materials used in combination with different transducing devices for on-chip DNA sensing devices. Many groups have reported electrochemical sensing of DNA with label[21-22] and label-free[23-25] detection strategies. Optical methods are also widely used for LOC DNA sensing.[26-28] Electrochemical and optical sensing tools are also favorite for tdEV detection.[29-32]

Although, many techniques with different transduction methods were reported by research laboratories for many years for DNA sensing, only a very few of those techniques were made available for clinical applications. One of the main reasons behind this is the reproducibility of the results of these methods/devices with high reliability in analyte quantification. Moreover, many of these reported sensing technologies are not capable of easy integration, not mass producible and also most of them require stringent measurement conditions. These reasons might have limited their development into useful methods for clinical applications. Consequently, the biosensing field still seeks reliable methods that can be used for highly selective and sensitive detection of these markers. Fragments of ctDNA (~100 - 200 base pairs) are ~30 - 60 nm long (each nucleotide is ~0.34 nm long).[33] Hence, biosensor devices with similar nanoscale features can facilitate improved signal-to-noise ratio.[34] Moreover, these devices enable the use of sample volumes in the range of a few microliters. Nanoscale devices are also suitable for rapid and multiplexed analysis of different sequences of DNA. tdEVs are also a few tens to hundreds of nanometers big. Here we attempt to develop such LOC devices for biosensing particularly for DNA and tdEVs.

## 1.3 Thesis outline

Accordingly, in this thesis, we explore the potential of three types of nanoscale electrodes for biosensing using electrical and electrochemical methods.

To start with, nanogap electrodes fabricated using edge lithography for DNA sensing are explained in **Chapter 2**. Here, the fabrication method of these electrodes and the functionalization of their surface in order to trap DNA across the gap are described. Also, DNA metallization for electrical detection is explained. We present successful fabrication of the nanogap electrodes, trapping of DNA across the gap, and electrical measurements confirming their presence.

In order to optimize the active sensing area of the sensor, a second type of electrode, nanoscale interdigitated electrodes (nIDEs), , were studied. **Chapter 3** explains the fabrication of these devices and their electrochemical validation. Electrochemistry turned out to be a  more promising method for biosensing especially on nIDEs owing to  the signal amplification provided  by redox cycling of redox-active mediator molecules. This chapter also describes the signal amplification obtained when the device is operated without any supporting electrolyte solution.

**Chapter 4** describes the use of nIDEs for DNA-sensing application. Sandwich assays with gold nanoparticles (NP) were used for sequence-specific detection and amplification of DNA. This chapter elucidates the immobilization of DNA-NP complexes on the electrode surface and their highly selective and sensitive electrochemical detection utilizing bipolar electrochemistry without supporting electrolyte.

As mentioned earlier, tdEVs are promising markers for cancer diagnostics. Hence, we also explored the detection of these particles using nIDE devices. **Chapter 5** describes the chemical surface functionalization of these electrodes, capturing tdEVs, and detecting their presence by electrochemical means. It also explains the scheme of detection of a sandwich immunosorbent assay on nIDEs, which gives a two-fold amplification: one from the electrochemical redox cycling on the nIDEs and another one from the enzymatic conversion. The data explained in this chapter reveal that the limit of detection of our scheme is unprecedented.

The next generation of biosensors demands the detection of biomolecules/bioparticles with ultra-high sensitivity. Although biosensing with the nIDEs using electrochemical methods was successful, we developed a third

type of electrode: nanodisc electrodes. **Chapter 6** explains the fabrication procedure for these electrodes and the proof-of-concept sensing experiments done with them. This chapter elucidates the capability of nanodisc electrodes for single-particle detection, which is a promising technique for the future.

We investigated the prospective of three types of nanoscale electrodes for biosensing: nanogap electrodes, nIDEs, and nanodisc electrodes using electrical and electrochemical methods. The scope of **Chapter 7** is to conclude and compare the work done with these electrodes and briefly explain the future scope of the research.

## 1.4 References

1.  World-Health-Organization Cancer: Key facts. https://www.who.int/news-room/fact-sheets/detail/cancer (accessed 29/01/2019).

2.  Coleman, M. P.; Estève, J., Trends in cancer incidence, survival and mortality. In *Imaging in Oncology, Second Edition*, CRC Press: 2004; pp 43-65.

3.  Gospodarowicz, M. K.; Brierley, J. D.; Wittekind, C., *TNM Classification of Malignant Tumours*. Wiley: 2017.

4.  Frangioni, J. V., New technologies for human cancer imaging. *Journal of clinical oncology* **2008,** *26* (24), 4012.

5.  Brawer, M. K.; Chetner, M. P.; Beatie, J.; Buchner, D. M.; Vessella, R. L.; Lange, P. H., Screening for prostatic carcinoma with prostate specific antigen. *The Journal of urology* **1992,** *147* (3), 841-845.

6.  Duffy, M. J.; Evoy, D.; McDermott, E. W., CA 15-3: uses and limitation as a biomarker for breast cancer. *Clinica chimica acta* **2010,** *411* (23-24), 1869-1874.

7.  Jacobs, I.; Bast Jr, R. C., The CA 125 tumour-associated antigen: a review of the literature. *Human reproduction* **1989,** *4* (1), 1-12.

8.  Motoyama, T.; Watanabe, H.; Yamamoto, T.; Sekiguchi, M., Production of β-human chorionic gonadotropin by germ cell tumors in vivo and in vitro. *Pathology International* **1988,** *38* (5), 577-590.

9.  Fletcher, R. H., Carcinoembryonic antigen. *Annals of internal medicine* **1986,** *104* (1), 66-73.

10. Bettegowda, C.; Sausen, M.; Leary, R. J.; Kinde, I.; Wang, Y.; Agrawal, N.; Bartlett, B. R.; Wang, H.; Luber, B.; Alani, R. M., Detection of circulating tumor DNA in early-and late-stage human malignancies. *Science translational medicine* **2014,** *6* (224), 224ra24-224ra24.

11. Galindo-Hernandez, O.; Villegas-Comonfort, S.; Candanedo, F.; González-Vázquez, M.-C.; Chavez-Ocaña, S.; Jimenez-Villanueva, X.; Sierra-Martinez, M.; Salazar, E. P., Elevated concentration of microvesicles isolated from peripheral blood in breast cancer patients. *Archives of medical research* **2013,** *44* (3), 208-214.

12. Julich, H.; Willms, A.; Lukacs-Kornek, V.; Kornek, M., Extracellular vesicle profiling and their use as potential disease specific biomarker. *Frontiers in immunology* **2014,** *5*, 413.

13. Lobb, R. J.; Lima, L. G.; Möller, A. In *Exosomes: key mediators of metastasis and pre-metastatic niche formation*, Seminars in cell & developmental biology, Elsevier: 2017; pp 3-10.

14. Jahr, S.; Hentze, H.; Englisch, S.; Hardt, D.; Fackelmayer, F. O.; Hesch, R.-D.; Knippers, R., DNA fragments in the blood plasma of cancer patients: quantitations and evidence for their origin from apoptotic and necrotic cells. *Cancer research* **2001,** *61* (4), 1659-1665.

15. Heitzer, E.; Ulz, P.; Geigl, J. B., Circulating tumor DNA as a liquid biopsy for cancer. *Clinical chemistry* **2015,** *61* (1), 112-123.

16. Coumans, F.; Dalum, G.; Terstappen, L. W. M. M., CTC Technologies and Tools. *Cytometry Part A* **2018,** *93* (12), 1197-1201.

17. Roy, S.; Chen, X.; Li, M.-H.; Peng, Y.; Anariba, F.; Gao, Z., Mass-produced nanogap sensor arrays for ultrasensitive detection of DNA. *Journal of the American Chemical Society* **2009,** *131* (34), 12211-12217.

18. Tang, X.; Bansaruntip, S.; Nakayama, N.; Yenilmez, E.; Chang, Y.-l.; Wang, Q., Carbon nanotube DNA sensor and sensing mechanism. *Nano letters* **2006,** *6* (8), 1632-1636.

19. Papadakis, G.; Murasova, P.; Hamiot, A.; Tsougeni, K.; Kaprou, G.; Eck, M.; Rabus, D.; Bilkova, Z.; Dupuy, B.; Jobst, G., Micro-nano-bio acoustic system

for the detection of foodborne pathogens in real samples. *Biosensors and Bioelectronics* **2018,** *111*, 52-58.

20.  Fu, Y. Q.; Luo, J.; Nguyen, N.-T.; Walton, A.; Flewitt, A. J.; Zu, X.-T.; Li, Y.; McHale, G.; Matthews, A.; Iborra, E., Advances in piezoelectric thin films for acoustic biosensors, acoustofluidics and lab-on-chip applications. *Progress in Materials Science* **2017,** *89*, 31-91.

21.  Umek, R. M.; Lin, S. W.; Vielmetter, J.; Terbrueggen, R. H.; Irvine, B.; Yu, C.; Kayyem, J. F.; Yowanto, H.; Blackburn, G. F.; Farkas, D. H., Electronic detection of nucleic acids: a versatile platform for molecular diagnostics. *The Journal of Molecular Diagnostics* **2001,** *3* (2), 74-84.

22.  Hsieh, K.; Ferguson, B. S.; Eisenstein, M.; Plaxco, K. W.; Soh, H. T., Integrated electrochemical microsystems for genetic detection of pathogens at the point of care. *Accounts of chemical research* **2015,** *48* (4), 911-920.

23.  Venkatesan, B. M.; Bashir, R., Nanopore sensors for nucleic acid analysis. *Nature nanotechnology* **2011,** *6* (10), 615.

24.  Zhang, J.; Song, S.; Zhang, L.; Wang, L.; Wu, H.; Pan, D.; Fan, C., Sequence-specific detection of femtomolar DNA via a chronocoulometric DNA sensor (CDS): Effects of nanoparticle-mediated amplification and nanoscale control of DNA assembly at electrodes. *Journal of the American Chemical Society* **2006,** *128* (26), 8575-8580.

25.  Steichen, M.; Decrem, Y.; Godfroid, E.; Buess-Herman, C., Electrochemical DNA hybridization detection using peptide nucleic acids and [Ru (NH3) 6] 3+ on gold electrodes. *Biosensors and Bioelectronics* **2007,** *22* (9-10), 2237-2243.

26.  Foudeh, A. M.; Daoud, J. T.; Faucher, S. P.; Veres, T.; Tabrizian, M., Sub-femtomole detection of 16s rRNA from Legionella pneumophila using surface plasmon resonance imaging. *Biosensors and Bioelectronics* **2014,** *52*, 129-135.

27.  Ramalingam, N.; Rui, Z.; Liu, H.-B.; Dai, C.-C.; Kaushik, R.; Ratnaharika, B.; Gong, H.-Q., Real-time PCR-based microfluidic array chip for simultaneous detection of multiple waterborne pathogens. *Sensors and Actuators B: Chemical* **2010,** *145* (1), 543-552.

28.    Hui, W. C.; Yobas, L.; Samper, V. D.; Heng, C.-K.; Liw, S.; Ji, H.; Chen, Y.; Cong, L.; Li, J.; Lim, T. M., Microfluidic systems for extracting nucleic acids for DNA and RNA analysis. *Sensors and Actuators A: Physical* **2007,** *133* (2), 335-339.

29.    Im, H.; Shao, H.; Park, Y. I.; Peterson, V. M.; Castro, C. M.; Weissleder, R.; Lee, H., Label-free detection and molecular profiling of exosomes with a nano-plasmonic sensor. *Nature biotechnology* **2014,** *32* (5), 490.

30.    Van Der Pol, E.; Hoekstra, A.; Sturk, A.; Otto, C.; Van Leeuwen, T.; Nieuwland, R., Optical and non-optical methods for detection and characterization of microparticles and exosomes. *Journal of Thrombosis and Haemostasis* **2010,** *8* (12), 2596-2607.

31.    Yadav, S.; Boriachek, K.; Islam, M. N.; Lobb, R.; Möller, A.; Hill, M. M.; Hossain, M. S. A.; Nguyen, N. T.; Shiddiky, M. J., An Electrochemical Method for the Detection of Disease-Specific Exosomes. *ChemElectroChem* **2017,** *4* (4), 967-971.

32.    Zhao, Z.; Yang, Y.; Zeng, Y.; He, M., A microfluidic ExoSearch chip for multiplexed exosome detection towards blood-based ovarian cancer diagnosis. *Lab on a Chip* **2016,** *16* (3), 489-496.

33.    Underhill, H. R.; Kitzman, J. O.; Hellwig, S.; Welker, N. C.; Daza, R.; Baker, D. N.; Gligorich, K. M.; Rostomily, R. C.; Bronner, M. P.; Shendure, J., Fragment length of circulating tumor DNA. *PLoS genetics* **2016,** *12* (7), e1006162.

34.    Sheehan, P. E.; Whitman, L. J., Detection limits for nanoscale biosensors. *Nano letters* **2005,** *5* (4), 803-807.

*"DNA was my only gold rush. I regarded DNA as worth a gold rush."*

*James Watson*

# 2

# Electrical detection of DNA on nanogap electrodes fabricated using edge lithography

**Abstract:** In this chapter, we describe a method for wafer-scale nanofabrication of nanogaps using edge lithography and DNA detection using them. Nanogaps between metallic electrodes are interesting devices for electric biosensing, especially for DNA detection. However, DNA itself is not sufficiently conducting to detect its presence inside the gap by electrical means. Before performing the trapping experiments on the nanogaps, we optimized the DNA metallization method to obtain conducting, DNA-templated nanowires. Metallized DNA chains were characterized using conductive-probe AFM. The current response to the applied voltage showed conduction along the metallized DNA chain. The surface functionalization for DNA trapping were studied using SPR and AFM. Later, the nanogaps were used for trapping biotin labelled DNA by streptavidin that were self-assembled on the Au electrode surface with biotinylated thiol. We measured current as a function of DNA concentration and metallization time on trapped and metallized DNA across the nanogap. As expected, higher concentration gave higher current at given voltage and similarly more metallization time enhanced the metallic nanowire growth along the DNA strands resulting again in higher current.

## 2.1 Introduction

Driven by the rapid advancement of micro-/nano-fabrication, nanogap devices have been fabricated and used for various sensing applications, such as electrical,[1-2] electrochemical,[3-4] plasmonic,[5-6] chemical,[7-8] and bio-sensing[9-11]. A typical nanogap device consists of a pair of electrodes separated by a gap of a few nanometers, either in a planar or vertical geometry. In the planar geometry, both electrodes are horizontally separated, while in the vertical geometry the gap is formed between two electrodes that are vertically separated by a dielectric. Both bottom-up and top-down nanofabrication approaches have been followed to produce nanogap devices by various research groups. For the top-down approach, mostly electron-beam lithography[12-13] and focused-ion-beam etching[14] are used to make nanogap structures. These are time-consuming or low-yield and high-cost techniques, and thus not suitable for high-throughput fabrication. Nanoimprint lithography[15] is an alternative nanofabrication technique suitable for batch processing, however it requires an expensive template and it lacks flexibility in design. For the bottom-up approach, mechanical-break-junction[16-17] and electromigration[18-19] methods are widely used. Again, these techniques are not suitable for mass production of devices, and the reproducibility is a point of concern. Electrochemical deposition[20] is another nanogap fabrication method, however, it has limitations in creating well-defined patterns. Nonetheless, research has shown that conventional optical lithography can also be used to fabricate nanogap electrodes.[11, 21-26] Although, most of these studies[11, 21-23] used expensive silicon-on-insulator wafers for fabrication limiting themselves to lateral nanogaps, Roy *et al*.[24-25] fabricated vertical nanogaps using a complex dry etching processes. They also used plasma-enhanced chemical vapor deposition to grow the dielectric layer in between the top and bottom electrodes, which has relatively inferior dielectric properties, resulting in an undesired leakage current. However, Van Megen *et al*.[26] used an easier fabrication process to obtain well-defined gaps with an high throughput using edge lithography on silicon rich nitride. Nonetheless, they also used a poor dielectric material (silicon-rich nitride) as insulating layer, which reduces the lifetime of the devices, especially for the electrochemical measurements they performed. Edge lithography is an easy, but unconventional nanolithography technique that can be used for wafer-scale nano-

patterning.[27-28] Here, we report a vertical nanogap fabrication method using edge lithography on silicon, however, with an highly insulating thermal oxide dielectric layer.

Being in the same order of magnitude of size with biomolecules, nanogaps have gained a lot of interest in the biosensing field especially for sensing or sequencing of DNA.[11, 21-25] Biomolecules can be trapped into the gap between the two electrodes, and their presence can be established by electrical measurement. Consequently, nanogap devices are able to directly transduce binding events of biomolecules on the functionalized electrodes across gaps into electrical signals, which can be measured by a change in current, resistance, capacitance, or field-effect.[10] DNA detection plays a vital role in pathogen detection, forensic profiling and screening of diseases like cancer. Consequently, DNA detection using nanogaps is an interesting field of research, and hence the electrical properties of DNA were investigated intensively. Although different groups have reported conductivity measurements through DNA, most of them are contradicting each other covering all possible results: insulating[29-30], semiconducting[31], ohmic[32] and even proximity-induced superconducting[33]. The difficulty in reproducing these results made the research community to conclude that these varying results come from the difference in experimental conditions. The electrical conductivity through double stranded DNA (dsDNA) depends on a variety of factors like base sequence, nature of the contact between dsDNA and the electrodes, thermal dependence (melting temperature) of dsDNA structure etc.[34] Although dsDNA is slightly more conducting than highly insulating single-stranded DNA (ssDNA), this difference in conductivity is not enough to detect DNA hybridization electrically, especially at low concentration. Consequently, conduction enhancement of dsDNA has been sought for.

Exploiting the negatively charged phosphate backbone of DNA, Braun *et al.* have demonstrated a DNA-templated conducting silver nanowire using silver ions.[29] Following this work, Roy *et al.*[35] reported ultrasensitive DNA detection using the formation of silver wires along DNA molecules bridging the electrodes of a vertical nanogap device. Cho *et al.*[21] also demonstrated similar conducting DNA bridges across planar nanogap electrodes using gold nanoparticles (NPs). Apart from

silver ions and gold NPs, other metallization procedures were used to study the conduction enhancement of DNA: magnetic nanowires[36-37], palladium nanowires[38], platinum nanowires[39], copper nanowires[40]. In addition to utilising the negatively charged phosphate backbone of DNA, other research focused on gold NPs as labels for DNA hybridisation with subsequent silver deposition to enlarge the gold NPs to build a conductive bridge across the nanogap (silver enhancement).[41] Also other complex methods for conduction enhancement have been reported by various groups including $Zn^{2+}$ ion replacement,[42] copper modified base pairs,[43] oxygen hole doping, [44] and increased humidity.[34] Nevertheless, conduction enhancement by the formation of a DNA-templated metal nanowire by electrostatically attracting metal ions onto the negative backbone of DNA is the most promising generic method, which can be used for all sequences of DNA in almost all conditions. Therefore, here we report DNA detection using this method of conduction enhancement on the vertical nanogaps fabricated using edge lithography. This study evoked three main challenges: (1) optimization of DNA conduction enhancement through metallization (2) fabrication of nanogaps using edge lithography, and (3) DNA trapping and electrical measurement along the nanogap. We discuss all these aspects in detail below.

## 2.1.1 DNA combing

Optimization studies of DNA metallization were done on flat $Si/SiO_2$ wafers, rather than on the nanogap devices directly. In order to visualize the metallization of individual DNA strands, we immobilized them on the substrate . Generally, DNA in solution with counter ions, has a random-coiled structure, and it prefers to stay coiled up, even when it is suspended on a flat surface out of the solution, which is entropically favorable. The technique used to stretch DNA along its length on a surface is termed "DNA combing". One of the easiest methods of DNA combing is retracting the meniscus of the DNA-containing solution at a constant rate along a hydrophobic surface as reported elsewhere.[45] At suitable pH, the interaction between the ends of the DNA strand and the hydrophobic surface helps DNA to stick to the surface. Under this condition, if the solution is allowed to recede along the surface as the meniscus retracts, surface retention creates a force that acts on the DNA to retain it in the liquid phase. However, this force is not strong

enough to overcome the DNA attachment to the surface. As a result, when the droplet recedes, the DNA is stretched along the direction of the water flow. Here, we improvised the method: rather than pulling the sample surface out of the DNA solution, we allowed droplets of DNA solution to slide over the surface that is kept 80° slanted with the horizontal, under gravity. Si/SiO$_2$ wafers were spin-coated with hexamethyl disilazane (HMDS) to obtain a hydrophobic surface. DNA suspended in acetate solution (pH 5.5) was pipetted onto the Si/SiO$_2$ wafer spin-coated with HMDS under inclination.

### 2.1.2 DNA Metallization

For the DNA conduction enhancement, we adopted the method from Braun *et al.*[29] with slight changes in the duration of metallization steps. The metallization of DNA involves three steps: (1) accumulation of positively charged Ag ions (Ag$^+$) on the negatively charged DNA backbone, (2) metal reduction at the Ag$^+$ sites, and (3) silver-growth enhancement. In a basic aqueous solution of silver salt, Na$^+$ ions attached to the negatively charged phosphate backbone of DNA will be exchanged with silver ions (0.1M AgNO$_3$ in aqueous ammonia buffer, pH 10.5). This process is called silver ion accumulation. The accumulated silver ions can be reduced to form small metallic silver aggregates stuck to the DNA backbone in a basic hydroquinone solution (silver reduction, 50mM hydroquinone in aqueous ammonia buffer, pH 10.5). These silver aggregates can be further used as nucleation centers to form a DNA-templated silver nanowire along the DNA backbone (silver growth enhancement) under low light conditions by electroless deposition of silver ions in an acidic solution of an excess of silver ions and the reducing agent hydroquinone (0.1M and 50mM hydroquinone in citrate buffer, pH 3.5). Three types of metallization samples were prepared with varying step duration: (*a*) 10 mins of accumulation, 10 mins of reduction and 2 mins of enhancement (10-10-2 mins); (*b*) 15 mins of accumulation, 15 mins of reduction and 3 mins of enhancement (15-15-3 mins), and (*c*) 15 mins of accumulation, 15 mins of reduction and 10 mins of enhancement (15-15-10 mins).
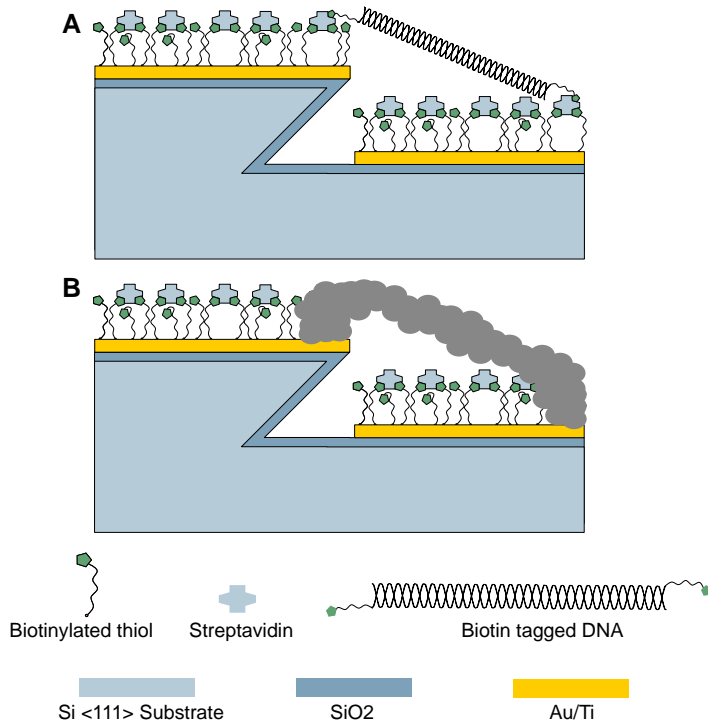
## *2.1.3 DNA trapping on nanogaps*



**Figure 2.1**: Scheme of the biotin-labelled DNA trapped and metallized across the nanogap. **(a)** Cross-sectional view of nanogap surface functionalized with biotinylated self-assembled monolayers with streptavidin and trapped biotin-labelled DNA on it. **(b)** Metallization of DNA for electrical measurements.

In order to validate the application of nanogap devices in the biosensing field, we specifically trapped DNA molecules across it using the scheme as depicted in **Figure 2.1**. The gold electrodes across the nanogap were first functionalized with biotinylated thiol molecules by self-assembly. Later, streptavidin (SA) was immobilized on these self-assembled monolayers (SAMs), utilizing the biotin-streptavidin affinity, one of the strongest non-covalent bonding mechanisms. Subsequently, biotin-labelled dsDNA was introduced onto the electrodes with SA. The SA has four *pockets* to which biotin can be attached. As a result, the DNA was captured using biotin-streptavidin interactions. The trapped DNA was metallized

as mentioned above with varying times for metallization. The DNA concentration was also varied to study its influence.

## 2.2 Results and discussion
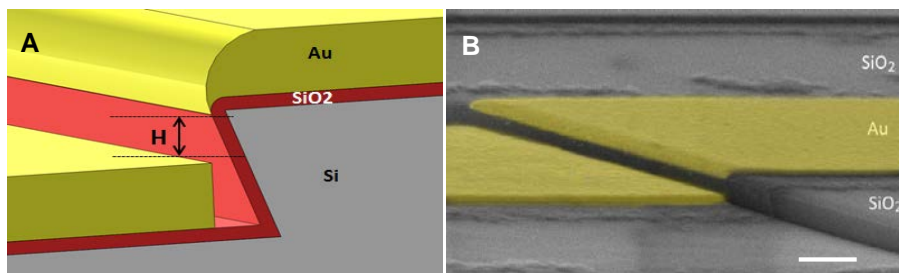
### 2.2.1 Fabrication of nanogaps



**Figure 2.2**: Cross-sectional view of nanogap. **(a)** Sketch of the undercut along the nanogap on silicon (grey), SiO2 (red) and metal (yellow) evaporated on it. Distance H indicates the nanogap height **(b)** Corresponding SEM image with false color for Au (scale bar = 200 nm)

The nanogap device fabrication involved seven steps. The first step was to make a thin oxide layer on the Si wafer, which would subsequently be used as an etching mask for <111> -plane-dependent etching. A 10 nm oxide layer was grown using an ultra-clean line thermal oxidation furnace. Ozone-stream cleaning was done to clean the wafers before the oxidation to remove any organic contamination. Later, by optical photolithography lines of 5 µm width were patterned to define the etch mask on the oxide layer. In the subsequent step, the underlying $SiO_2$ layer was etched using 1% HF, with etching stopping at the silicon surface. After etching, the remaining photoresist was rinsed-off with acetone, leaving the oxide mask layer intact. Successively, a plane-dependent etching of silicon <111> was done with this patterned oxide layer as the mask using 25% tetramethylammonium hydroxide (TMAH). This creates a step edge as shown in **Figure 2.2**. The step height determines the nanogap size. The step edge can be varied by adjusting the etch time. Here, we made a step edge of with different sizes: 100 nm, 50 nm and 20 nm. Later we used 20 nm devices for DNA detection experiments. TMAH was

preferred over KOH because, although it etches the $SiO_2$ layer, the etch rate is slower than that of KOH. Moreover, KOH etching would leave $K^+$ ions on the substrate, which requires another cleaning step.

After the plane-dependent etching, the remaining oxide layer was removed using HF etching. After removal of the SiO2 etch mask, the silicon is again homogeneously oxidized by thermal oxidation at 1000°C. This new high-quality oxide layer can work as the insulator under the electrodes at the nanogap to prevent current leakage. The oxidation temperature has an influence on the sharpness of the edge. On Si <111>, lower oxidation temperatures (<950°C) give sharper edges, while higher oxidation temperatures give rounded edges.[46] For the molecular junction devices like ours, rounded edges are more favorable because it provides uniform oxide thickness along the step edge. Moreover, the $SiO_2$ fabricated at low temperature can withstand electric fields of ~1V/nm. Here, we grew an oxide layer of 20 nm thickness to assure good isolation of the device. Later, a second photolithography step was done to pattern nanogap electrodes and large contact pads for electrical measurements. The final step involved metal evaporation on the resist-patterned substrate. E-beam evaporation, which is a physical vapor deposition technique, is used here to utilize its highly directional nature of deposition. If the substrate is kept stationary (not rotating), the shadowing effect of deposition helps in producing electrodes that are not connected to each other. A 2-3 nm Ti layer is first evaporated as adhesion layer, followed by an Au layer of 20 nm. After evaporation photoresist was lifted-off in acetone.
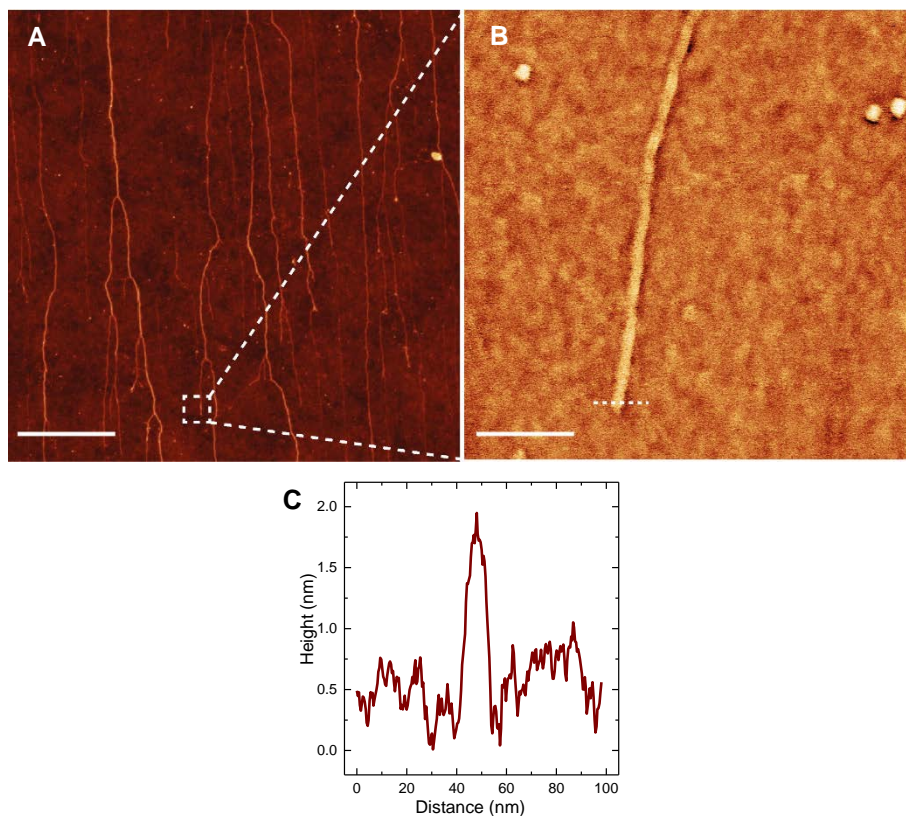
## 2.2.2 DNA on an unpatterned surface



**Figure 2.3:** **(a)** Atomic force micrograph of combed DNA on an HMDS-coated (hydrophobic) surface. DNA strands aligned in the same direction, revealing that DNA combing has stretched them along the flow direction of the droplet (downwards). Multiple braided strands of DNA can also be seen. (scale bar = 1 μm) **(b)** Zoom-in of a single chain of combed dsDNA (scale bar = 100 nm) **(c)** Height profile of the DNA strand along the white dashed line in (b). Height of the DNA strand is ~1.8 nm.

In order for the DNA fragment to be anchored to the Si surface, the surface has to be modified to make it hydrophobic, either by chemical modification or by polymer coating. Hence, small pieces of Si substrates spin- coated with HMDS were used for DNA combing. DNA of 50 Kbp was used for this study, which is

around ~15 μm in length. However, smaller fragments of DNA were also present in the solution.
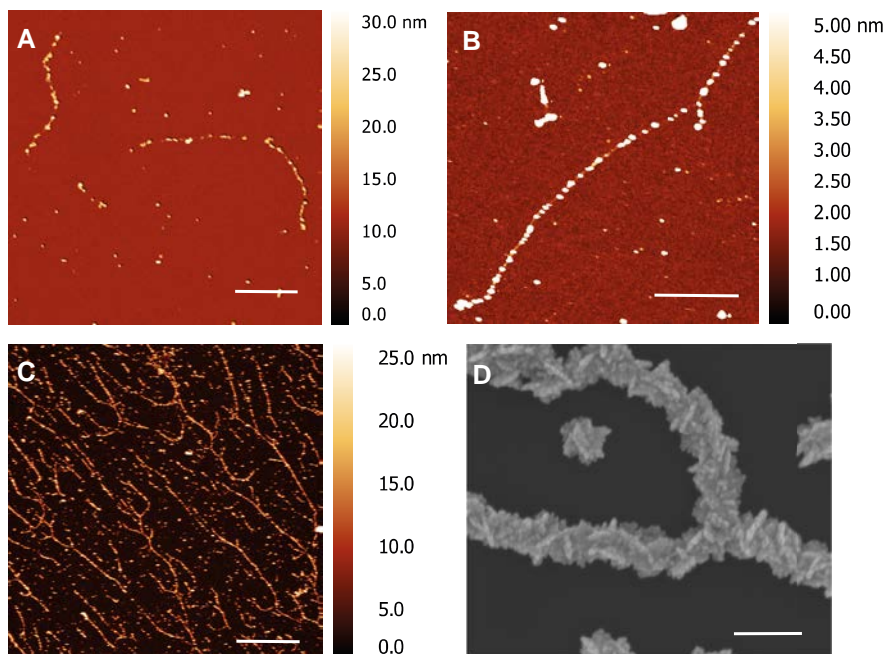


**Figure 2.4**: Atomic force micrographs of the metallized DNA on an HMDS-coated surface. **(a)** Metallization for 15-15-3 mins: (relatively) continuously metallized DNA strands (scale bar = 500 nm) **(b)** Metallization for 10-10-2 mins: metallization is not continuous, separated metal particles can be seen (scale bar = 500 nm) **(c)** Metallization for 15-15-10 mins: continuously metallized longer DNA strands (scale bar = 2 μm) **(d)** Scanning electron micrograph of metallized DNA strands after metallization for 15-15-10 mins: continuously metallized longer DNA strands (Scale bar = 200 nm)

The atomic force microscope (AFM) image (shown in **Figure 2.3 (a)**) of the combed DNA on Si surface shows that long DNA strands were flawlessly stretched along the surface. All the DNA strands were aligned along the direction of the flow of the droplet of the solution containing the DNA. The height of the DNA was measured to be around 1.8 nm, which is slightly lower than the double helix diameter (2 nm) of the DNA. This suggests that the DNA on the surface does not have a double helix confirmation. This might be due to the hydrophobic

interaction of the DNA bases with the hydrophobic surface at the denatured DNA ends, and also due to the capillary and adhesion forces between the hydrophobic surface and the DNA.

In a successive step, we metalized the strands of combed DNA with the same three-step method mentioned above. The duration of each metallization step was varied to study the extensiveness of the metallization along the DNA chain. As shown in **Figure 2.4**, for a sample with 10-10-2 mins, the metallization was not continuous over the DNA's full length. However, it appeared continuous for shorter length less than 50 nm. Nonetheless, for 15-15-3 mins, the metallization appeared thicker and continuous for longer extent along the DNA strands. Furthermore, the metalized samples with 15-15-10 mins of metallization showed the most promising result with thick and continuously metallized DNA strands spanning micrometers. The height of the metallized DNA strands increased to 15-25 nm. However, 15-15-10 mins samples also displayed pieces of metal lying on the surface. This might be metallized DNA recoiled in the presence of (salt) solution. Nevertheless, it can also be unspecifically bound metal pieces that are formed during the enhancement step. Hence, based on the size of the nanogaps that we fabricated and the size of the biotin-labelled DNA, we were convinced not to use the 15-15-10 metallization scheme on the nanogaps in order to avoid false negative signals.
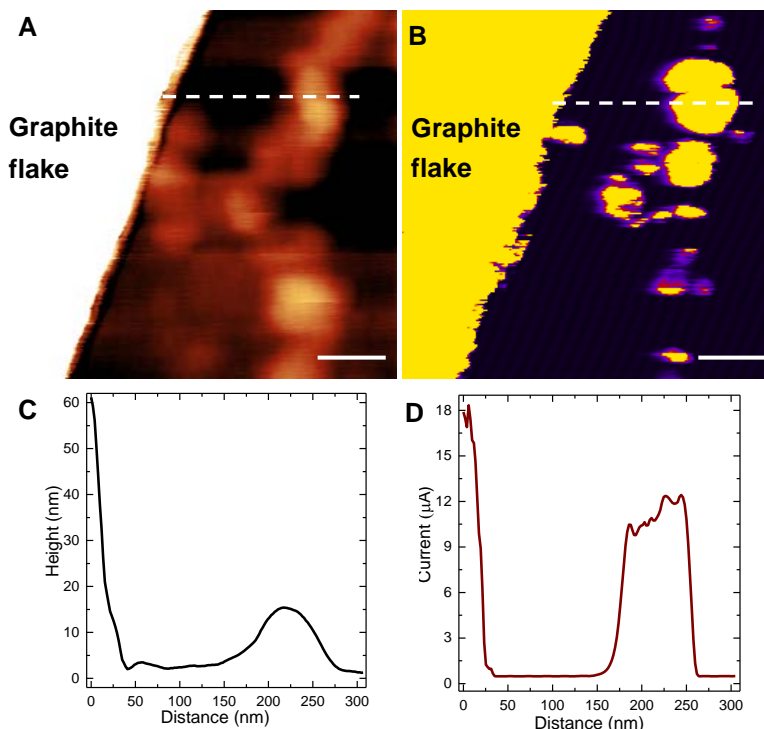
**Figure 2.5: (a)** Atomic force height micrograph captured by contact mode using a conductive tip. A graphite flake is seen on the left side of the image and on right side the metallized DNA strand, which extends under the graphite flake. **(b)** Conductive probe atomic force current micrograph on the image shown in (a). Current transport along the DNA chain is seen. **(c)** Height profile and **(d)** current profile taken along the white dashed line on (a) and (b), respectively.

The conductive-probe AFM (CP-AFM) was used to investigate the electrical properties of the metallized DNA strands lying on the flat surface. Imaging was performed with a conductive tip on an atomic force microscope in which a current to voltage converter and amplifier was incorporated. In order to have a closed electrical circuit for CP-AFM measurements, at first, the metallized DNA strands were connected to the measurement system with the help of graphite flake and silver paste. A graphite flake was chosen in order to have a sharp edge between the DNA and the contact. It was deposited on the sample with metallized DNA chains (15-15-3) as described in the experimental methods **section 2.4**. **Figure 2.5**

shows the height image and the current image, using contact-mode CP-AFM. The graphite flake and the metallized DNA strand extending under the flake are visible in the height image. The height profile shows that the metallized DNA was about 15 nm high. The current response (~10 µA) to the applied voltage (5 V) shows conduction along the metallized DNA chain. However, for a metallic nanowire, one would expect a lower resistance. The relatively high resistance (~500 kΩ) might be due to (1) the oxide layer formed on the surface of the Ag grain along the DNA strand and (2) high interface resistance between the graphite flake and the oxidized outer layer of the Ag nanowire. The oxidation of Ag nanowire and the reduction in conductance as result, is also reported earlier.[47] The comparison between **Figure 2.5 (a)** and **(b)** provides more evidence for the oxidation of the Ag grains. From the CP-AFM height image it is clear that although the nanowire is continuous, it comprises of multiple metal particles/grains. Nonetheless, the continuous nanowire should allow a uniform continuous conduction along it. However, from the CP-AFM current image it can be observed that, although the nanowire was conducting, the conductance was not uniform throughout the nanowire. Some Ag grains appeared more conductive while some others show very low conductance. This suggests that for the grains with low conductance, the outer surface (shell) of the nanowire is (more) oxidized while its core is metallic and as a result, the grains with thicker oxide shell were not appeared in the current image. Nonetheless, even the grain with the lowest resistance showed ~500 kΩ suggesting that it might also have an oxidized shell layer but thinner than the other grains.
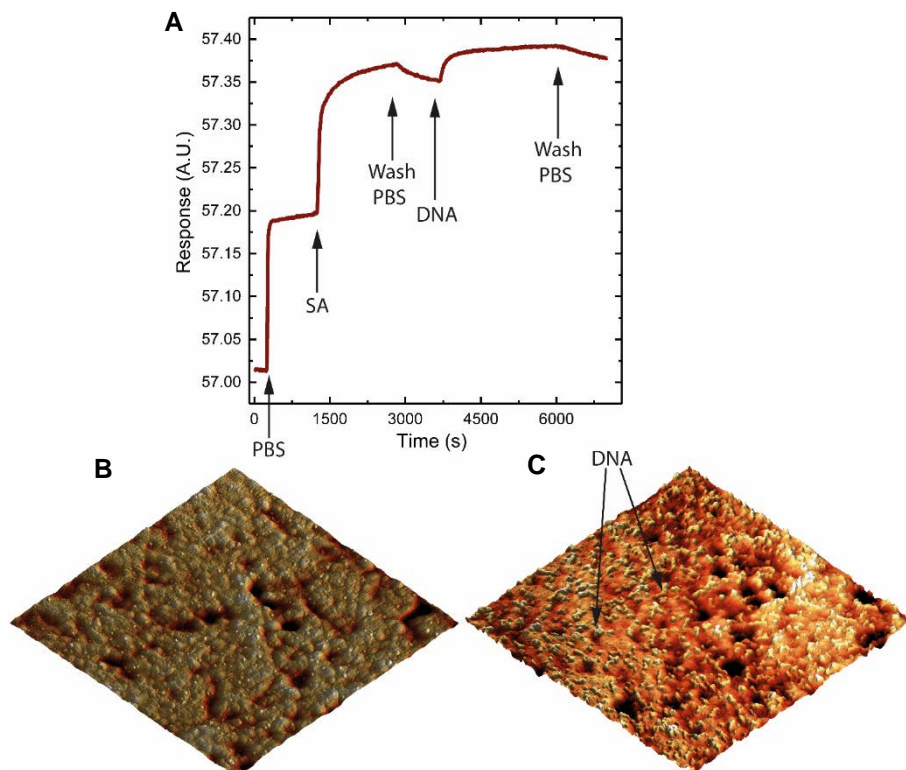
**Figure 2.6**: **(a)** Surface plasmon resonance sensogram; arrows show the introduction points of different solutions **(b)** 3D view of atomic force micrograph of Au surface functionalized with biotinylated SAMs and streptavidin **(c)** 3D view of atomic force micrograph of surface as in (b) and also with immobilized biotin-labelled DNA strands. Comparison with (b) confirms the DNA strands lying on the surface.

Before functionalizing the nanogap electrodes with the SAM, and trapping biotin-tagged DNA across the gap, the binding chemistry of the molecules was examined using surface plasmon resonance (SPR) measurements. SPR is a powerful tool in probing the layer-by-layer self-assembly of molecules. **Figure 2.6** shows the sensogram from SPR dynamic measurements on a Au surface previously functionalized with biotinylated thiols. Initially, Milli-Q was flushed over the surface and soon after, the measurement buffer, phosphate-buffered saline (PBS) solution, was introduced and a new background baseline was obtained. After 20

mins from the start of the experiment, SA (1 µM) in PBS solution was administered. This resulted in a rise in the sensogram, suggesting the binding of SA on the surface with biotinylated thiol. The surface was allowed to saturate with SA for 25 mins and later washed with PBS for 20 mins to get rid of any unspecfically bound SA on the surface. A small decrease in the signal can be observed, suggesting cleaning of the surface. Later, 1 µM biotin-tagged DNA was added. An increase in signal was immediately observed, confirming the binding of biotin tags to the remaining *affinity pockets* of SA. Later, the surface was cleaned by PBS. The samples used for SPR measurements were examined with AFM afterwards. **Figure 2.6 (a)** shows the AFM image of SPR sample with self-assembly till SA and **(b)** shows the immobilization of biotin-labeled DNA strands on the surface.

## *2.2.3 Electrical measurements on the nanogap*
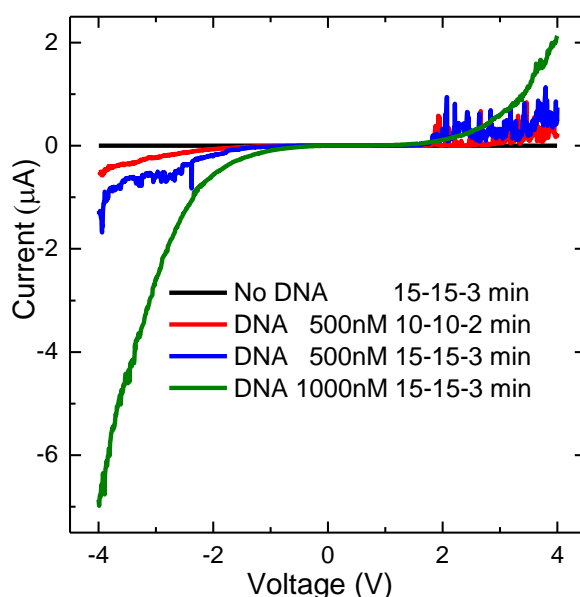


**Figure 2.7**: IV characteristics of 20 nm nanogap electrodes for different concentration and different metallization time: without DNA but with 15-15-3 mins metallization (black), 500 nM DNA with 10-10-2 mins metallization (red), 500 nM DNA with 15-15-3 mins metallization (blue) and 1000 nM DNA with 15-15-3 mins metallization (green). Curves show the average of 3 measurements.

Later, the gold electrodes across the nanogap were functionalized with biotin-thiol monolayers. Subsequently, the biotin-thiol-functionalized electrodes were incubated with SA in PBS buffer with a 1 µM concentration. Previous experiments (data not shown) have provided us data that our recipe with a mixed monolayer, N-(1-mercapto-11-undecyl)-biotin amide and 11-mercapto-1-undecanol, provides a monolayer of SA on thiol-functionalized electrodes. Nanogap electrodes were tested after each functionalization procedure to confirm that before DNA trapping and metallization the gaps were electrically open. Later, we introduced double-stranded DNA (80 bp) with biotin tags at both ends with different concentrations. These biotin tags on the DNA bound to the SA binding pockets so that the nanogap was bridged. The length of each DNA strand is around 25 nm which is compatible with our device of 20 nm nanogaps. After trapping the DNA, they were metallized with the same metallization procedure mentioned previously in **section 2.1.2** with different duration of the metallization steps: (a) 10-10-2 mins and (b) 15-15-3 mins. After the metallization, a voltage sweep was taken across the electrodes with nanogaps and *IV* curves were obtained as shown in **Figure 2.7**. From No DNA sample to DNA samples, there was six orders of magnitude increase in current. As expected, higher concentration of DNA gave higher current especially at negative voltage. The higher concentration of DNA results in the formation of more DNA bridges between the nanogap subsequently producing more silver nanowires between the electrodes yielding higher conductance. Similarly, more metallization time enhanced the metallic nanowire growth along the DNA strands resulting in higher current. However, in all the cases, the curves were nonlinear and asymmetric with respect to zero bias similar to that observed by Roy *et al.*[35] and Braun *et al.*[29] The non-linearity can be due to the discontinuous nanowire formation. It is evident from the AFM images in **Figure 2.5 (a)** and **(b)** that the metallization process does not yield a continuous metallic nanowire for 10-10-2 mins and 15-15-3 mins samples. Qualitatively, this can result in simultaneous charging of a large number of Ag particles in series giving rise to high resistance at low bias voltage. Another, reason of non-linearity might be metal-insulator-metal (M-i-M) structure at the electrode interface. The electrode is fabricated with Au while the metallized DNA is with Ag. As seen from the CP-AFM measurements, the deposited Ag nanowire suffer from corrosion resulting in silver core and silver oxide shell. Hence at the electrode, an Au-silver

oxide-Ag (M-i-M) interface is formed resulting in tunnel junctions. Asymmetry of the curves might be due to the asymmetric interfaces on both the electrodes across the nanogap. More experiments has to be done in order to provide a comprehensive and quantitative explanation for both of these effects.

## 2.3 Conclusion

Nanogap electrode devices were fabricated using e-beam metal evaporation across a pre-patterned step-edge using edge lithography. The nanogap size can be tuned by the etching time and the electrode metal thickness. Since the step-edge was defined in Si, we could later thermally oxidize it to obtain a high-quality isolation layer, which is significant for the electrical measurements. In order to study the potential of nanogaps for biosensing applications, we formulated a scheme for trapping DNA across the nanogaps. Before performing the trapping experiments on the nanogaps, we optimized the DNA metallization method to obtain conducting, DNA-templated nanowires. AFM images confirmed the metallization of combed DNA on a Si surface. CP-AFM measurements verified the electrical properties of the metallized DNA wires. Metallized DNA chain showed high resistance than expected and also CP-AFM current image provided insights into the oxidized outer layer of the metallized nanowires. We also investigated the binding chemistry of the molecules using SPR and AFM. Later, the nanogaps were used for trapping biotin labelled DNA by SA that were self-assembled on the Au electrode surface with biotinylated thiol. We were able to measure current as a function of DNA concentration and metallization time on trapped and metallized DNA across the nanogap. As expected, higher concentration gave higher current at given voltage and similarly more metallization time enhanced the metallic nanowire growth along the DNA strands resulting again in higher current. However, one of the main concerns of this method is the false positive signals obtained especially at low concentrations of DNA. The first two metallization steps are specific, i.e., the silver ions are accumulated on the negatively charged DNA back bone and hence, when reduced, these ions form metal seeds on the DNA backbone. However, the metal growth enhancement step is non-specific and it initiates the electroless deposition of metal on all metallic substances including the electrodes themselves. Hence, the nanogap can be bridged by a non-

specifically deposited metal particle between the nanogap rather than the DNA. This results in false positive signals. Consequently, for small gap devices, the metallization times has to be truncated in order to avoid false positives which limits the detection of low concentration of DNA. At low concentration, the DNA bridging the nanogap will be less. The less the bridged DNA molecules, the less the silver nanowires are expected across the nanogap. With a reduced metallization time, this will result in a much lower conductance hampering the detection of low DNA concentrations.

Furthermore, for a nanogap, fabricated using edge lithography, the ratio of the *dead* sensing area to the active sensing area is high. The part of the electrode which does not contribute to the sensing can be considered as *dead* sensing area. Although the vertical distance between the electrodes are only a few nanometers, the other dimensions of electrodes are a few micrometers. The electrode area along the step edge can be considered active sensing area, however, the extent of the active sensing area away from the step edge diminishes linearly with length of the DNA strands of interest. Hence, after the DNA binds on one electrode, there is only a fraction of the area on the second electrode which can contribute to a successful bridging of the gap. Therefore, even if passivated, the large *dead* area of the electrodes can capture lot of DNA molecules without contributing to the active sensing. Thus the problem false positive results and *dead* sensing area makes this method and device less suitable for high sensitive biosensing .

## 2.4 Materials and Methods

### 2.4.1 Chemicals and Reagents

N-(1-mercapto-11-undecyl)-biotin amide (MUBA) 99% (Prochimia, Poland), 11-mercapto-1-undecanol (MUD) 99% and 11-mercaptoundecanoic acid 99% (Sigma-Aldrich, Germany) were used without any modifications. Streptavidin ( lyophilized, ≥13 U/mg protein), Silver Nitrate (AgNO$_3$) ≥99.0%, anhydrous Ammonia (NH3) ≥99.99%, Trisodium citrate dihydrate and Citric acid monohydrate, Hexamethyldisilazane (HMDS) 99.9%, Acetic acid ≥99.7%, Sodium

acetate ≥99.0%, hydroquinone ≥99% (all from Sigma-Aldrich, Germany) were also procured and used. Phosphate buffered saline (PBS) solution was prepared using PBS powder pouch (pH 7.4 at 25°C, Sigma-Aldrich, Gemany)by dissolving one litre of deionized water yielding 0.01 M PBS (NaCl 0.138 M; KCl - 0.0027 M). Deionized water for buffer preparation and washing was obtained from Millipore multicartridge system (Milli-Q Ultra-Pure water system). HPLC grade organic solvents (Merck, Germany) like ethanol (for thiol incubation) acetone and 2-isopropyl alcohol (IPA) were used. Streptavidin (MWSA ≈ 60kDa, lyophilized powder, ≥13 units/mg protein) (Sigma-Aldrich, Germany) was stored at -20°C. After thawing, it was restored in PBS (1mg/ml) preparing aliquots of 100µl and stored at 4°C without further freeze/thaw cycles. Streptavidin (SA) tagged (at 5' end) 80bp complimentary DNA strands were obtained from Eurofins Scientific, the Netherlands (SA-5'-GGCCCGGCGGTCGCCACACCAATTCGTTACTCAGGGACGTTACCACGGCTACTA TCGTCGCAATTCAGTCAGGGATCTCG-3' and 3'-CCGGGCCGCCAGCGGTGTGGTTAAGCAATGAGTCCCTGCAATGGT GCCGATGATAGCAGCGTTAAGTCAGTCCCTAGAGC-5'-SA). 50 Kbp linear dsDNA was also purchased for DNA combing experiments.

### 2.4.2 Devices

Nanogap devices were fabricated as mentioned in Section #.#. For metallization of immobilized biotin-tagged DNA on an SA monolayer, nanogaps with a gap size of 20 nm were used, which is smaller than the length of DNA used (~30 nm). For metallization of the combed DNA on a Si surface, 2 cm × 2 cm chips of Si n-type wafer pieces were used and for metallization of negatively charged SAM molecules, 2 cm × 2 cm chips of Si n-type wafer pieces with 30nm thick gold layer and 5nm Ti adhesive layer on top were used. Chips were cleaned in acetone and ethanol using ultrasonication and by oxygen plasma (at 40W for 300s) under vacuum (180 millitorr).

### 2.4.3 Buffer preparation

*Citrate Buffer:* 70.75 ml of 0.1 M solution of monohydrate citric acid in deionized water and 29.25 ml of 0.1 M solution of dihydrate trisodium citrate in deionized water were mixed to form citrate buffer with pH 3.5 at 20°C. *Acetate Buffer:* 54.4

g of sodium acetate was dissolved in 50 ml of deionized water at 35°C. After cooling, 10 ml of anhydrous acetic acid was slowly added and later diluted to 100ml with deionized water to obtain pH 5.5 at 20°C. *Ammonia solution:* Aqueous ammonia solution was prepared by diluting 1ml of anhydrous ammonia in 500ml of deionized water giving pH 10.5 at 20°C.

### 2.4.4 DNA combing

After plasma cleaning, for metallization of combed DNA experiments, HMDS was spin coated on the Si chips at 1500rpm. 20ng/µl of 50 kbp linear dsDNA was suspended in acetate buffer at pH 5.5. HMDS coated hydrophobic chips were held at 85° angle to horizontal surface and 5µl of DNA suspended in acetate solution was pipetted onto the chip so that droplet flows down the chip surface under gravity. Later, chip is rinsed with deionized water and blow dried under nitrogen stream.

### 2.4.5 DNA Metallization

Devices were incubated in 0.1M $AgNO_3$ in aqueous ammonia buffer (pH 10.5) for 10 min. After a thorough rinsing with deionized water and drying in nitrogen stream, the adsorbed silver ions were reduced by 50mM hydroquinone in aqueous ammonia buffer (pH 10.5) for 10 min. After the silver ion collection and reduction steps, 0.1M $AgNO_3$ in citrate buffer (pH 3.5) and 50mM hydroquinone in citrate buffer (pH 3.5) were mixed under less light ambient and the chips were incubated in the solution for 2-10 mins.

### 2.4.6 Conductive-probe atomic force microscope

Atomic force microscope (AFM), DI- Dimension 3100 Series AFM, Digital Instruments, CA, USA, was used to image the height of the DNA samples and the nanogap devices. Together with the AFM, an IV converter and amplifier was used for conductive probe AFM (CP-AFM). A constant sample bias of voltage (1 V) between the sample and the conducting cantilever tip was applied and current was measured in CP-AFM mode.

A scotch tape was used to exfoliate layers of graphite from an HOPG sample. Thin layers of graphite were then separated from the tape using a tweezer and laid carefully on the Si chip with metallized DNA on it. Silver paste was used to

electrically connect the graphite flake to the measurement system. CP-AFM measurements were conducted along the edge of the flake where the layer thickness was relatively less.

### 2.4.7 Immobilization of SA tagged DNA

For metallization of immobilized biotin tagged DNA on SA monolayer, cleaned devices were rinsed in ethanol for 30s and ultrasonicated in ethanol for 5mins to remove possible oxide residues. After sonication, devices were rinsed with ethanol and Milli-Q water and dried under a stream of nitrogen flow. 1 mM of thiol solutions (overall concentration of both MUBA and MUD thiols together in solution) in HPLC grade ethanol are prepared with 1:18 ratio of MUBA to MUD (as described in chapter 3). Later the solution was purged with argon before incubation to avoid oxidation of thiols. All devices were incubated for 24h by immersing it in 5mL of thiol solution in argon ambient (again to limit oxidation of thiols to sulfonates). After incubation, devices were rinsed thoroughly with ethanol and Milli-Q water several times and dried under a stream of nitrogen. In order to get rid of any unattached thiol molecules on the surface, the devices were ultrasonicated in fresh ethanol for 5min and thereafter rinsed with water and dried with stream of nitrogen. 1μM SA was suspended in PBS and the chips with biotinylated electrodes were incubated in the solution for 30 mins with gentle agitation using rocking motion. Subsequently the chips were rinsed with PBS tween and deionized water and were incubated with SA tagged DNA in PBS with different concentrations (1 μM and 500 nM) for 30 mins. For SPR studies, a partially home-built setup was used.

### 2.4.8 Electrical characterization

The two terminal current-voltage characteristics were obtained in room temperature (dry condition: without any solution) using probe station (Janis ST-500) connected to a semiconductor characterization system (Keithley 2400) controlled by a home-built LabVIEW program.

## 2.5 References

1.  Moth-Poulsen, K.; Bjørnholm, T., Molecular electronics with single molecules in solid-state devices. *Nature nanotechnology* **2009,** *4* (9), 551.

2.  Liang, W.; Shores, M. P.; Bockrath, M.; Long, J. R.; Park, H., Kondo resonance in a single-molecule transistor. *Nature* **2002,** *417* (6890), 725.

3.  Zevenbergen, M. A.; Wolfrum, B. L.; Goluch, E. D.; Singh, P. S.; Lemay, S. G., Fast electron-transfer kinetics probed in nanofluidic channels. *Journal of the American Chemical Society* **2009,** *131* (32), 11471-11477.

4.  Mahapatro, A. K.; Ying, J.; Ren, T.; Janes, D. B., Electronic transport through ruthenium-based redox-active molecules in metal– molecule– metal nanogap junctions. *Nano letters* **2008,** *8* (8), 2131-2136.

5.  Im, H.; Bantz, K. C.; Lindquist, N. C.; Haynes, C. L.; Oh, S.-H., Vertically oriented sub-10-nm plasmonic nanogap arrays. *Nano letters* **2010,** *10* (6), 2231-2236.

6.  Kubo, W.; Fujikawa, S., Au double nanopillars with nanogap for plasmonic sensor. *Nano letters* **2010,** *11* (1), 8-15.

7.  Lee, J.; Shim, W.; Noh, J. S.; Lee, W., Design rules for nanogap-based hydrogen gas sensors. *ChemPhysChem* **2012,** *13* (6), 1395-1403.

8.  Minh, Q. N.; Tong, H.; Kuijk, A.; van de Bent, F.; Beekman, P.; van Rijn, C. M., Gas sensing performance at room temperature of nanogap interdigitated electrodes for detection of acetone at low concentration. *RSC advances* **2017,** *7* (79), 50279-50286.

9.  Nevill, J. T.; Di Carlo, D.; Liu, P.; Jeong, K.-H.; Lee, L. P. In *Detection of protein conformational changes with a nanogap biosensor*, The 13th International Conference on Solid-State Sensors, Actuators and Microsystems, 2005. Digest of Technical Papers. TRANSDUCERS'05., IEEE: 2005; pp 1668-1671.

10. Chen, X.; Guo, Z.; Yang, G.-M.; Li, J.; Li, M.-Q.; Liu, J.-H.; Huang, X.-J., Electrical nanogap devices for biosensing. *Materials Today* **2010,** *13* (11), 28-41.

11. Kim, S. K.; Cho, H.; Park, H.-J.; Kwon, D.; Lee, J. M.; Chung, B. H., Nanogap biosensors for electrical and label-free detection of biomolecular interactions. *Nanotechnology* **2009,** *20* (45), 455502.

12. Negishi, R.; Hasegawa, T.; Terabe, K.; Aono, M.; Ebihara, T.; Tanaka, H.; Ogawa, T., Fabrication of nanoscale gaps using a combination of self-assembled molecular and electron beam lithographic techniques. *Applied physics letters* **2006,** *88* (22), 223111.

13. Fischbein, M. D.; Drndić, M., Nanogaps by direct lithography for high-resolution imaging and electronic characterization of nanostructures. *Applied physics letters* **2006,** *88* (6), 063116.

14. Nagase, T.; Gamo, K.; Kubota, T.; Mashiko, S., Direct fabrication of nano-gap electrodes by focused ion beam etching. *Thin Solid Films* **2006,** *499* (1-2), 279-284.

15. Büyükköse, S.; Vratzov, B.; van der Wiel, W. G., High-quality global hydrogen silsequioxane contact planarization for nanoimprint lithography. *Journal of Vacuum Science & Technology B, Nanotechnology and Microelectronics: Materials, Processing, Measurement, and Phenomena* **2011,** *29* (2), 021602.

16. Martin, C. A.; van Ruitenbeek, J. M.; van der Zant, H. S., Sandwich-type gated mechanical break junctions. *Nanotechnology* **2010,** *21* (26), 265201.

17. Tian, J.-H.; Liu, B.; Li, X.; Yang, Z.-L.; Ren, B.; Wu, S.-T.; Tao, N.; Tian, Z.-Q., Study of molecular junctions with a combined surface-enhanced Raman and mechanically controllable break junction method. *Journal of the American Chemical Society* **2006,** *128* (46), 14748-14749.

18. Sordan, R.; Balasubramanian, K.; Burghard, M.; Kern, K., Coulomb blockade phenomena in electromigration break junctions. *Applied physics letters* **2005,** *87* (1), 013106.

19. Trouwborst, M.; Van Der Molen, S.; Van Wees, B., The role of Joule heating in the formation of nanogaps by electromigration. *Journal of applied physics* **2006,** *99* (11), 114316.

20. Kim, J.-H.; Moon, H.; Yoo, S.; Choi, Y.-K., Nanogap Electrode Fabrication for a Nanoscale Device by Volume-Expanding Electrochemical Synthesis. *Small* **2011,** *7* (15), 2210-2216.

21. Cho, H.; Kim, S. K.; Jung, Y.; Jung, J.; Chung, B. H., Electric detection of target DNA by fabricating gold nanowire bridges on planar nanogap electrodes. *Chemical Communications* **2011,** *47* (20), 5756-5758.

22.  Dhahi, T. S.; Hashim, U.; Ali, M.; Ahmed, N., Fabrication of 6? nm gap on silicon substrate for power-saving appliances. *Int. J. Phys. Sci.* **2012,** *7*, 2414-2421.

23.  Ali, M. E.; Dhahi, T. S.; Das, R.; Hashim, U., DNA hybridization detection using less than 10-nm gap silicon nanogap structure. *Sensors and Actuators A: Physical* **2013,** *199*, 304-309.

24.  Roy, S.; Chen, X.; Li, M.-H.; Peng, Y.; Anariba, F.; Gao, Z., Mass-produced nanogap sensor arrays for ultrasensitive detection of DNA. *Journal of the American Chemical Society* **2009,** *131* (34), 12211-12217.

25.  Chen, X.; Roy, S.; Peng, Y.; Gao, Z., Electrical sensor array for polymerase chain reaction-free messenger RNA expression profiling. *Analytical chemistry* **2010,** *82* (14), 5958-5964.

26.  Van Megen, M.; Bomer, J. G.; Olthuis, W.; van den Berg, A., Solid state nanogaps for electrochemical detection fabricated using edge lithography. *Microelectronic engineering* **2014,** *115*, 21-25.

27.  Haneveld, J.; Berenschot, E.; Maury, P.; Jansen, H., Nano-ridge fabrication by local oxidation of silicon edges with silicon nitride as a mask. *Journal of micromechanics and microengineering* **2006,** *16* (6), S24.

28.  Yagubizade, H.; Berenschot, E.; Jansen, H. V.; Elwenspoek, M.; Tas, N. R. In *Silicon nanowire fabrication using edge and corner lithography*, Nanotechnology Materials and Devices Conference (NMDC), 2010 IEEE, IEEE: 2010; pp 128-131.

29.  Braun, E.; Eichen, Y.; Sivan, U.; Ben-Yoseph, G., DNA-templated assembly and electrode attachment of a conducting silver wire. *Nature* **1998,** *391* (6669), 775-778.

30.  Storm, A. J.; Van Noort, J.; De Vries, S.; Dekker, C., Insulating behavior for DNA molecules between nanoelectrodes at the 100 nm length scale. *Applied Physics Letters* **2001,** *79* (23), 3881-3883.

31.  Porath, D.; Bezryadin, A.; De Vries, S.; Dekker, C., Direct measurement of electrical transport through DNA molecules. *Nature* **2000,** *403* (6770), 635-638.

32.  Fink, H. W.; Schönenberger, C., Electrical conduction through DNA molecules. *Nature* **1999,** *398* (6726), 407-410.

33.   Kasumov, A. Y.; Kociak, M.; Guéron, S.; Reulet, B.; Volkov, V. T.; Klinov, D. V.; Bouchiat, H., Proximity-induced superconductivity in DNA. *Science* **2001,** *291* (5502), 280-282.

34.   Maeda, Y.; Okamoto, A.; Hoshiba, Y.; Tsukamoto, T.; Ishikawa, Y.; Kurita, N., Effect of hydration on electrical conductivity of DNA duplex: Green's function study combined with DFT. *Computational Materials Science* **2012,** *53* (1), 314-320.

35.   Roy, S.; Chen, X.; Li, M. H.; Peng, Y.; Anariba, F.; Gao, Z., Mass-produced nanogap sensor arrays for ultrasensitive detection of DNA. *Journal of the American Chemical Society* **2009,** *131* (34), 12211-12217.

36.   Watson, S. M. D.; Mohamed, H. D. A.; Horrocks, B. R.; Houlton, A., Electrically conductive magnetic nanowires using an electrochemical DNA-templating route. *Nanoscale* **2013,** *5* (12), 5349-5359.

37.   Mohamed, H. D. A.; Watson, S. M. D.; Horrocks, B. R.; Houlton, A., Magnetic and conductive magnetite nanowires by DNA-templating. *Nanoscale* **2012,** *4* (19), 5936-5945.

38.   Richter, J.; Mertig, M.; Pompe, W.; Mönch, I.; Schackert, H. K., Construction of highly conductive nanowires on a DNA template. *Applied Physics Letters* **2001,** *78* (4), 536-538.

39.   Mertig, M.; Ciacchi, L. C.; Seidel, R.; Pompe, W.; De Vita, A., DNA as a Selective Metallization Template. *Nano Letters* **2002,** *2* (8), 841-844.

40.   Monson, C. F.; Woolley, A. T., DNA-templated construction of copper nanowires. *Nano Letters* **2003,** *3* (3), 359-363.

41.   Park, S. J.; Taton, T. A.; Mirkin, C. A., Array-based electrical detection of DNA with nanoparticle probes. *Science* **2002,** *295* (5559), 1503-1506.

42.   Rakitin, A.; Aich, P.; Papadopoulos, C.; Kobzar, Y.; Vedeneev, A. S.; Lee, J. S.; Xu, J. M., Metallic conduction through engineered DNA: DNA nanoelectronic building blocks. *Physical Review Letters* **2001,** *86* (16), 3670-3673.

43.   Liu, H.; Li, G.; Ai, H.; Li, J.; Bu, Y., Electronic enhancement effect of copper modification of base pairs on the conductivity of DNA. *Journal of Physical Chemistry C* **2011,** *115* (45), 22547-22556.

44.     Lee, H. Y.; Tanaka, H.; Otsuka, Y.; Yoo, K. H.; Lee, J. O.; Kawai, T., Control of electrical conduction in DNA using oxygen hole doping. *Applied Physics Letters* **2002,** *80* (9), 1670-1672.

45.     Allemand, J.; Bensimon, D.; Jullien, L.; Bensimon, A.; Croquette, V., pH-dependent specific binding and combing of DNA. *Biophysical journal* **1997,** *73* (4), 2064-2070.

46.     Kozhummal, R.; Berenschot, E.; Jansen, H.; Tas, N.; Zacharias, M.; Elwenspoek, M., Fabrication of micron-sized tetrahedra by Si< 1 1 1> micromachining and retraction edge lithography. *Journal of micromechanics and microengineering* **2012,** *22* (8), 085032.

47.     Liu, C.-H.; Yu, X., Silver nanowire-based transparent, flexible, and conductive thin film. *Nanoscale research letters* **2011,** *6* (1), 75.

*"I was taught that the way of progress was neither swift nor easy."*

*Marie Curie*

3

# Electrochemical redox cycling on nano-interdigitated electrodes

**Abstract:** Optimization of the active sensing area by minimizing the non-active (*dead*) sensing area is a crucial device design consideration for sensors. Here, we fabricated interdigitated electrode arrays with the width, gap and height of the interdigitated nanogap electrodes in nanoscale dimensions, using electron-beam lithography, thus improving the ratio of *dead* to active sensing a rea. Electrochemical biosensors (*e.g.* glucose sensors) are well established sensing systems for many years. Hence, instead of an electrical measurement technique, here we used electrochemical measurement methods in order to avoid false positive events which may occur as a result of metallization of DNA as discussed in chapter 2. Signal amplification due to redox cycling of the redox-active molecules between the nano-interdigitated electrodes was studied. We also explored the possibility of using alternative measurement techniques, like differential pulse voltammetry and cyclic voltammetry in the absence of a supporting electrolyte.

## 3.1 Introduction

In the previous chapter, we discussed the fabrication of nanogap devices using edge lithography and the electrical characterization of metallized DNA across these nanogaps. For these nanogaps, the ratio of the *dead* sensing area to active sensing area was high. Consequently, a large number of analyte molecules were lost in this "dead" sensing area without contributing to active sensing. Accordingly, in order to reduce the ratio of the dead sensing area to the active sensing area, we modified the geometry of our nanogap sensor to a nano-interdigitated electrode (nIDE) array. An nIDE consists of a pair of comb electrode structures that mesh with each other. By reducing the width of the electrodes using the electron-beam lithography (EBL), the dead sensing area can be minimized considerably, depending on the size of the analyte molecules. However, apart from high dead sensing area, the DNA metallization method also encountered problems with false positive signals as discussed in **chapter 2**. Consequently, instead of electrical biosensing, we shifted our focus to more conventional electrochemical methods of biosensing. Micro-/nano-devices, particularly interdigitated electrode arrays,[1-6] have been extensively investigated electrochemically for more than two decades. Electrochemical redox cycling on mirco-/ nano devices, provides amplification of current in dual mode, small double layer capacitance, and fast time response. Moreover, the advantage of devices with an easily accessible open structure (like nDIEs,[7] ring-disc electrodes[8-9]) over more enclosed redox cycling systems (like nanogap cells,[10-11] nanogap channels[6, 12]) is the ease of chemical functionalization of the electrode surface, which is an important factor in biosensing. Furthermore, these enclosed systems require fluidic systems with microchannel in parallel to the nanochannel between the electrode gap. Consequently, only a fraction of the analyte reaches the electrode surface through the nanochannel and the bulk of the analyte bypasses the electrodes through the microchannel. Moreover, opposed to ring-disk electrodes, nIDEs provide symmetrical collector and generator electrodes, thus improving the active sensing area and redox cycling on it. Here, in this chapter we study the electrochemical redox cycling on nIDEs to investigate their potential for biosensing.

### 3.1.1 Generator-collector dual mode

Generally, an electrochemical cell involves a working electrode, an auxiliary electrode and a reference electrode. However, for a generator-collector (GC) electrochemical system, there are two working electrodes where one electrode generates oxidized or reduced species of the redox analyte, while the other collects these electrogenerated species. As a result of the diffusive shuttling of the redox species between the electrodes (termed as redox cycling) that dominates the mass transfer, a steady-state current is achieved. Normally, in the generator-collector dual mode configuration, the collector electrode is held at a constant potential, while the potential is swept on the generator electrode across the formal potential of the analyte of interest. Usually, the constant potential on the collector is chosen based on the chemically stable form of the redox analyte. If the reduced form is more stable, then the potential at the collector electrode is kept well below the formal potential, while the generator potential is scanned from low to high potential well above the formal potential, such that reduction reaction happens on the collector and oxidation happens on the generator. In the GC dual mode operation, redox cycling helps in amplifying the current of the reversible redox analyte species, providing enhanced faradaic currents. It also gives reduced non-faradaic charging and discharging current through the double layer capacitance, especially on the collector electrode where the potential is kept constant making the dual mode interesting for fast scan cyclic voltammetry.[13-14] Although the dual mode amplification is not achieved for non-reversible redox active species, this mode can also help in selective and amplified detection of reversible redox active species in the presence of non-reversible redox active species. It can also provide information about the diffusion coefficients of redox species[15], fast electron transfer kinetics[6], rate of the electrochemical reaction[16], lifetime of intermediate products generated during electrochemical reactions.[17-18]

One of the important parameters in the dual mode operation is the collection efficiency of the IDEs. It is the measure of how effectively the collector electrode can collect the redox species generated at the generator. The distance between the two working electrodes is crucial, since deceasing the gap between the electrodes helps in getting a better collection efficiency. The collection efficiency is given by

$$\Phi = \frac{I_c}{I_g}, \tag{3.1}$$

where $I_c$ and $I_g$ are the limiting currents of the collector and generator, respectively, and for a symmetrical collector and generator geometry, the number of redox cycling events, $N_{rc}$[1], is

$$N_{rc} = \frac{1}{1 - \Phi^2}. \tag{3.2}$$

Unlike the conventional thin-film interdigitated electrodes, elevated electrodes further improve the collection efficiency of the electrochemical system by providing redox cycling on the sidewalls of the electrode as well. The magnitude of the limiting current of the nIDEs with elevated electrodes can be approximated using the following equation[19-21]

$$I = mbn_i FC_i D_i \left[ \left\{ 1.9 \frac{h_e}{w_g} \right\} + \left\{ 0.637 \ln(2.55 (1 + \frac{w_e}{w_g})) \right\} - \left\{ \frac{0.19}{(1 + \frac{w_e}{w_g})^2} \right\} \right], \tag{3.3}$$

where $m$ is the number of electrodes, $b$ is the length of each electrode, $n_i$ is the number of electrons involved in the redox reaction, $F$ is the Faraday constant, $D_i$ is the diffusion constant and $C_i$ is the concentration of the redox mediator, respectively, $h_e$ is the height and $w_e$ is the width of the electrode and $w_g$ is the gap between the adjacent IDEs. This equation considers that the dominant factor of the limiting current is diffusion. That is, the equation holds true only when there is an excess of supporting electrolyte, and the system is undisturbed.

### 3.1.2 Mass transport

The mass transport of redox mediator molecules to the working electrode in an electrochemical cell is influenced by three processes: diffusion, electromigration, and convection. According to the Nernst-Planck equation, the total flux, $J_i(x)$, of the reactant molecules, $i$, to an electrode is given by[22]

$$J_i(x) = \underbrace{-D_i \frac{\partial C_i(x)}{\partial x}}_{\textbf{Diffusion}} - \underbrace{\frac{n_i F}{RT} D_i C_i \frac{\partial \phi(x)}{\partial x}}_{\textbf{Migration}} + \underbrace{C_i v(x)}_{\textbf{Convection}} , \quad \text{(3.4)}$$

where $D_i$ is the diffusion constant and $\frac{\partial C_i(x)}{\partial x}$ is the concentration gradient of the redox mediator, respectively, $n_i$ is the number of electrons involved in the redox reaction $F$, is the Faraday constant, $R$ is the gas constant, $T$ is the temperature, $\frac{\partial \phi(x)}{\partial x}$ is electric potential gradient, and $v(x)$ is the velocity profile of the solution. The diffusion is the net movement of molecules from higher concentration region to a lower concentration region. Initially, the concentration of the redox species is constant throughout the electrochemical cell. However, as the reaction progresses on the working electrode, the concentration of one species (redox or oxidized species depending on the potential on the electrode) near the electrode increases. This results in the diffusion of that particular species away from the electrode surface, and other species towards the electrode. On the other hand, the migration is the movement of the charged species in the solution due to the applied potential. As the current passes through the solution, it generates a potential gradient along the solution between the electrodes. In a system with supporting electrolyte when a potential is applied on an electrode, the counter ions will move towards the surface of the electrode to screen the change in net charge. Usually in electrochemistry, ten to hundred times excess of supporting electrolyte is added. These extra ions can screen the charge of the redox ions and hence the flux contribution due to migration becomes negligible. If the solution is physically undisturbed (unstirred), the velocity profile is negligible. As a result, in an undisturbed solution with excess of supporting electrolyte, the dominant flux towards the electrode surface is due to the diffusion of the redox molecules. On the other hand, in a low concentration of the supporting electrolyte, the ionic strength of the solution is low, and it can influence the mass transport due to the ion migration. In this chapter, we also study the effect of the absence of supporting electrolyte in redox cycling.

## 3.2 Results and discussion
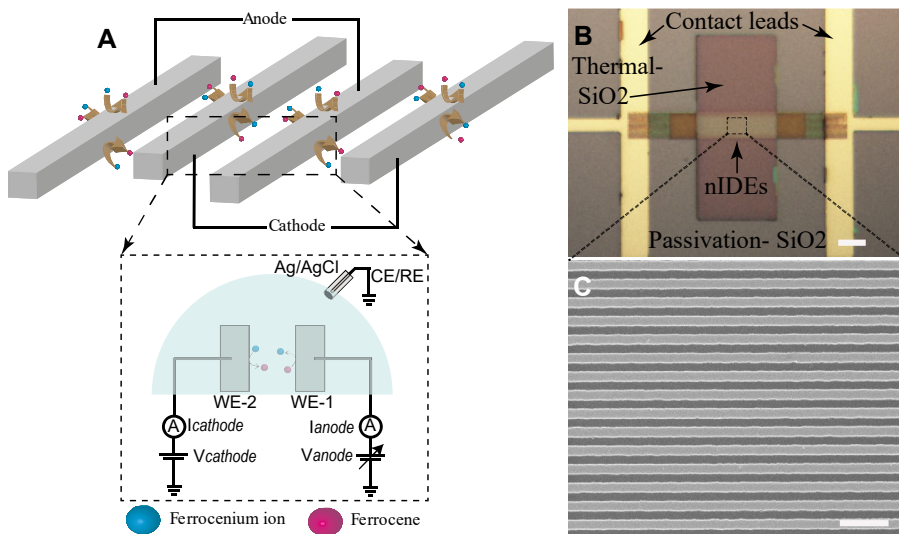
### 3.2.1 Fabrication of nIDEs



**Figure 3.1: (a)** Schematic cross-sectional view of nIDEs and redox cycling on them (top), measurement setup of the device (bottom). **(b)** Optical micrograph of the device showing nIDEs, contact leads, top passivation SiO2 layer and bottom insulation SiO2 layer (scale bar = 10 µm) **(c)** Scanning electron micrograph showing zoom-in of the nIDEs (scale bar = 500 nm).

The nIDEs were fabricated using a combination of optical and electron-beam lithography. The fabrication started with thermally (1000° C, dry) oxidizing a Si <100> wafer with a 300 nm oxide layer. This oxide layer acts as the insulation layer, preventing current leakage through the electrodes. Subsequently, a positive photoresist was patterned using optical lithography, defining the contact pads and lead wires for electrical measurements, and markers for EBL patterning. Later, metals (Ti 5 nm followed by Pt 80 nm) were evaporated directionally using an e-beam evaporator. The Ti/Pt film formed on the photoresist was then removed using a lift-off method in acetone with ultrasonic agitation leaving the contact pads, leads and markers on the substrate. Afterwards, A4 PMMA resist was spin coated (250 nm) on the substrate and patterned into 100 nm wide structures with a pitch of 200 nm (providing 100 nm gap) using EBL. The substrate

was developed in an MIBK and IPA (1:3) solution for 45 sec. A CHF$_3$-based, selective plasma etching of SiO$_2$ (5 nm) was performed to recess the adhesive metal layer into the substrate. Later the metals (Ti 5 nm, adhesive layer, and Pt 100 nm) defining the nIDEs were evaporated, using an e-beam evaporator and the metal film was lifted-off in warm (80° C) DMSO solution without acoustic agitation to obtain well-defined nano features. **Figure 3.1 (a)** shows the schematic diagram of the nIDEs, while **(b)** and **(c)** show optical and scanning-electron-micrograph images of the fabricated devices.
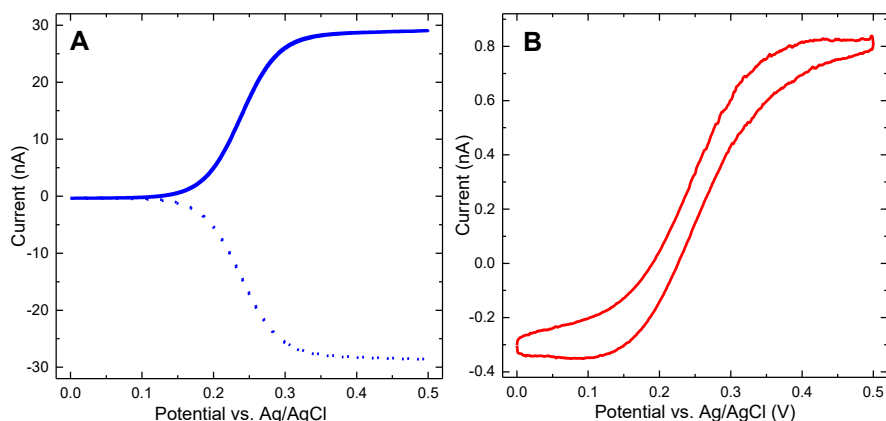
### 3.2.2 Redox cycling on nIDEs



**Figure 3.2:** Comparison of **(a)** GC dual mode and **(b)** non-GC modes of cyclic voltammograms of 2 mM of ferrocenium dimethanol (Fc(MeOH)$_2$ ) in 2 M KCl at 50 mV/s scan rate on 100 nm gap nIDEs. For GC dual mode, the collector was biased at 0 V and for non-GC mode the collector was floating. Solid line shows the generator current and the dotted line shows the redox-cycling current on the collector.

Electrochemical measurements were performed on the fabricated nIDEs and the obtained cyclic voltammograms are shown in **Figure 3.2** for ferrocenium dimethanol (Fc(MeOH)$_2$) in 2 M KCl at 50 mV/s scan rate. In the GC mode, the collector was biased at 0 V, while in the non-GC mode the collector was left floating. In both cases, the voltammograms resembled the shape of a sigmoid function indicating diffusion-limited current as expected. In the non-GC mode, the limiting current at 0.5 V was 0.81 nA, and for the GC mode it was 29 nA, resulting

in an amplification factor of ~36. The amplification factor is much higher than other open-system redox-cycling devices owing to the long, close and elevated electrode array.[7-9, 23-24] In GC mode the current through the generator electrode (solid line) was essentially the inverse of that through the collector electrode (dotted line) due to RC. The generator electrode limiting current was 29 nA, while that of the collector electrode is 28.6 nA, yielding a collection efficiency of 98.6%, which is slightly better than previously reported open redox-cycling devices.[7-9]

Normally, CV is sensitive to non-faradaic current, like charging of the double layer capacitance due to the continuously ramping voltage on the working electrode. In the redox cycling systems in the GC mode, since the collector potential is kept constant, generally, the collector does not suffer from this. Nonetheless, in order to obtain a very small double layer capacitance on the generator electrode, the potential scan rate is usually lowered to 5 -10 mV/s.  Unlike many redox-cycling-based devices, we observed no hysteresis even at relatively higher scan rate of 50 mV/s, confirming that the double layer capacitance at GC mode is very small for nIDEs. This in turn reduces the capacitive current, and thus the offset due to non-faradaic current in the total current is eliminated. This also makes our device suitable for fast-scan cyclic voltammetry.
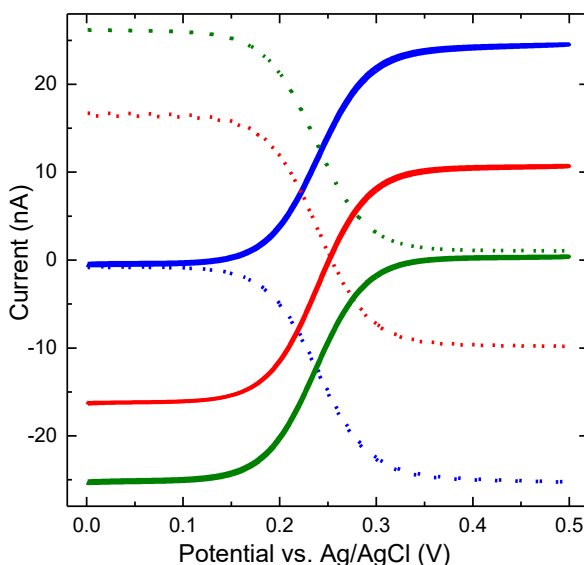
**Figure 3.3**: Dependence of voltammetric response on collector potential. The potential of the generator electrode was swept from 0 V to 0.5 V, while the collector electrode was held at 0.1 V (blue), 0.25 V (red) and 0.5 V (green). Solid curves show the generator current and the dotted curves show the redox-cycling current on the collector.

**Figure 3.3** shows the voltammograms obtained by varying the potential on the collector electrode (a) 0.1 V as reductive potential, (b) 0.25 V near the formal potential, and (c) 0.5 V as oxidative potential. In all the three cases, the current through the generator electrode was the inverse of that through the collector electrode due to redox cycling. When the fixed potential on the collector electrode is 0.1 V, a cathodic current is observed on the collector and an anodic current on the generator. Meanwhile, for a collector voltage of 0.5 V, this is reversed; an anodic current is seen on the collector and a cathodic current on the generator. A crossover region is observed when the collector potential is in the range of 0.2 to 0.3 V. This suggests that the redox species concentration profile inside the device is in steady state throughout. Consequently, when the voltage on the collector is a reductive potential, the collector undergoes reduction and the opposite reaction occurs on the generator, resulting in an anodic current on generator and vice versa.

Differential pulse voltammetry (DPV) is an electrochemical measurement technique that is normally used to extract faradaic current from an electrochemical reaction without the influence of non-faradaic current, like charging and discharging through double layer capacitance. DPV consists of a series of pulses each with a fixed amplitude superimposed on a gradually ramping base potential. Current from every consecutive pulse is measured and subtracted to obtain the differential current. At formal potential, the differential current reaches a maximum, and decreases to zero as the current becomes diffusion controlled. *I.e.,* the current shows a peak at the formal potential and falls to zero/minimum for potentials below and above the formal potential.
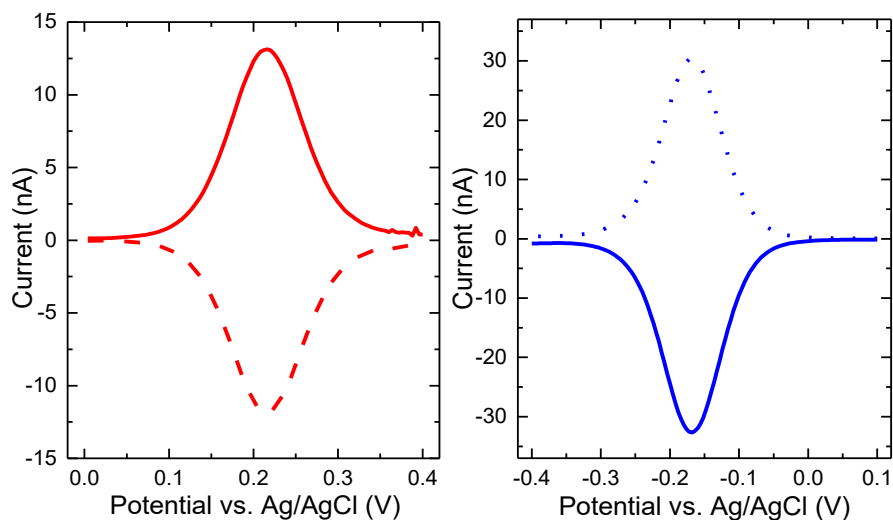


**Figure 3.4**: Differential pulse voltammograms in GC mode of **(a)** Fc(MeOH)$_2$ with collector voltage -0.1 V **(b)** ruthenium hexamine (Ru(NH$_3$)$_6$Cl$_3$) with collector voltage 0.3 V. Solid lines show the generator differential current and the dotted lines show the differential redox-cycling current on the collector.

Since, our nIDE devices show a very small double layer capacitance when worked in GC mode, one would expect that DPV is not a worthwhile technique for nIDEs as it is for electrochemical studies with macro electrodes. Nonetheless, DPV in dual mode is a useful and easy to-interpret tool for selective and amplified detection of reversible redox-active species in the presence of non-reversible redox active species, because redox cycling only amplifies reversible redox

reactions. *E.g.,* DPV in dual mode can be used for simultaneous and amplified detection of dopamine in the presence of uric acid and ascorbic acid, where dopamine undergoes reversible redox reaction, while the other two do not. As a proof of concept, DPV dual mode was performed on nIDEs with $Fc(MeOH)_2$ and ruthenium hexamine ($Ru(NH_3)_6Cl_3$) as redox- active molecules. **Figure 3.4** shows the differential pulse voltammograms of $Fc(MeOH)_2$ and $Ru(NH_3)_6Cl_3$. Here, both of these molecules undergo reversible redox reactions, and hence both the generator and the collector currents are observed and are similar. A current peak is observed at 0.215 V for $Fc(MeOH)_2$ and -0.17 V for $Ru(NH_3)_6Cl_3$ which is more easily discerned from DPV compared to CV.

### 3.2.3 Redox cycling without supporting electrolyte

In order to study the effect on the redox cycling current on nIDEs in the absence and presence of a supporting electrolyte, we used three different redox-active species: (a) $Ru(NH_3)_6Cl_3$, (b) $Fc(MeOH)_2$ and (c) potassium ferricyanide, $K_3(Fe(CN)_6)$. 2 M KCl was used for measurements with a supporting electrolyte, while for measurements in the absence of supporting electrolyte the redox species were dissolved in Mill-Q water. In all cases, the concentration of the redox species was kept at 2 mM. **Figure 3.5** shows cyclic voltammograms on the nIDEs with and without the supporting electrolyte at 50 mV/s scan rate for $Ru(NH_3)_6Cl_3$, $Fc(MeOH)_2$ and $K_3(Fe(CN)_6)$. For $Ru(NH_3)_6Cl_3$ and $Fc(MeOH)_2$ we observed a significant current enhancement (50 and 100% respectively) in the absence of the supporting electrolyte, and a smaller increase (8%) for $K_3(Fe(CN)_6)$.
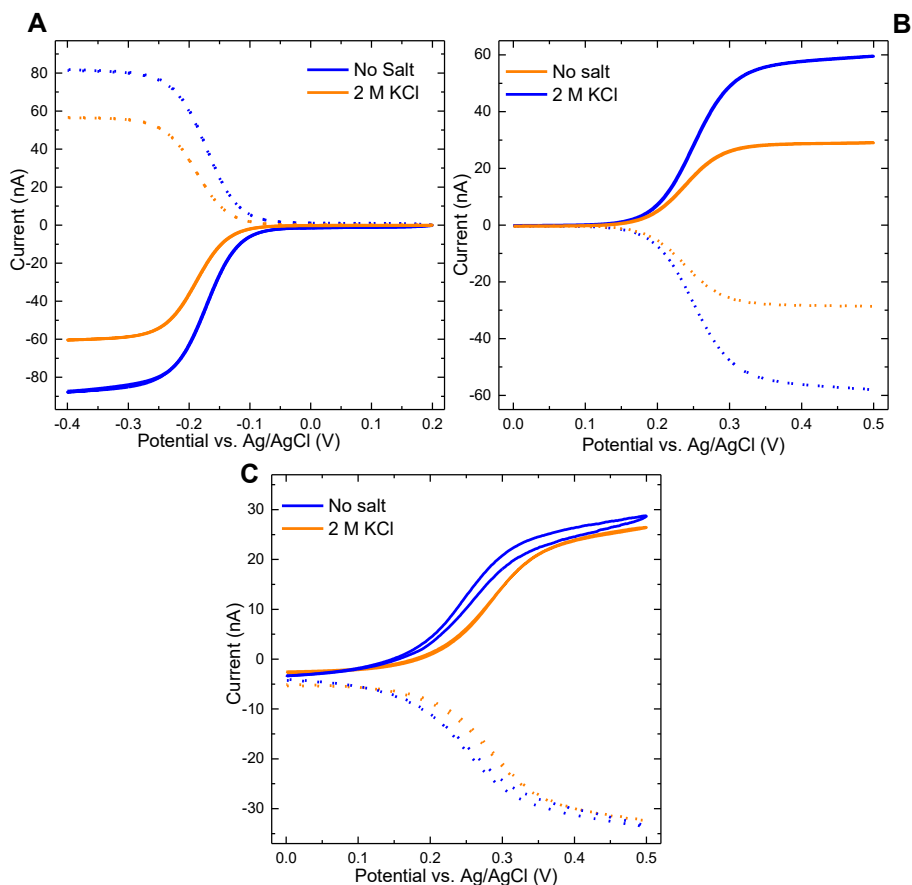
**Figure 3.5**: Cyclic voltammograms on nIDEs with and without supporting electrolyte (2 M KCl) at 50 mV/s scan rate of **(a)** $Ru(NH_3)_6$ **(b)** $Fc(MeOH)_2$ **(c)** $K_3(Fe(CN)_6)$. Solid lines show the generator current and the dotted lines show the redox cycling current on the collector.

We attribute the current enhancement to two phenomena, (1) electrostatically driven ion enrichment due to surface charge and (2) ion migration. As described in **Section 3.1.2**, when there is an excess of supporting electrolyte in the solution, the mass transfer of the redox species is dominated by diffusion. However, in solution without the supporting electrolyte, other mass transfer processes can become relevant. Consider the adjacent collector and generator electrodes of the nIDEs. When a water-based solution is applied on the nIDEs, the volume of solution contained between these two adjacent electrodes is in contact with the

cathode on one side, the anode on the other side and $SiO_2$ at the bottom. The latter occurs because the nIDEs were fabricated on a thermally grown silicon oxide layer. Submerged in water, the $SiO_2$ surface develops a negative surface charge due to the dissociation of the terminal silanol groups. This negative surface charge attracts mobile counter ions from the solution, whereas it repels co-ions to maintain overall electroneutrality. In the presence of a supporting electrolyte, the counter ions consist predominantly of $K^+$ ions, which are present in a large excess. With no supporting electrolyte, on the other hand, the main cationic species in solution originates from the redox mediator salt. These are either the positive redox mediator ions such as $Ru(NH_3)_6^{3+/2+}$ and ferrocenium ions, or the $K^+$ counterions to $Fe(CN)_6^{-3}$. For cationic redox species, this results in ion enrichment, *i.e.*, an increase in concentration of the redox ions near the surface compared to the bulk solution. As a rough estimate, one expects that the ion enhancement due to surface charge becomes the dominant contribution to transport between the electrodes when the number of redox molecules per unit volume in the bulk is less than that needed to screen the surface charge density of the $SiO_2$ insulating layer. For our geometry and concentration of redox species, to be a dominant mechanism, the surface charge density of the $SiO_2$ insulating layer is estimated to be at least ~100 mC/m$^2$, in good agreement with the typical surface charge value of glass.[25-26] This mechanism does not enhance the $Fe(CN)_6^{3-/4-}$ redox cycling current, on the other hand, as these anionic species are repelled from the $SiO_2$ surface. In order to keep the neutrality of the surface charge of the $SiO_2$ layer, a larger number of monovalent ferrocenium counter ions is required compared to the divalent and trivalent $Ru(NH_3)_6^{3+/2+}$ ions, resulting in a higher ion enhancement due to surface charge for $Fc(MeOH)_2$. The change in the limiting current for $Fc(MeOH)_2$ is ~2 fold whereas for $Ru(NH_3)_6Cl_3$ it is ~ 1.5 fold.

The second consequence of working without supporting electrolyte is that migration becomes a relevant transport mechanism, next to diffusion. In nanoscale redox cycling devices, this results in a complex interplay between sharp diffusive gradients and spatially dependent electric fields, as investigated experimentally and numerically by the Bohn and White groups.[8, 11] The small increase (8%) in the limiting current for $K_3(Fe(CN)_6)$ suggests similar effects in our system as well. However, more experimental investigation has to be done in order

to conclusively explain this complex interplay. Although more prominent for $K_3(Fe(CN)_6)$, we also observed that for all the three redox species, in the absence of the supporting electrolyte, the limiting current is not entirely saturated; there is a gradual increase (small slope) in current with the overpotential. This can be due to ion migration and/or increase in local concentration of the redox ions. For example, for $Ru(NH_3)_6Cl_3$, as the cathode potential is decreased, in order to equilibrate the net ionic charge between the electrodes, more ions have to diffuse from the bulk, resulting in a higher average concentration of both the redox-active ions, in the absence of supporting electrolyte. A similar effect also occurs for both $Fc(MeOH)_2$ and $K_3(Fe(CN)_6)$.

## 3.3 Conclusion

In order to improve the ratio of *dead* to active sensing area, and to minimize the false positive events we proposed to use nanoscale interdigitated electrodes. In this chapter, we fabricated nIDEs with 100 nm electrode width and 100 nm gap and electrochemically validated them. We passivated the top surface of the device, which helped to perform measurements without current leakage and any complex fluidic system. It also provides an open device structure that is useful for a better chemical functionalization of the electrode surface for biosensing in the future. With the redox cycling on the nIDEs, a current amplification of ~36 fold was observed with respect to the single mode which is quite high for an open electrode system reported. In the future the electrode spacing can be further reduced to yield more efficient mass transport, potentially resulting in even higher amplification. Moreover, for experiments in the absence of supporting electrolyte, an additional 2 fold amplification was observed due to the surface charge within the nIDEs. This can be an interesting observation to consider while designing future detection schemes in the bionanosensing field. Due to the easy fabrication process, improved performance with high signal amplification due to redox cycling, the ability to perform in different conditions (salt or no salt), the ability for simultaneous and amplified detection of reversible reactions with DPV and the possibility for integration, nIDEs are suitable for lab-on-a-chip biosensing applications.

## 3.4 Materials and Methods

### 3.4.1 Chemicals and reagents

$Fc(MeOH)_2$, , $Ru(NH_3)_6Cl_3$, $K_3(Fe(CN)_6)$ and KCl, were purchased from Sigma-Aldrich B.V, the Netherlands. All solutions were prepared using Milli-Q water and experiments were carried out at room temperature.

### 3.4.2 Electrochemical measurements

Electrochemical experiments were carried out using a CH Instruments 842D (USA) bipotentiostat system. A commercial Ag/AgCl (3 M KCl) reference electrode (BASi Inc., USA) were used for measurements. Since the current produced by the nIDEs are in the order of nanoamperes, both the counter electrode and reference electrode leads of the bipotentiostat were connected together to the Ag/AgCl reference electrode. Generator-collector cyclic voltammetry was performed with one set of electrodes of nIDEs at fixed potential and the other set potential scanning. The working electrode 1 of the bipotentiostat was connected to the generator (anode) electrode set while the working electrode 2 was connected to the collector (cathode) electrode set.

## 3.5 References

1.  Niwa, O.; Morita, M.; Tabei, H., Electrochemical behavior of reversible redox species at interdigitated array electrodes with different geometries: consideration of redox cycling and collection efficiency. *Analytical Chemistry* **1990,** *62* (5), 447-452.

2.  Menon, V. P.; Martin, C. R., Fabrication and evaluation of nanoelectrode ensembles. *Analytical Chemistry* **1995,** *67* (13), 1920-1928.

3.  Paeschke, M.; Wollenberger, U.; Köhler, C.; Lisec, T.; Schnakenberg, U. ; Hintsche, R., Properties of interdigital electrode arrays with different geometries. *Analytica Chimica Acta* **1995,** *305* (1-3), 126-136.

4.  Nagale, M. P.; Fritsch, I., Individually addressable, submicrometer band electrode arrays. 1. Fabrication from multilayered materials. *Analytical Chemistry* **1998,** *70* (14), 2902-2907.

5.  Howell, J. O.; Wightman, R. M., Ultrafast voltammetry and voltammetry in highly resistive solutions with microvoltammetric electrodes. *Analytical Chemistry* **1984,** *56* (3), 524-529.

6.  Zevenbergen, M. A.; Wolfrum, B. L.; Goluch, E. D.; Singh, P. S.; Lemay, S. G., Fast electron-transfer kinetics probed in nanofluidic channels. *Journal of the American Chemical Society* **2009,** *131* (32), 11471-11477.

7.  Skjolding, L.; Spegel, C.; Ribayrol, A.; Emnéus, J.; Montelius, L. In *Characterisation of nano-interdigitated electrodes*, Journal of Physics: Conference Series, IOP Publishing: 2008; p 052045.

8.  Ma, C.; Contento, N. M.; Bohn, P. W., Redox cycling on recessed ring-disk nanoelectrode arrays in the absence of supporting electrolyte. *Journal of the American Chemical Society* **2014,** *136* (20), 7225-7228.

9.  Ma, C.; Contento, N. M.; Gibson, L. R.; Bohn, P. W., Redox cycling in nanoscale-recessed ring-disk electrode arrays for enhanced electrochemical sensitivity. *Acs Nano* **2013,** *7* (6), 5483-5490.

10. Kätelhön, E.; Hofmann, B.; Lemay, S. G.; Zevenbergen, M. A.; Offenhäusser, A.; Wolfrum, B., Nanocavity redox cycling sensors for the detection of dopamine fluctuations in microfluidic gradients. *Analytical chemistry* **2010,** *82* (20), 8502-8509.

11. Chen, Q.; McKelvey, K.; Edwards, M. A.; White, H. S., Redox cycling in nanogap electrochemical cells. The role of electrostatics in determining the cell response. *The Journal of Physical Chemistry C* **2016,** *120* (31), 17251-17260.

12. Rassaei, L.; Singh, P. S.; Lemay, S. G., Lithography-based nanoelectrochemistry. ACS Publications: 2011.

13. Pathirathna, P.; Balla, R. J.; Amemiya, S., Simulation of Fast-Scan Nanogap Voltammetry at Double-Cylinder Ultramicroelectrodes. *Journal of The Electrochemical Society* **2018,** *165* (12), G3026-G3032.

14. Dengler, A. K.; Wightman, R. M.; McCarty, G. S., Microfabricated Collector-Generator Electrode Sensor for Measuring Absolute pH and Oxygen Concentrations. *Analytical chemistry* **2015,** *87* (20), 10556-10564.

15. Amatore, C.; Sella, C.; Thouin, L., Electrochemical time-of-flight responses at double-band generator-collector devices under pulsed conditions. *Journal of Electroanalytical Chemistry* **2006,** *593* (1-2), 194-202.

16.    Menshykau, D.; Cortina-Puig, M.; del Campo, F. J.; Muñoz, F. X.; Compton, R. G., Plane-recessed disk electrodes and their arrays in transient generator–collector mode: The measurement of the rate of the chemical reaction of electrochemically generated species. *Journal of Electroanalytical Chemistry* **2010,** *648* (1), 28-35.

17.    Postlethwaite, T. A.; Hutchison, J. E.; Murray, R.; Fosset, B.; Amatore, C., Interdigitated Array Electrode as an Alternative to the Rotated Ring– Disk Electrode for Determination of the Reaction Products of Dioxygen Reduction. *Analytical Chemistry* **1996,** *68* (17), 2951-2958.

18.    Menshykau, D.; O'Mahony, A. M.; del Campo, F. J.; Munõz, F. X.; Compton, R. G., Microarrays of ring-recessed disk electrodes in transient generator-collector mode: theory and experiment. *Analytical chemistry* **2009,** *81* (22), 9372-9382.

19.    Aoki, K.; Morita, M.; Niwa, O.; Tabei, H., Quantitative analysis of reversible diffusion-controlled currents of redox soluble species at interdigitated array electrodes under steady-state conditions. *Journal of electroanalytical chemistry and interfacial electrochemistry* **1988,** *256* (2), 269-282.

20.    Hayashi, K.; Takahashi, J.-i.; Horiuchi, T.; Iwasaki, Y.; Haga, T., Development of nanoscale interdigitated array electrode as electrochemical sensor platform for highly sensitive detection of biomolecules. *Journal of The Electrochemical Society* **2008,** *155* (9), J240-J243.

21.    Morita, M.; Hayashi, K.; Horiuchi, T.; Shibano, S.; Yamamoto, K.; Aoki, K. J., Enhancement of redox cycling currents at interdigitated electrodes with elevated fingers. *Journal of The Electrochemical Society* **2014,** *161* (4), H178-H182.

22.    Zoski, C. G., *Handbook of Electrochemistry*. Elsevier Science: 2007.

23.    Han, D.; Zaino III, L. P.; Fu, K.; Bohn, P. W., Redox cycling in nanopore-confined recessed dual-ring electrode arrays. *The Journal of Physical Chemistry C* **2016,** *120* (37), 20634-20641.

24.    Zafarani, H. R.; Mathwig, K.; Sudhölter, E. J.; Rassaei, L., Electrochemical redox cycling in a new nanogap sensor: design and simulation. *Journal of Electroanalytical Chemistry* **2016,** *760*, 42-47.

25.    Iler, R. K.; K, I. R., *The Chemistry of Silica: Solubility, Polymerization, Colloid and Surface Properties and Biochemistry of Silica*. Wiley: 1979.

26.    Stein, D.; Kruithof, M.; Dekker, C., Surface-charge-governed ion transport in nanofluidic channels. *Physical Review Letters* **2004,** 93 (3), 035901.

*"The most beautiful thing we can experience is the mysterious."*

*Albert Einstein*

4

# Electrochemical DNA sensing on nano-interdigitated electrodes using metallic nanoparticle amplification

**Abstract:** A nanoparticle (NP) immobilized between two closely spaced electrodes having a concentration gradient can function as bipolar electrode which can cause a current amplification. Moreover, in chapter 3 we observed an amplification in limiting current in the absence of salt solution. Here, we report a DNA sensor utilizing ion enrichment in the absence of supporting electrolyte and the bipolar behavior of the NP immobilized between the nano-interdigitated electrodes (nIDEs) in a concentration gradient solution. Our DNA sensor is based on a sandwich assay consisting of the capture probe DNA, the reporter probe DNA with NPs, and the target DNA, which is complementary to both the other probes. For a specific binding, the NP DNA sandwich complex is bound on the nIDE. Due to ion enrichment in the absence of supporting electrolyte and the bipolar behavior of NP trapped between the cathode and anode, we observed a ~4 fold current amplification. As a result of this, our DNA sensor could detect ~10 picomolar concentration of DNA targets with excellent selectivity.

## 4.1 Introduction

Sequence-specific detection of DNA and RNA has facilitated in the advancements of medical diagnostics for pathogen analysis, genetic disorder diagnostics and detection of non-infectious diseases.[1-3] However, portable, rapid and inexpensive DNA sequencing techniques are required for the screening of diseases (such as cancer among high-risk populations), DNA profiling in forensics, detection of pathogens in predicting the food safety hazards, in limiting epidemic outbreaks and for biodefense. Due to the limitation of the existing detection techniques, DNA samples are mostly amplified using polymerase chain reaction (PCR) technique.[4] However, being expensive, time-consuming, resource-demanding and less portable, PCR is less interesting for point-of-care (POC) applications. Although studies have been done to develop on-chip PCR devices, the required protocol with multiple thermal cycles makes it challenging to perform PCR on chip.[5-6] Fluorescence labeling together with optical detection methods are generally used together with PCR for DNA detection. Integration difficulties makes optical tools less attractive. Moreover, photobleaching of fluorescence labels is a major limitation for the accurate quantification of DNA. As a label-free technique, surface plasmon resonance attracted much interest in the biosensing field. However, it is prone to non-specific interactions, and it also requires complex optics, resulting in expensive devices. Quartz crystal microbalance and micro/nano cantilevers, other label-free techniques, which are based on mass readout, are also susceptible to non-specific interactions and thermal drifts.[7-10]

Nevertheless, one of the compelling label-free detection alternatives is the electrochemical nucleic acid sensing. These sensors are popular for their low cost and ability to operate faster with limited instrumentation, making it easily integrable into a portable POC device. Also, electroactive molecules deteriorate less compared to other molecules, for example fluorescent dyes, which photobleach as mentioned earlier. Moreover, electrochemical methods are in general well suited for the integration of the device since it provides an electrical signal without another transduction equipment. The commercial success of electrochemical biosensors, like glucose sensors, corroborates the potential of electrochemistry in the field of POC biosensing. Nonetheless, most of the existing electrochemical nucleotide sensing strategies use (i) intercalation of the redox

label on to the double stranded DNA[11-12], (ii) reporter DNA strand with a redox-active label[13-14], or (iii) use redox cations[15-18] which bind to the negatively charged backbone of the DNA. For the labeling methods, to obtain a high signal to background current, the concentration of the labeled DNA should be high, thus lowering the sensitivity of the detection method and for redox cation method, measurement technique is often based on coulometric measurements. Compared to coulometric detection techniques, an amperometric method allows direct readout without any complex data analysis algorithms or any another transduction strategies, making it more suitable for POC applications. Hence, amperometric electrical DNA sensors are highly sought for. Here we report an electrochemical, *amperometric* DNA sensor with a sandwich assay of gold nanoparticles (NPs).

### 4.1.1 Nanoparticle sandwich assay

NPs have been used for various biological applications including separation and purification, labeling and sensing of biomolecules, diagnostic imaging and targeted drug delivery or hyperthermia for therapeutics.[19-20] NP based nucleic acid sensors were demonstrated previously using electrical,[21-22] electrochemical[15, 23-24] and optical[25-27] detection methods. Here, we use a NP *sandwich* assay strategy as illustrated in *Figure 4.1*. It consists of the capture probe DNA (SH-DNA), the target DNA (T-DNA) and the reporter probe DNA (R-DNA). The T-DNA has half of its nucleotides complementary to the SH-DNA and another half to the R-DNA. Both the SH-DNA and the R-DNA are modified with thiol groups at 5' and 3' respectively. The thiol on the R-DNA is used to anchor these nucleotides onto the Au NP forming R-DNA/NP biconjugate, while the thiol on the SH-DNA is used to anchor them on the Pt nIDEs. At first, the SH-DNA was self-assembled on the nIDEs. Then nIDEs were backfilled with 6-mercapto-1-hexanol (MCH) to displace any non-specifically adsorbed DNA and to help hybridization of oligos in following steps. After the functionalization with MCH, nIDEs were incubated with the T-DNA to capture them by hybridization on SH-DNA. Later, the electrodes were incubated with R-DNA/NP complex and were immobilized by hybridization with T-DNA, thus completing the *sandwich* assay.
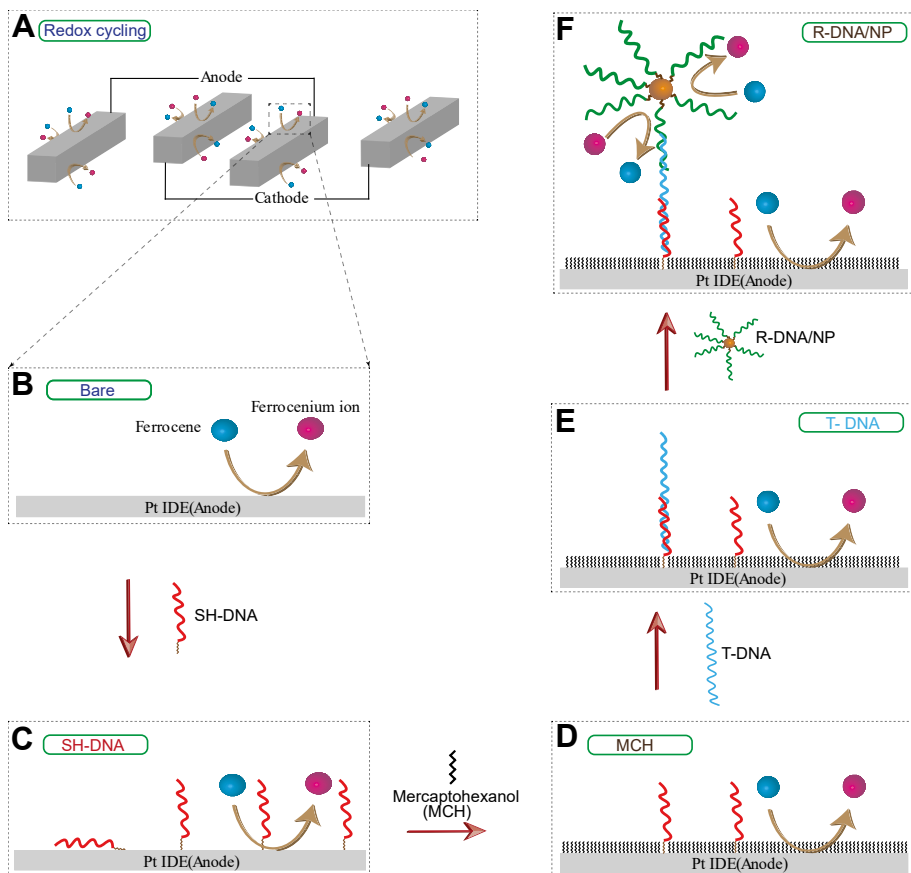
**Figure 4.1:** Schematic diagram depicting the DNA sensor using NP sandwich assay on the nIDEs. A neutral redox mediator, 1, 1' –ferrocene dimethanol (Fc(MeOH)$_2$), is used for amperometric measurements. **(a)** Redox cycling of Fc(MeOH)$_2$ on bare IDE surface where redox active molecules shuttle between the anode and cathode (two sets of adjacent interdigitated electrodes are shown; our device has 50 pairs of electrodes) **(b)** Zoom-in on the bare anode IDE surface where ferrocene is oxidized to ferrocenium ion **(c)** Bare nIDE is functionalized with thiolated capture DNA (SH-DNA) **(d)** IDE surface is backfilled with 6-mercapto-1-hexanol (MCH) for the better hybridization of the nucleotides **(e)** Target DNA (T-DNA) strands complementary to SH-DNA are immobilized on the backfilled nIDE surface **(f)** Reporter DNA functionalized on Au NP (R-DNA/NP) which is

complementary to the T-DNA is captured on the nIDE. Oxidation and/or reduction reactions of are also illustrated in each step with curvy arrows.

### 4.1.2 Ion enrichment with DNA on nIDEs

In **Chapter 3**, we discussed redox cycling on nIDEs in the absence and presence of a supporting electrolyte. We observed a 100% current enhancement in the absence of the supporting electrolyte for ferrocenium dimethanol ($Fc(MeOH)_2$). This was due to electrostatically driven ion enrichment due to surface charge and ion migration on nIDEs. Bashir and coworkers reported amplification of ionic current due to electrical gating of surface current in a nanochannel due to the charge on the DNA molecules.[28] The DNA backbone is negatively charged and as a result when suspended in an ionic solution, DNA molecules attract positive counter ions around them. Thus, when DNA molecules were passed through the nanochannel, they induced extra cations into the channel along with them resulting in an increase in ionic current.

We can expect a similar behavior on nIDE devices with DNA. When DNA molecules are immobilized on nIDE electrode surface, negatively charged DNA backbone will attract positive counter ions onto the surface to keep the electroneutrality. In the absence of a supporting electrolyte, the main cationic species in solution originates from the redox mediator salt *e.g.* ferrocenium ions in the case of $Fc(MeOH)_2$. For cationic redox species, this results in ion enrichment, *i.e.*, an increase in concentration of the redox ions near the surface compared to the bulk solution. This ion enrichment can result in limiting current amplification of nIDEs.

### 4.1.3 Nanoparticle bipolar electrode

Although bipolar electrochemistry has been known for almost half a century now, it has not been in the limelight until early years of the last decade.[29-31] As a result, bipolar electrodes (BPEs) were also investigated for its potential for sensing purposes.[32-34] Zhu et al.[35] used BPEs for selective detection of dopamine in the presence of ascorbic acid and Chow et al.[33] reported DNA sensor based on BPE microarray. Hence here we tried to explore further the possibilities of BPE in biosensing.

Under high external electric field, electrically isolated conductor (*floating electrode with no external connection*) submerged in a solution, functions as a BPE which acts as both cathode and anode that are spatially separated regions on its surface.[36] With the bipolar behavior induced by the potential gradient across the solution, redox active species can undergo electrochemical oxidation on the anode side and reduction on the cathode side of the BPE. While this bipolar behavior can be detrimental if overlooked during electrochemical system design and validation, it can also be utilized for specific applications.[37-38] In the sensing methods reported earlier[32-34], since BPEs are not electrically connected, optical readout mechanisms were employed for signal acquisition. Electrical readout systems are highly sought for integrated sensing applications. In order to have an electrical readout method, there should be an electrical or electrochemical coupling of the signal on the BPE with the working electrode of which the current is measured. This is hard to realize on a BPE that depends on the potential gradient across the solution. Nevertheless, a floating electrode can also undergo bipolar behavior when it is subjected to a gradient of diffusional concentration of redox species surrounding it. Amatore group has previously shown the concentration gradient based bipolar behavior of floating electrode on a plane-recessed microelectrode array where the presence BPE is enhances the device performance.[35, 39] In order to drive a *floating* particle to function as an electrochemical BPE, a significant concentration gradient of redox species is required around it. This demands the working and counter electrodes to be closely spaced and the *floating* BPE is immobilized between them. Owing to the small gap between these electrodes, the solution yields a steep diffusion gradient of the redox molecules over the gap between the electrodes. This steep diffusion gradient can be exploited to drive the particle to function as a BPE. Hence if the particles are in nanometer scale, the devices like nanoscale interdigitated electrodes (nIDE)[40-41] or nanogap electrodes[42-43] are required to drive it as a BPE. Nonetheless, unlike nanogap electrodes, nIDEs with open structure does not need complex fluidics to pump the solution through the nanochannel which also helps in better chemical functionalization of the electrode surface.

Furthermore, here we use a metallic NP based sandwich assay for DNA detection. These *floating* metallic nanoparticles trapped between the nIDEs can also work as

BPE. Nonetheless, an analytical study is required to comprehend the bipolar influence of NP on redox cycling in nIDEs. Consequently, we start with focusing on diffusive mass transport. In the steady state, the concentrations of reduced and oxidized species ($c_R$ and $c_O$, respectively) obey the diffusion equation,

$$D\nabla^2 c_{R,O}(\boldsymbol{r}) = D\left(\frac{1}{r^2}\frac{\partial}{\partial r}\left(r^2 \frac{\partial c_{R,O}(r,\theta)}{\partial r}\right)\right. \tag{4.1}$$

$$\left. + \frac{1}{r^2 \sin\theta}\frac{\partial}{\partial \theta}\left(\sin\theta \frac{\partial c_{R,O}(r,\theta)}{\partial \theta}\right)\right) = 0,$$

where the second expression is in spherical coordinates and assumes azimuthal symmetry. Here $D$ is the diffusion coefficient, which we assume for simplicity to be identical for the reduced and oxidized forms; under these conditions, $c_R(\boldsymbol{r}) + c_O(\boldsymbol{r}) = c_b$, where $c_b$ is the bulk concentration of redox species. We use the geometry of **Figure 4.2 (a)**, in which the NP is represented by a sphere of radius $R$ centered at the origin. Two infinite planar electrodes separated by a distance $\Delta z$ and labeled 1 and 2 are located at $z = -z_0$ and $z = \Delta z - z_0$, respectively. We treat the reaction as fully reversible, such that the ratio $c_O/c_R$ is constant over the surface of the NP and is set by the Nernst equation,

$$\frac{c_O(R,\theta)}{c_R(R,\theta)} = \frac{c_O(R,\theta)}{c_b - c_R(R,\theta)} = e^{(E-E^{0'})/kT}. \tag{4.2}$$

Here, $E$ is the potential of the floating NP, $E^{0'}$ is the formal potential of the redox reaction, $k$ is Boltzmann's constant and $T$ is the absolute temperature. In the steady-state, the value of $E$ is set by the condition that no net reduction or oxidation of the NP takes place (that is, $E$ adjusts such that the total rate of charge transfer integrated over the surface of the NP vanishes). The concentrations at the electrodes are also fixed with values $c_{O,R}^1$ and $c_{O,R}^2$.
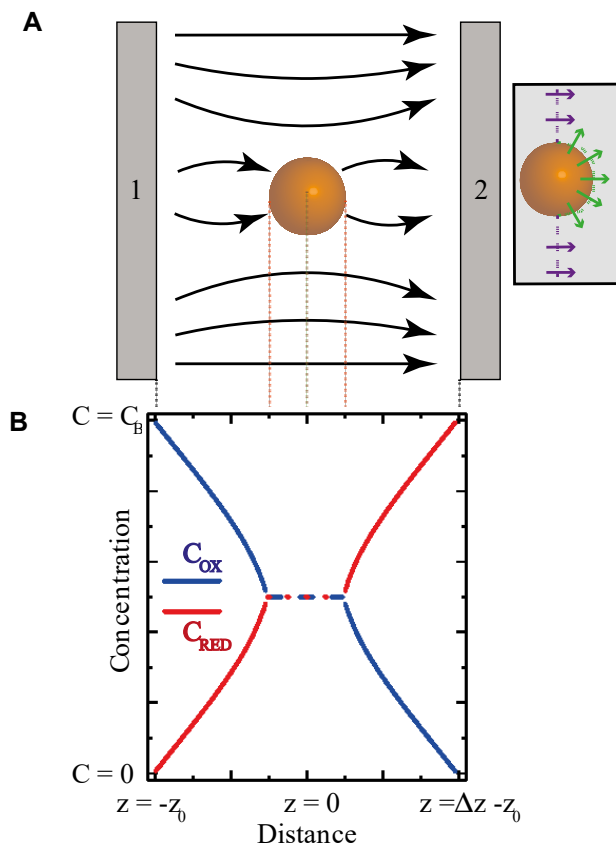
**Figure 4.2: (a)** Sketch of the geometry employed for calculations. A single spherical NP is located between two infinite planar electrodes at which redox cycling takes place. The NP acts as a bipolar electrode, driving reduction and oxidation reactions in opposite hemispheres due to the concentration gradient imposed by the electrodes. This in turn concentrates the fluxes of redux species in the vicinity of the particle, as represented schematically by the flux lines for the oxidized species. **(b)** Concentration profiles along the zenith direction ($z-$axis), as given by **Equation (4. 4)**. The green line represents the linear concentration profile in the absence of the NP, showing how the NP causes the concentration gradients to become steeper. **Inset:** The current through the NP can be evaluated by integrating the concentration gradient of the redox species over one hemisphere (green arrows). The resulting drop in flux in the region near the equator of

the NP can be evaluated by integrating over the region shown by purple arrows.

In the absence of a NP, the concentrations simply exhibit linear gradients,

$$c_{R,O}(\boldsymbol{r}) = c_{R,O}^1 + \frac{c_{R,O}^2 - c_{R,O}^1}{\Delta z}(z + z_0) \tag{4.3}$$

When a NP is present, we first consider the case where it is located far from the electrodes ($z_0 \gg R$, $\Delta z - z_0 \gg R$). The calculation then becomes analogous to the classic electrostatics problem of a metallic sphere in a uniform electric field with solution[44]

$$c_{R,O}(\boldsymbol{r}) = c_{R,O}^1 + \frac{c_{R,O}^2 - c_{R,O}^1}{\Delta z}(z + z_0) - \frac{c_{R,O}^2 - c_{R,O}^1}{\Delta z}\frac{R^3}{r^2}\cos\theta. \quad (3) \tag{4.4}$$

The first two terms in this expression again correspond to a linear concentration gradient between the electrodes while the last term represents the perturbation caused by the NP. This concentration distribution is plotted in **Figure 4.2 (b)** showing that the presence of the particle causes the concentration gradient to become steeper in the vicinity of the poles of the NP ($\theta = 0$ and $\theta = \pi$). The fluxes of redox species are given by

$$\boldsymbol{j}_{R,O} = -D\nabla c_{R,O}(\boldsymbol{r}), \tag{4.5}$$

which reduces to simple expressions for the radial fluxes at the particle surface:

$$j_{r,O}(\theta) = -D\left.\frac{\partial c_O}{\partial r}\right|_{r=R} = -3D\frac{c_O^2 - c_O^1}{\Delta z}\cos\theta \tag{4.6}$$

$$j_{r,R}(\theta) = -D\left.\frac{\partial c_R}{\partial r}\right|_{r=R} = -j_{r,O}(\theta). \tag{4.7}$$

This result indicates that net oxidation takes place in one hemisphere and net reduction takes place in the opposite hemisphere of the NP. As illustrated

schematically in **Figure 4.2 (a)**, the NP focuses the flux lines in its vicinity and acts a bipolar electrode, the opposite reactions at the two hemispheres exactly compensate each other such that the NP remains at a fixed potential. The total current passing through the NP is

$$I_{\mathrm{NP}} = ne \iint \boldsymbol{j_{r,0}} \cdot \boldsymbol{dA} = -3\pi neDR^2 \frac{c_O^2 - c_O^1}{\Delta z}, \qquad (4.8)$$

where $n$ is the number of electrons transferred per molecule and $-e$ is the charge of the electron. The integral is taken over one hemisphere of the particle (green arrows in the inset of **Figure 4.2**). There is no change in the total current flowing between the redox cycling electrodes, however, as the current through the NP is exactly compensated by a decrease in the current flowing around the NP (purple arrows in the inset of **Figure 4.2**). This behavior can be traced to the assumption that the electrodes are far from the NP ($z_0 \gg R$, $\Delta z - z_0 \gg R$). When this condition is not satisfied, the perturbation around the particle can interact more directly with the electrodes, leading to a net change in the total current. Although there is perturbation, the effect on redox cycling current is not evident. Hence, we performed a detailed finite element analysis to study the effect further and this result is explained in next section.

## 4.2 Results and discussion

### 4.2.1 Finite element analysis

The analytical solution to **Equation** (4.1) in the case where the NP is near an electrode takes the form of an infinite series of Legendre polynomials and is not readily tractable analytically. We therefore used finite element calculations (COMSOL Multiphysics® 5.3) to obtain the concentration profiles and fluxes in this case. The calculation were performed in cylindrical coordinates in two dimensions using the geometry of **Figure 4.2**, with the exception that the electrodes had a finite radius. The same boundary conditions as described above were used, where the correct value of $E$ was determined for each case by iteration of the complete calculation. For each case, the magnitude of the perturbation in the redox cycling current introduced by the NP, $\Delta I$, was determined by integrating

the total flux at one of the two electrodes and subtracting the corresponding current in the absence of a NP. The radius of the circular electrodes was selected as $20R$; this was large enough that further increasing this value did not affect $\Delta I$ significantly.
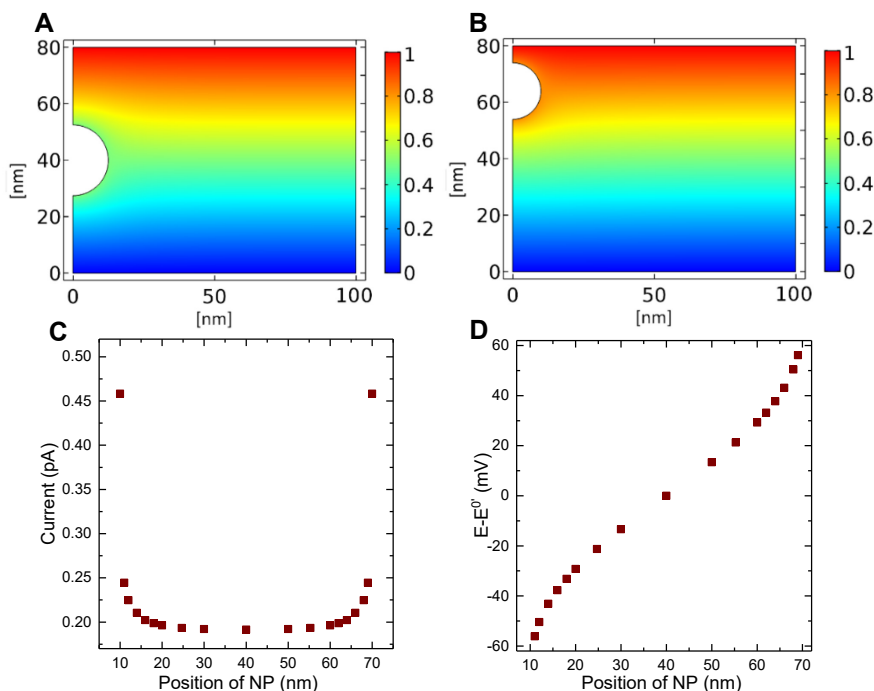


**Figure 4.3:** Numerical simulations. Concentration distribution showing the perturbation of the concentration gradient by a NP in a nanogap **(a)** when NP is centered in middle of the nanogap and **b)** when NP (center) is 24.7 nm away from the cathode. The false color scales show concentration profile in mol/m³. **(c)** Increase in current upon the introduction of the NP versus position in the nanogap. **(d)** Overpotential of the floating NP versus position in the nanogap.

*Figure 4.3 (b)* shows the calculated concentration profile for typical experimental parameters (electrode spacing, $\Delta z = 80$ nm; NP radius, $R = 10$ nm; particle position, $z_0 = 24{,}7$ nm, corresponding to a fully extended 44 bp ds-DNA tether;

diffusion coefficient $D = 10^{-9}$ m²/s; number of electron transferred $n = 1$; concentrations $c_b = 1$ mM, $c_O^1 = c_R^2 = 1$ mM and $c_O^2 = c_R^1 = 0$ mM). Once again the NP acts as a bipolar electrode that enhances the concentration gradient in its vicinity. The main difference is that the concentration gradient is further accentuated as a result of the vicinity of an electrode to the NP. This is more readily seen by integration of the flux, which yields an enhancement in the current of $\Delta I = +0.19$ pA upon introducing the NP. The value of $\Delta I$ depends on $z_0$: as shown in **Figure 4.3 (c)**, it is maximal when the NP is close to contact with an electrode and exhibits a minimum at the center of the nanogap. The corresponding NP overpotential is plotted in **Figure 4.3 (d)**. It exhibits a nonlinear dependence of $E - E^{0'}$ on position, again highlighting the enhanced perturbation of the linear gradient when the NP is close to an electrode.

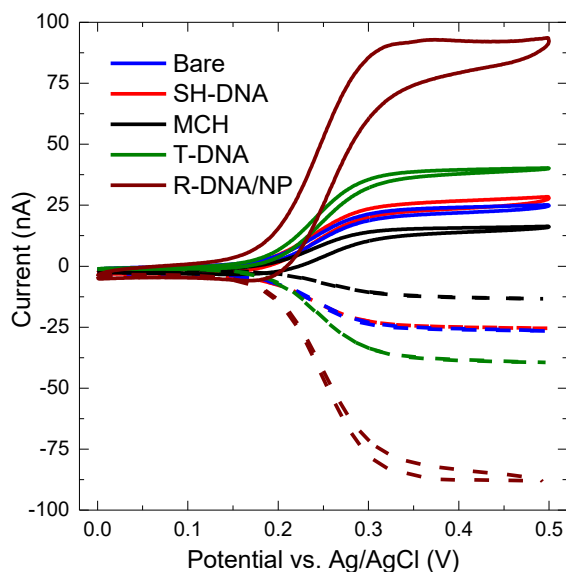### 4.2.2 DNA sensing using NP sandwich assay



**Figure 4.4**: Cyclic voltammograms 80 nm nIDEs with bare electrodes (blue), modified with SH-DNA (black), back-filled with MCH (red), hybridized with T-DNA (green) and amplified R-DNA/NP (brown) with 1 mM Fc(MeOH)₂ at scan rate of 50 mV/s. Solid lines show the anode current and the dashed lines show the redox cycling current on cathode.

For DNA sensing, the nIDE (80 nm gap) were surface functionalized as described in *section 4.4.4*. The cyclic voltammetry measurements were carried out with 1 mM (Fc(MeOH)$_2$) without a supporting electrolyte at a scan rate of 50 mV/s keeping the cathode (collector) potential at -0.1 V. *Figure 4.4* shows the cyclic voltammograms of nIDE at different stages of surface functionalization with solid curves representing the anode current and dashed lines indicating the cathode current. The cyclic voltammogram of oxygen plasma cleaned bare nIDE was recorded first (blue curve). After the measurement, the nIDE was cleaned again with oxygen plasma and incubated in SH-DNA. It was again electrochemically analyzed after the SH-DNA functionalization (red curve). Both the anode and the cathode currents were similar to the previous bare electrode measurement. Generally, single-stranded DNA molecules prefer to stick to the surface of the noble metals due to the electrostatic attraction preventing the hybridization of DNA molecules in subsequent steps. Hence, the nIDE was incubated with MCH for backfilling the electrode surface. This backfilling helps the SH-DNA molecules to orient upwards on the electrode surface, thus helping them in the hybridization process with T-DNA. A cyclic voltammetry measurement after the backfilling showed that the limiting current was reduced (black curve). Qualitatively, an additional layer on the electrode will hinder the charge transfer from the redox ion to the electrode, resulting in a reduction of the current. With surface functionalization on electrode, Pan *et al.* also observed a similar decrease in current as result of increase in charge transfer resistance.[45]

Subsequently, the nIDE was incubated with the complementary T-DNA in order to hybridize it with the SH-DNA. The voltammogram after this stage, showed a significant increase in the limiting current even higher than the bare electrode current.   The possible reason would be the electrostatically driven ion enrichment[46] in the absence of supporting electrolyte as mentioned in **Section 4.1.2**. Qualitatively, the hybridization of DNA increases the net charge (negative) within the sensing area. This increased charge attracts counter ions from the solution to the device surface. In the absence of supporting electrolyte, ferrocenium ions (the main cationic species) in solution are attracted to neutralize the change in charge resulting in an increase in concentration of these ions near the surface compared to the bulk solution. This local increase in concentration

provides an increase in current. However, compared to the current change after SH-DNA binding, the increase in current was more prominent after T-DNA binding. One likely explanation is that the more stiffer hybridized T-DNA, stay more orthogonal to and away from the electrode surface facilitating enhanced charge transfer of the redox species to the electrode.[45]

As the last functionalization step, the nIDE was incubated with R-DNA/NP and consequently R-DNA was hybridized with T-DNA and as a result the NP complex was also immobilized between the electrodes. Cyclic voltammogram after this incubation showed around four fold (3.72) increase in the limiting current compared to the bare electrode. This high amplification can be attributed to two factors. As discussed earlier, NPs immobilized between the electrodes function as BPEs yielding an enhancement in the current. The large hysteresis of the voltammogram after this step, compared to any other functionalization stages, indicates the charging and discharging through the NP as expected with the NP BPE. Meanwhile, a single 20 nm particle in a 80 nm gap can only enhance the current by 190 fA. Consequently, a very high surface coverage of NP is required to produce four fold amplification as we observed. Hence, on top of this effect, another factor that allowed the current amplification might be ion enrichment. The NP has more R-DNA bound to its surface than the one that is hybridized with the T-DNA. This further increases the net charge on the electrode and attracts counter ions (ferrocenium ions) from the solution thus increasing the local concentration of the species resulting in high current.
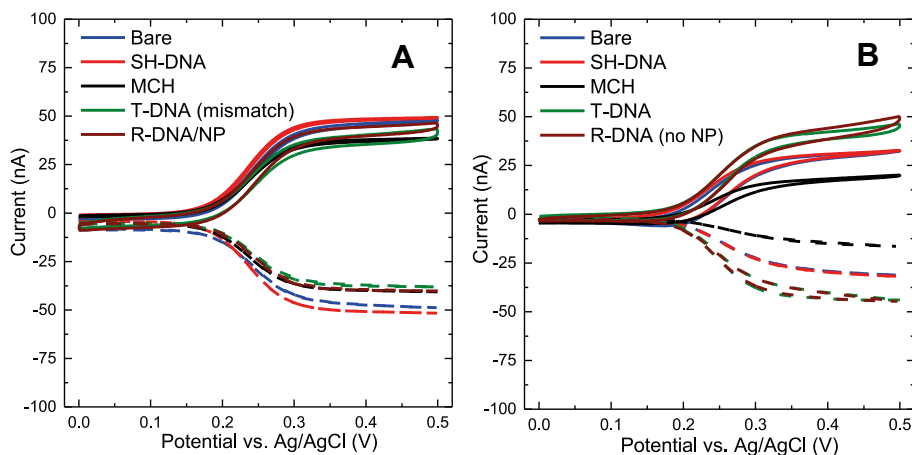
**Figure 4.5**: Cyclic voltammograms nIDEs with control samples: **(a)** non-complementary T-DNA sequence and **(b)** R-DNA with no NP. Curves show bare electrodes (blue), modified with thiolated-DNA molecules (black) and back-filled with MCH (red). For (a), IDEs were hybridized with target-DNA (green) which was non-complementary while for (b), target-DNA (green) was fully complementary. Similarly in (a), R-DNA was with the NPs (brown) but in (b) R-DNA was with NP (brown). Measurements were done with 1 mM $Fc(MeOH)_2$ at a scan rate of 50 mV/s on 80 nm nIDE. Currents shown are $I_{anode}$ (sold lines) and $I_{cathode}$ (dashed lines).

In order to study the selectivity of the sandwich assay and the amplification due to the NP, we prepared two different control samples: (a) non-complementary T-DNA sequence and (b) R-DNA with no NP. For both the samples, the first two steps of functionalization was similar to the non-control sample: firstly, IDE surface were decorated with SH-DNA and then backfilled with MCH. Later, for (a), the IDE was incubated in solution with non-complementary T-DNA while for (b) IDE was incubated with fully complementary T-DNA as in the non-control sample. However, in the subsequent step for (b) IDE was incubated with R-DNA without the NPs and for (a), IDE was incubated with R-DNA with NPs as in the case of non-control sample. In the control sample (a), we expect that the non-complementary T-DNA cannot hybridize with the SH-DNA, thus even when incubated with R-DNA/NP, the NPs cannot be immobilized and hence resulting in no amplification. On the contrary, for control sample (b), fully complementary T-DNA could

hybridize with SH-DNA and R-DNA. Nonetheless, since the R-DNA does not have NP on it, (b) also results in no amplification. *Figure 4.5* shows the cyclic voltammograms of sample (a) and (b). In both cases it can be easily noticed that the amplification (brown) is not present after the R-DNA incubation. Similar to the non-control sample, for both control samples, the limiting current after the SH-DNA anchoring (red) was more or less same as that of the bare electrodes (blue) and also the current reduced after the backfilling of MCH (black). As with control sample (a) where the T-DNA was non-complementary, there was no significant increase in limiting current (green) as compared to that of (b) where the T-DNA was complementary. This was expected as explained previously where hybridized T-DNA attracts the ferrocenium ions to it.
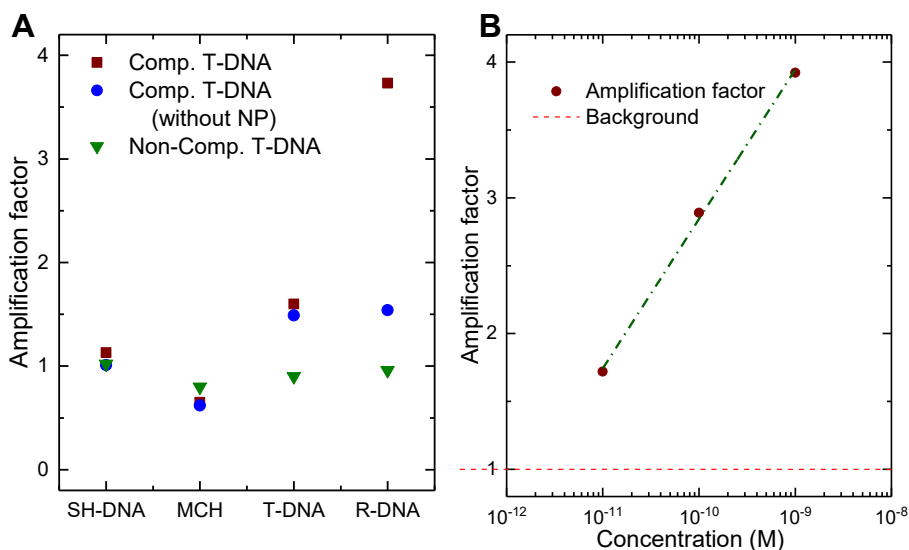


Figure 4.6: (a) Amplification responses at the nIDEs with respect to step by step functionalization of the electrode surface. Three situations are compared: 1) with complementary T-DNA, 2) non-complementary DNA and 3) complementary T-DNA and R-DNA without NP. (b) Amplification responses at the nIDEs with NP sandwich assay with varying T-DNA concentrations. The NP amplification shows a logarithmic dependence on the T-DNA concentration within the range of concentrations that were analyzed (from 10 pM to 1 nM).

The change in the limiting current after each functionalization step is studied as shown in *Figure 4.6* **(a)**. The three experimental conditions (non-control and control) were carefully reflected: 1) with complementary T-DNA, 2) non-complementary DNA and 3) complementary T-DNA but with R-DNA without NP. The amplification factor is calculated as the ratio of the limiting current after each surface functionalization step to the limiting current of the bare electrode. The change in the limiting current after the SH-DNA functionalization step is negligible while after the MCH backfilling the limiting current is reduced. In both cases the amplification factor for all the three conditions under consideration were similar. However, after T-DNA functionalization, the condition were complementary T-DNA (condition: 1 and 3) were used relatively higher amplification compared to the non-complementary T-DNA as expected. Finally, after the R-DNA modification, for condition 1), the amplification factor was 3.74 while for other two cases the amplification did not change from the previous step. This confirms the effect of NP amplification. More IDEs were functionalized and analyzed with varying concentration of complementary T-DNA in order to investigate the dependence of amplification factor to the concentration variations. Three different concentrations were examined for this study. The same trend of amplification (as for the first sample) was also observed in all the different stages of functionalization. The observations of the measurements are summarized and plotted in *Figure 4.6* **(b)**. The amplification factor of the R-DNA/NP step showed a logarithmic dependence on the concentration of T-DNA within the range of concentrations (from 10 pM to 1 nM) that were analyzed. This suggests that these concentrations may be spanning within and beyond the dynamic range of the detection method.

## 4.3 Conclusions

Herein we reported a label-free electrochemical DNA sensing on nanoscale interdigitated electrodes using gold nanoparticle amplification by bipolar behavior and ion enrichment. We have established the high selectivity of our device compared to two control samples and samples with different concentrations. This amperometric sensing method can be easily integrated with a readout circuitry for developing a portable POC testing device. Operation

simplicity, stability and reproducibility makes it furthermore appealing. By using array of IDEs and by multiplexing, the device can be used for detection of different DNA sequence. This method can also be used for prognosis and personalized medication and validating its efficacy and the recurrence of the disease. Although device optimization has to be done in order to create an extremely sensitive sensor with a large dynamic range of detection, clearly, our method is a promising alternative to most of the state-of-the-art POC nucleotide sensors. Nonetheless, for ultra-low concentration DNA measurements, an alternative method by which one can count single binding events will be more appropriate. Such a measurement method is proposed in **chapter 6**.

## 4.4 Materials and Methods

### 4.4.1 Chemicals and reagents

1, 1' –ferrocene dimethanol, $Fc(MeOH)_2$, as redoxactive mediator, 6-mercapto-1-hexanol, gold nanoparticles (~20 nm) and PBS tablets were purchased from Sigma-Aldrich B.V, the Netherlands. All solutions were prepared using Milli-Q water and experiments were carried out at room temperature. The DNA sequences were ordered form Eurofins Genomics GmbH, Germany and stored at -20°C. Lyophilized thiol modified oligos (capture probe and reporter probe) were suspended in 200 µl of 10mM TCEP and shook for 1 hour at room temperature to cleave any disulfide bonds.  Later, the oligos were precipitated by incubating 20 min at -20°C in 150 µl of 3 M Sodium-Acetate and ethanol. Subsequently, the pellet was centrifuged for 5 min at 13000 rpm and the supernatant was discarded and then dried at room temperature. It was then suspended in  milli-Q water, and aliquots of 100 µM were prepared and stored at  4°C.

### 4.4.2 Preparation of R-DNA/NP bioconjugates

Reporter DNA (R-DNA) modified gold NP (R-DNA/NP) complexes were prepared according to previously reported method with slight modification.[7]   From previously prepared aliquot, 35 µl of 100 µM R-DNA was mixed with 1 ml Au NPs solution and incubated at 4 °C for 12 hours. After incubation, 20 µL of 1% sodium dodecyl sulfate was added to stabilize the Au NPs with shaking at room

temperature for 1 hour. Then the R-DNA/NP complex was aged for 12 hours by slowly adding 100 μL of 0.5 M NaCl solution. To remove excess reagents, the solution was centrifuged at 12,000 rpm for 20 min. The wine red R-DNA/NP precipitate was washed 2 times by centrifugation with 0.01 M PBS solution (pH 7.4), and then resuspended in 0.5 ml PBS for future use.

### 4.4.3 nIDE fabrication

nIDEs were fabricated using a combination of optical and electron-beam lithography (EBL) and metal evaporation and lift-off process. 300 nm $SiO_2$ was thermally grown on a 10 cm Si 100 wafer at $1000^\circ$ C. First optical lithography step was carried out followed by Pt metal evaporation and lift-off for making markers for EBL. Subsequently, nIDEs were patterned using EBL with Ti/Pt evaporation (5/80 nm) and lift-off. Later, the nIDEs were connected to contact pads via contact leads using second optical lithography followed by another metal evaporation (120 nm) and lift-off. The third optical lithography step was used to pattern and later passivated and insulated the contact leads using evaporated $SiO_2$ (30 nm). The passivation layer covers everything except the contact pads and a rectangular window over the nIDEs. Thus effectively each electrode of the nIDEs is 30 μm long and are 120 nm wide and 80 nm high with 80 nm gap between each other. The passivation layer prevents current leakage through the contact leads and also enables the use of the nIDEs without fluidic systems, by simply placing an analyte droplet on top of the IDEs.

### 4.4.4 Chemical functionalization

The DNA stock solution was diluted to the appropriate probe concentration in PBS. The nIDE surface was cleaned using oxygen plasma treatment for 1 min. The freshly cleaned nIDE was then immersed into 1 μM HS-DNA solution for 2.5 hours for probe immobilization. Following immobilization, the nIDE was rinsed with copious amounts of Milli-Q water, and then immersed in a 2 mM MCH solution in water for 1 hour. Afterwards, the DNA hybridization was done by incubating the nIDE with 1 μM T-DNA solution for 1 hour at room temperature. Subsequently, 500 μL of R-DNA/NP bioconjugates were incubated for 1 hour to hybridize with the T-DNA. After each step, the nIDE was rinsed with Milli-Q water, and dried with nitrogen. All the incubation were done with shaking of the sample.

### 4.4.5 Electrochemical measurements

Electrochemical experiments were carried out using a CH Instruments 842D (USA) bipotentiostat system. A commercial Ag/AgCl (3 M KCl) reference electrode (BASi Inc., USA) were used for measurements. Since the current produced by the nIDEs are in the order of nanoamperes, both the counter electrode and reference electrode leads of the bipotentiostat were connected together to the Ag/AgCl reference electrode. Generator-collector cyclic voltammetry was performed with one set of electrodes of nIDEs at fixed potential and the other set potential scanning. The working electrode 1 of the bipotentiostat was connected to the generator (anode) electrode set while the working electrode 2 was connected to the collector (cathode) electrode set. The cathode was kept at -0.1 V, while the anode was being swept from 0 to 0.5 V against the Ag/AgCl reference electrode at a rate of 50 mV/s, unless mentioned.

## 4.5 References

1. Burtis, C. A.; Ashwood, E. R.; Bruns, D. E., *Tietz Textbook of Clinical Chemistry and Molecular Diagnostics - E-Book*. Elsevier Health Sciences: 2012.

2. Tang, Y.-W.; Procop, G. W.; Persing, D. H., Molecular diagnostics of infectious diseases. *Clinical chemistry* **1997,** *43* (11), 2021-2038.

3. Smith, A. M.; Dave, S.; Nie, S.; True, L.; Gao, X., Multicolor quantum dots for molecular diagnostics of cancer. *Expert review of molecular diagnostics* **2006,** 6 (2), 231-244.

4. Halford, W. P., The essential prerequisites for quantitative RT-PCR. *Nature biotechnology* **1999,** *17* (9), 835.

5. Lagally, E. T.; Emrich, C. A.; Mathies, R. A., Fully integrated PCR-capillary electrophoresis microsystem for DNA analysis. *Lab on a Chip* **2001,** *1* (2), 102-107.

6. El-Ali, J.; Perch-Nielsen, I. R.; Poulsen, C. R.; Bang, D. D.; Telleman, P.; Wolff, A., Simulation and experimental validation of a SU-8 based PCR thermocycler chip with integrated heaters and temperature sensor. *Sensors and Actuators A: Physical* **2004,** *110* (1-3), 3-10.

7.  Zhang, J.; Song, S.; Wang, L.; Pan, D.; Fan, C., A gold nanoparticle-based chronocoulometric DNA sensor for amplified detection of DNA. *Nature protocols* **2007,** *2* (11), 2888.

8.  Drummond, T. G.; Hill, M. G.; Barton, J. K., Electrochemical DNA sensors. *Nature biotechnology* **2003,** *21* (10), 1192.

9.  Helmerhorst, E.; Chandler, D. J.; Nussio, M.; Mamotte, C. D., Real-time and label-free bio-sensing of molecular interactions by surface plasmon resonance: a laboratory medicine perspective. *The Clinical Biochemist Reviews* **2012,** *33* (4), 161.

10. Wang, J.; Jiang, M.; Palecek, E., Real-time monitoring of enzymatic cleavage of nucleic acids using a quartz crystal microbalance. *Bioelectrochemistry and bioenergetics* **1999,** *48* (2), 477-480.

11. Kelley, S. O.; Boon, E. M.; Barton, J. K.; Jackson, N. M.; Hill, M. G., Single-base mismatch detection based on charge transduction through DNA. *Nucleic Acids Research* **1999,** *27* (24), 4830-4837.

12. Boon, E. M.; Ceres, D. M.; Drummond, T. G.; Hill, M. G.; Barton, J. K., Mutation detection by electrocatalysis at DNA-modified electrodes. *Nature biotechnology* **2000,** *18* (10), 1096.

13. Umek, R. M.; Lin, S. W.; Vielmetter, J.; Terbrueggen, R. H.; Irvine, B.; Yu, C.; Kayyem, J. F.; Yowanto, H.; Blackburn, G. F.; Farkas, D. H., Electronic detection of nucleic acids: a versatile platform for molecular diagnostics. *The Journal of Molecular Diagnostics* **2001,** *3* (2), 74-84.

14. Fojta, M.; Havran, L.; Billova, S.; Kostecka, P.; Masarik, M.; Kizek, R., Two-surface strategy in electrochemical DNA hybridization assays: detection of osmium-labeled target DNA at carbon electrodes. *Electroanalysis: An International Journal Devoted to Fundamental and Practical Aspects of Electroanalysis* **2003,** *15* (5-6), 431-440.

15. Zhang, J.; Song, S.; Zhang, L.; Wang, L.; Wu, H.; Pan, D.; Fan, C., Sequence-specific detection of femtomolar DNA via a chronocoulometric DNA sensor (CDS): Effects of nanoparticle-mediated amplification and nanoscale control of DNA assembly at electrodes. *Journal of the American Chemical Society* **2006,** *128* (26), 8575-8580.

16.    Yu, H.-Z.; Luo, C.-Y.; Sankar, C. G.; Sen, D., Voltammetric procedure for examining DNA-modified surfaces: quantitation, cationic binding activity, and electron-transfer kinetics. *Analytical chemistry* **2003,** *75* (15), 3902-3907.

17.    Steichen, M.; Decrem, Y.; Godfroid, E.; Buess-Herman, C., Electrochemical DNA hybridization detection using peptide nucleic acids and [Ru (NH3) 6] 3+ on gold electrodes. *Biosensors and Bioelectronics* **2007,** *22* (9-10), 2237-2243.

18.    Lao, R.; Song, S.; Wu, H.; Wang, L.; Zhang, Z.; He, L.; Fan, C., Electrochemical interrogation of DNA monolayers on gold surfaces. *Analytical chemistry* **2005,** *77* (19), 6475-6480.

19.    Sperling, R. A.; Gil, P. R.; Zhang, F.; Zanella, M.; Parak, W. J., Biological applications of gold nanoparticles. *Chemical Society Reviews* **2008,** *37* (9), 1896-1908.

20.    Mody, V. V.; Siwale, R.; Singh, A.; Mody, H. R., Introduction to metallic nanoparticles. *Journal of Pharmacy and Bioallied Sciences* **2010,** *2* (4), 282.

21.    Park, S.-J.; Taton, T. A.; Mirkin, C. A., Array-based electrical detection of DNA with nanoparticle probes. *Science* **2002,** *295* (5559), 1503-1506.

22.    Fang, C.; Fan, Y.; Kong, J.; Gao, Z.; Balasubramanian, N., Electrical detection of oligonucleotide using an aggregate of gold nanoparticles as a conductive tag. *Analytical chemistry* **2008,** *80* (24), 9387-9394.

23.    Liu, L.; Xia, N.; Liu, H.; Kang, X.; Liu, X.; Xue, C.; He, X., Highly sensitive and label-free electrochemical detection of microRNAs based on triple signal amplification of multifunctional gold nanoparticles, enzymes and redox-cycling reaction. *Biosensors and Bioelectronics* **2014,** *53*, 399-405.

24.    Wang, W.-J.; Li, J.-J.; Rui, K.; Gai, P.-P.; Zhang, J.-R.; Zhu, J.-J., Sensitive electrochemical detection of telomerase activity using spherical nucleic acids gold nanoparticles triggered mimic-hybridization chain reaction enzyme-free dual signal amplification. *Analytical chemistry* **2015,** *87* (5), 3019-3026.

25.    Cao, Y. C.; Jin, R.; Mirkin, C. A., Nanoparticles with Raman spectroscopic fingerprints for DNA and RNA detection. *Science* **2002,** *297* (5586), 1536-1540.

26.    Verdoold, R.; Gill, R.; Ungureanu, F.; Molenaar, R.; Kooyman, R. P., Femtomolar DNA detection by parallel colorimetric darkfield microscopy

of functionalized gold nanoparticles. *Biosensors and bioelectronics* **2011,** *27* (1), 77-81.

27.    Elghanian, R.; Storhoff, J. J.; Mucic, R. C.; Letsinger, R. L.; Mirkin, C. A., Selective colorimetric detection of polynucleotides based on the distance-dependent optical properties of gold nanoparticles. *Science* **1997,** *277* (5329), 1078-1081.

28.    Chang, H.; Kosari, F.; Andreadakis, G.; Alam, M.; Vasmatzis, G.; Bashir, R., DNA-mediated fluctuations in ionic current through silicon oxide nanopore channels. *Nano letters* **2004,** *4* (8), 1551-1556.

29.    Backhurst, J.; Coulson, J.; Goodridge, F.; Plimley, R.; Fleischmann, M., A preliminary investigation of fluidized bed electrodes. *Journal of the Electrochemical Society* **1969,** *116* (11), 1600-1607.

30.    Arora, A.; Eijkel, J. C.; Morf, W. E.; Manz, A., A wireless electrochemiluminescence detector applied to direct and indirect detection for electrophoresis on a microfabricated glass device. *Analytical Chemistry* **2001,** *73* (14), 3282-3288.

31.    Zhan, W.; Alvarez, J.; Crooks, R. M., Electrochemical sensing in microfluidic systems using electrogenerated chemiluminescence as a photonic reporter of redox reactions. *Journal of the American Chemical Society* **2002,** *124* (44), 13265-13270.

32.    Bouffier, L.; Arbault, S.; Kuhn, A.; Sojic, N., Generation of electrochemiluminescence at bipolar electrodes: concepts and applications. *Analytical and bioanalytical chemistry* **2016,** *408* (25), 7003-7011.

33.    Chow, K.-F.; Mavré, F.; Crooks, R. M., Wireless electrochemical DNA microarray sensor. *Journal of the American Chemical Society* **2008,** *130* (24), 7544-7545.

34.    Zhang, X.; Chen, C.; Li, J.; Zhang, L.; Wang, E., New insight into a microfluidic-based bipolar system for an electrochemiluminescence sensing platform. *Analytical chemistry* **2013,** *85* (11), 5335-5339.

35.    Zhu, F.; Yan, J.; Pang, S.; Zhou, Y.; Mao, B.; Oleinick, A.; Svir, I.; Amatore, C., Strategy for increasing the electrode density of microelectrode arrays by utilizing bipolar behavior of a metallic film. *Analytical chemistry* **2014,** *86* (6), 3138-3145.

36. Fosdick, S. E.; Knust, K. N.; Scida, K.; Crooks, R. M., Bipolar electrochemistry. *Angewandte Chemie International Edition* **2013,** *52* (40), 10438-10456.

37. Sarkar, S.; Lai, S.; Lemay, S. G., Unconventional electrochemistry in micro-/nanofluidic systems. *Micromachines* **2016,** *7* (5), 81.

38. Oleinick, A. I.; Battistel, D.; Daniele, S.; Svir, I.; Amatore, C., Simple and clear evidence for positive feedback limitation by bipolar behavior during scanning electrochemical microscopy of unbiased conductors. *Analytical chemistry* **2011,** *83* (12), 4887-4893.

39. Oleinick, A.; Yan, J.; Mao, B.; Svir, I.; Amatore, C., Theory of Microwell Arrays Performing as Generators–Collectors Based on a Single Bipolar Plane Electrode. *ChemElectroChem* **2016,** *3* (3), 487-494.

40. Cohen, A. E.; Kunz, R. R., Large-area interdigitated array microelectrodes for electrochemical sensing. *Sensors and Actuators B: Chemical* **2000,** *62* (1), 23-29.

41. Finot, E.; Bourillot, E.; Meunier-Prest, R.; Lacroute, Y.; Legay, G.; Cherkaoui-Malki, M.; Latruffe, N.; Siri, O.; Braunstein, P.; Dereux, A., Performance of interdigitated nanoelectrodes for electrochemical DNA biosensor. *Ultramicroscopy* **2003,** *97* (1-4), 441-449.

42. Zevenbergen, M. A.; Wolfrum, B. L.; Goluch, E. D.; Singh, P. S.; Lemay, S. G., Fast electron-transfer kinetics probed in nanofluidic channels. *Journal of the American Chemical Society* **2009,** *131* (32), 11471-11477.

43. Hüske, M.; Stockmann, R.; Offenhäusser, A.; Wolfrum, B., Redox cycling in nanoporous electrochemical devices. *Nanoscale* **2014,** *6* (1), 589-598.

44. Griffiths, D. J., *Introduction to Electrodynamics*. Cambridge University Press: 2017.

45. Pan, S.; Rothberg, L., Chemical control of electrode functionalization for detection of DNA hybridization by electrochemical impedance spectroscopy. *Langmuir* **2005,** *21* (3), 1022-1027.

46. Chen, Q.; McKelvey, K.; Edwards, M. A.; White, H. S., Redox cycling in nanogap electrochemical cells. The role of electrostatics in determining the cell response. *The Journal of Physical Chemistry C* **2016,** *120* (31), 17251-17260.

*"Enzymes are things invented by biologists that explain things which otherwise require harder thinking."*

*Jerome Lettvin*

# 5

# Electrochemical detection of tumor-derived extracellular vesicles on nano-interdigitated electrodes

**Abstract**: Tumor derived extracellular vesicles (tdEVs) are receiving much attention as a promising cancer biomarkers. The sample collection using less invasive *liquid* biopsy methods has also fueled interest of tdEVs. Although they are much more abundant in the blood than circulating tumor cells, tdEVs in patients' blood is still very low. Consequently, a highly sensitive tdEV detection method is sought for. Here, we report an electrochemical biosensor consisting of nIDEs for highly sensitive detection of tdEVs, after their selective capture on the electrodes. The tdEVs were immobilized on the electrodes using a cancer-specific antibody and detected with an antibody-conjugated reporter enzyme that converts a non-electrochemically active substrate to an electrochemically active mediator. A two-fold selectivity is realized by use of a sandwich assay using antibodies, while high sensitivity is attained by the redox cycling of enzymatically amplified electroactive species over the electrodes separated by nano-scale distances. Our enzyme based electrochemical sensor can detect physiologically relevant concentrations, as low as 10 tdEVs/µl (well above the background) with a detection range sprawling over 6 orders of magnitude.

## 5.1 Introduction

Liquid biopsies are an emerging tool in metastatic cancer disease management. In this non-invasive approach, a sample of blood is screened for the presence of circulating tumor cells (CTCs).[1] It has been established that the concentration of CTCs is indicative of the patient outcome. Compared to MRI, CTC quantification in liquid biopsies has a better prognostic value[2] and is significantly less demanding. As such, this approach can be repeated at higher frequency (e.g., few times per month vs. few times per year for MRI) and can be used in real-time monitoring of a patient's response to therapy. A challenge to be overcome for liquid biopsies is the low abundance of CTCs. For every CTC (typically <10 per ml of blood), there can be millions of white blood cells and even billions of red blood cells. This "signal to noise ratio" is more favorable for tumor-derived extracellular vesicles (tdEVs). These biological nanoparticles are produced by cancer cells and occur in blood at a frequency of $10^5$-$10^9$ tdEVs/ml.[3] Extracellular vesicles (EVs) are nanometer sized (30-150 nm) particles consisting of a phospholipid bilayer membrane containing intracellular proteins, transmembrane proteins, DNA, mRNA, miRNA and phospholipids which give information on their tissue of origin.[4-6] EVs are shed by all cell types and found in all bodily fluids. Nowadays, it is well-established that EVs play an important role in (inter)cellular communication since they can transfer proteins, lipids and nucleic acids between cells.[7] All EVs have generic membrane proteins that are unique to EVs but do not represent the cells of origin (*e.g.*, CD9, CD63, CD81 are present on the vast majority of blood cell-derived EVs present in blood).[8-9] In addition, EVs present antigens/membrane proteins, which are characteristic of the cells from which they were derived from, *e.g.*, cancer biomarkers HER2, EGFR, or epithelial cell adhesion molecule (EpCAM).[2, 10-11] Most notably, EpCAM is widely used for the identification for tdEVs since it has been shown that the concentration of all objects of epithelial origin correlates with cancer patient outcome.[2] tdEVs are found in blood from the early stages of the disease to metastasis and their concentration varies depending on the progression of the tumor.[12-15] Consequently, EpCAM is a promising marker in metastatic cancer patient management tools.

However, before tdEVs can be clinically targeted in liquid biopsies, reliable methods for their quantification need to be developed. Their low availability and

small size necessitate specialized and sensitive equipment for detection. The most important complication in their detection is the complex environment surrounding the EVs. In blood, considering only particles in the same size range, there are protein aggregates, lipoproteins, cell debris and, most notably, non-cancerous EVs from which the tdEVs need to be distinguished. This imposes a demand for high specificity on any tdEV quantification tool. Being of interest to clinicians, EVs are often studied using tools available for the characterization of cells, *e.g.* flow cytometry, or fluorescent microscopy.[16-22] Although these techniques can give molecular information on the studied EVs, like expressed membrane proteins, they often lack the sensitivity required to detect the smaller particles and also require substantial sample volumes. Therefore, these methods are not ideal for quantification of tdEVs with high sensitivity. There are methods available that can detect single EVs, e.g., atomic force microscopy[23], nanoparticle tracking analysis[24] or resistive pulse sensing.[24] However, these methods are not suitable for distinguishing tdEVs from blood cell EVs and also they tend to suffer from poor throughput as they take longer time for the analysis of available sample volume.

Hence, reliable sensing methods for quantification of EVs with high selectivity and sensitivity are highly sought after. Zhang *et al.* employed a surface immobilization technique targeting generic EV markers and subsequent fluorescent detection of captured tdEVs.[17] This technique was reportedly sensitive enough to detect fluorescent signals at 50 EVs/μl, also with enzymatic amplification. The complexity of integration and photobleaching of fluorescence labels make optical methods less attractive for lab-on-a-chip (LOC) applications. Moreover, they also lack the sensitivity required to detect the smaller EVs which are more abundant than the bigger ones. Reategui *et al.* reported immunocapturing tdEVs on the surfaces of EGFR-coated microfluidic herringbone structrures.[10] Using downstream droplet PCR, tdEVs could be quantified down to a concentration of 100 EVs/μl. Nonetheless, on-chip PCR is difficult to realize reliably due to the multiple thermal cycles that are involved in the process. Furthermore, they also used fluorescent detection after PCR amplification. Xu *et al.* used magnetic precipitation with beads modified with antibodies recognizing lipids in phospholipid shells to capture EVs.[25] These complexes could then be detected using differential pulse voltammetry

(DPV) with a limit of detection (LOD) of 76/μl. Although DPV is a powerful electrochemical measurement technique, the magnetic precipitation is not a consistent method for LOC applications as it is a difficult technique for device integration and also it requires considerable sample volumes. Moreover, this group targeted more generic markers rather than specific cancer markers. Nevertheless, electrochemical sensors are popular alternatives for LOC applications owing to their low cost, easy integration and electrical signal output which does not require other transduction. Here, we report ultrasensitive electrochemical detection of tdEV using a sandwich immunoassay scheme suitable for LOC applications.

### 5.1.1 Sandwich immunoassay on interdigitated electrodes

One of the major challenges in sensing is detection of a low signal corresponding to a low analyte concentration. This is also true for electrochemical sensing methods. The electrochemical oxidation/ reduction involves the transfers of one or a few electrons per reacting redox mediator molecule. Therefore, qualitatively, at low analyte concentration, without amplification, the electrical signal might be too small, *i.e.* beyond the detection limit of the electrical measurement setup. Hence, signal amplification is highly desirable to realize sensitive devices. Accordingly, signal amplification via redox cycling can be a useful method involving electrochemically reversible reactions. As discussed in **Chapter 3**, it is a process of repeated diffusive shuttling of the redox mediator ions between the closely spaced anode and cathode electrodes, undergoing oxidation and reduction reactions on them, thus amplifying the signal.[26] In addition to device based amplification, an enzyme based concentration amplification of the cleaved substrate can also improve both the sensitivity and selectivity. Therefore, here we use a two-level amplification strategy with electrochemical redox cycling on interdigitated electrodes (IDEs) and an alkaline phosphatase (ALP) enzyme based substrate cleaving and amplification as described below. This two-level amplification is a key factor of the detection scheme. An additional attribute of the device is the nano-scale dimensions. Having an electrode width and spacing in the same order of magnitude as the targeted EVs (∽ 100 nm) does not only facilitate efficient capturing, but more notably, it tremendously enhances redox

cycling, as the redox species have smaller distances to diffuse and thus the current is much higher.
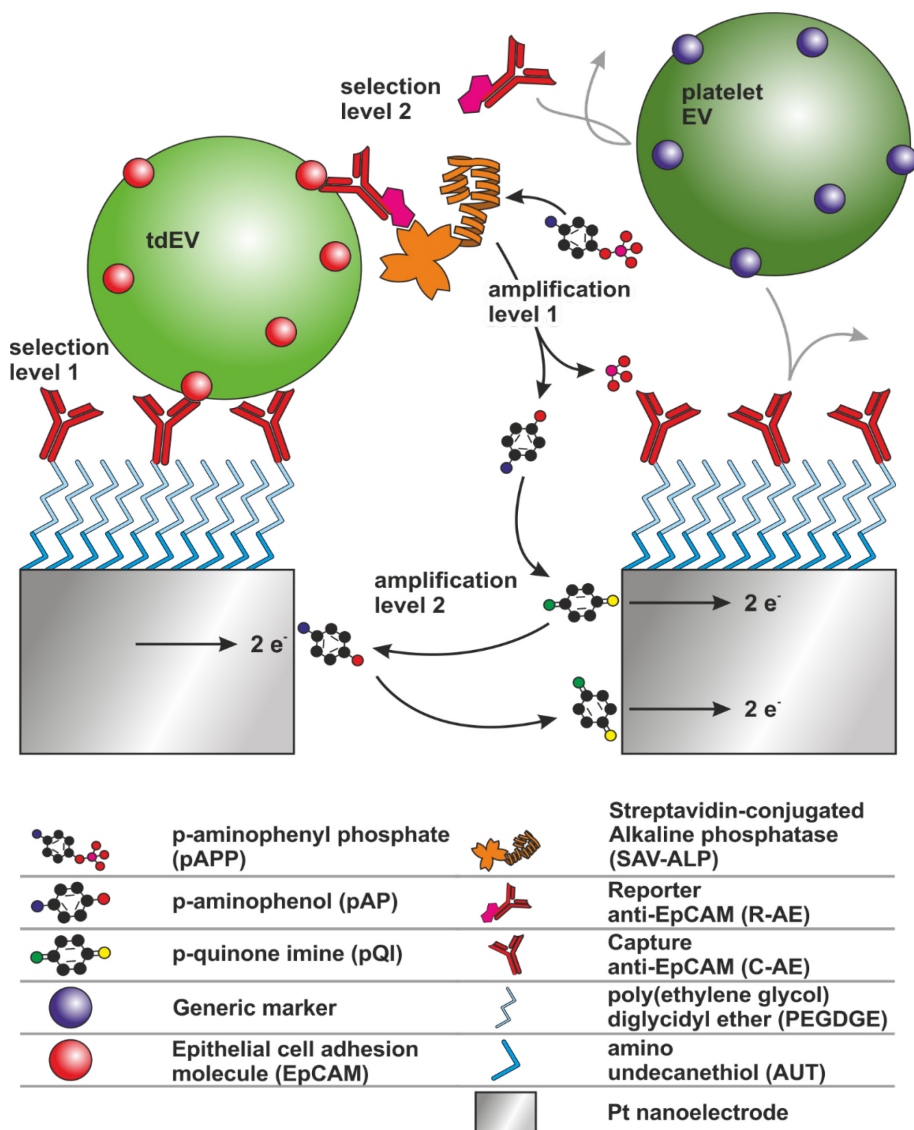


**Figure 5.1:** Schematic representation of the sandwich enzyme immunosensor for tdEV detection using ezymatic amplification of pAPP to pAP by ALP and thereafter pAP is oxidized to pQI and is redox cycled between the electrodes of IDE.

The sandwich immunoassay-based strategy involves a capture anti-EpCAM antibody that captures the tdEVs and a reporter antibody (also anti-EpCAM ) with a label for detection, as  illustrated in *Figure 5.1*. Oxygen plasma cleaned (and activated) electrode surface was functionalized with an amine-terminated thiol (amino-undecane thiol, AUT) and reacted with an amine-reactive bifunctional poly(ethylene glycol) polymer (PEGDGE). To this anti-fouling layer, anti-EpCAM antibodies (C-AE) were covalently linked to specifically capture tdEVs derived from EpCAM-expressing human prostate adenocarcinoma cell lines (LNCaP). Later, the devices were incubated with tdEVs and were captured on the electrodes. The captured tdEVs were next let to interact with reporter anti-EpCAM antibody coupled to biotin (R-AE). This provides a multi-level selectivity since non-cancerous EVs (e.g., blood cell-derived) are not recognized by either the C-AE or the R-AE.  Streptavidin-conjugated alkaline phosphatase (SA-ALP) was next introduced in solution to the device to bind to the biotin moiety of R-AE, enabling an enzyme based sandwich immunosorbent assay. ALP can convert p-aminophenyl phosphate (pAPP) to p-aminophenol (pAP). Thus, the IDEs were subsequently incubated with pAPP. Later, an electrochemical detection is performed on IDEs that amplifies the signal through electrochemical redox cycling. pAPP is electrochemically inactive, however, the ALP converted pAPP to pAP which is redox active and can undergo reversible redox reaction. For control measurements we use platelet derived EVs (pdEV) instead of tdEV which are not recognized by anti-EpCAM antibody. We also compared the performance of the nanoscale IDEs (nIDEs), with the microscale IDEs (µIDEs).

## 5.2 Results and Discussion

### 5.2.1 Surface functionalization and capture validation

The surface functionalization method was performed on bare, Pt-coated silica chips (with no patterned structures), and was characterized using XPS and AFM. XPS was used to study the self-assembly of AUT and PEGDGE. The successful formation of an AUT monolayer and the successive attachment of PEGDGE were confirmed using XPS (data not shown).  XPS data showed a strong S 2p and N 1s peak (at 164 eV and 400 eV, respectively) after formation of the first layer and

their full attenuation after the second layer, indicating only C 1s (285 eV) and O 1s (532 eV). This confirms the formation of the self-assembled layer. AFM of the dried samples (data not shown) confirmed the successful selective capture of tdEVs on anti-EpCAM antibody functionalized Pt surfaces, spherical objects of 10 nm ± 1 nm height and 0.1 - 1 µm in width were observed in all studied regions of 10x10µm$^2$, suggesting the capture of tdEvs. In contrast, for negative control samples [(1) no addition of PEGDGE, (2) no antibody conjugation, (3) no incubation with EVs, or (4) incubation with EpCAM-negative EVs derived from PC3 cell lines], no EV was captured, indicating that the EV isolation was specific to tdEVs.
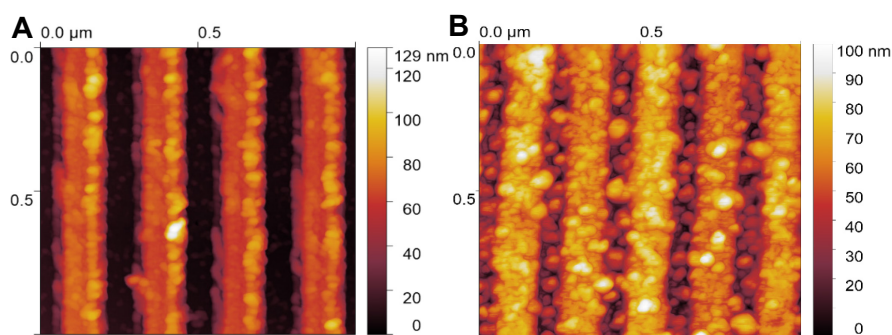


**Figure 5.2**: Atomic force microscope height images before (**a**) and after (**b**) capture of EpCAM-positive tdEVs derived from LnCAP cell lines on nIDEs. The spherical particles found in (b) have sizes 10 - 15 nm, in good agreement with that of EVs.

After validation of the surface functionalization and characterization on Pt surfaces, the experiment was repeated on nIDEs. As before, nIDEs were functionalized with an AUT-based self-assembled monolayer, onto which the PEGDGE linker was grafted, and finally C-AE was covalently conjugated. **Figure 5.2** shows the AFM images before and after the capture of tdEV on the C-AE functionalized electrodes. Spherical objects of 10 - 15 nm can be seen on the electrodes after the capture similar to what we observed on the Pt-coated silica chips (with no patterned structures).

### 5.2.2 tdEV detection on nIDEs

Both nIDEs and µIDEs were used for electrochemical characterization of tdEVs. For nIDEs, the electrodes were 120 nm wide and 70 nm high with 80 nm gap

between the adjacent electrodes. For the µIDEs, the electrodes were 3 µm wide and 70 nm high with a 3 µm gap. The total surface area of both the nIDEs and µIDEs was kept the same, enabling a comparative study. Exchange of reagents was accomplished by micropipetting directly in PDMS microchannels (200 µm × 3mm × 7mm, see SI X). Although ALP prefers alkaline media for optimal performance, EVs prefer a physiological pH and consequently, all the incubations were done in PBS (pH 7.4) at room temperature. IDEs were functionalized as described in **Section 5.1.1**. The devices were first surface functionalized with PEGDGE, AUT and C-AE consecutively. Later, the devices were incubated with tdEVs ($10^6$ tdEVs/µl). After 90 minutes of tdEV incubation, the microchannels were flushed with PBS solution to clean the non-specifically adsorbed particles on the electrodes. Soon after, the devices were incubated with R-AE and SA-ALP sequentially with an incubation time of 30 minutes each followed by cleaning with PBS. Finally, 1 mM pAPP in PBS was added to the device and incubated for 45 minutes.
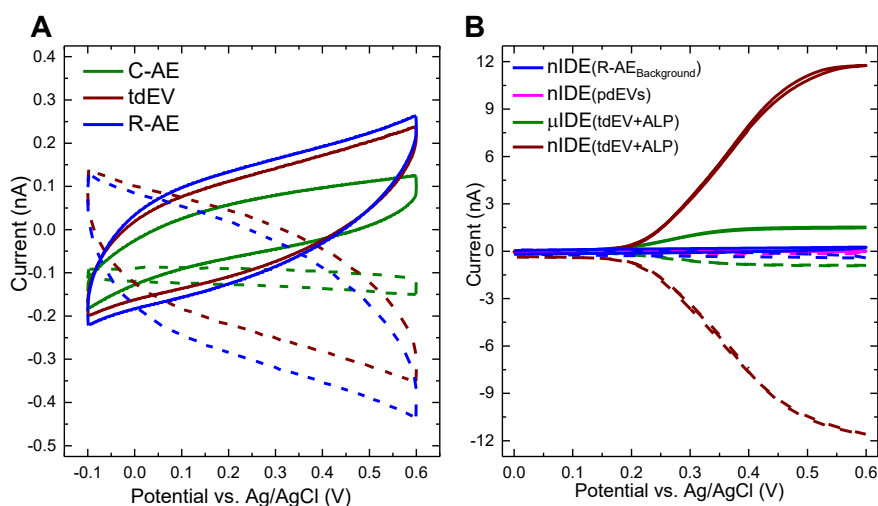


**Figure 5.3:** Cyclic voltammograms for 1 mM of pAPP in PBS (pH7.4) at a scan rate of 50 mV/s **(b)** on nIDEs after C-AE surface modification (green), after tdEV capture (brown) and after sandwich assay formation with R-AE (blue) . **(b)** After SA-ALP immobilization on nIDEs (brown) and on µIDEs (green) with background signal after sandwich assay formation with R-AE (blue) and on control sample after incubation with pdEVs (magenta). The currents $I_{anode}$

(solid lines) and $I_{cathode}$ (dashed lines) represent the current measured at the generator and collector set of electrodes of the nIDEs/µIDEs, respectively.

The nIDEs and µIDEs were electrochemically analyzed at various points during functionalization: (1) after C-AE functionalization, (2) after tdEV capture, (3) R-AE immobilization, and (4) after SA-ALP functionalization. For control experiments, nIDE device was incubated with pdEVs instead of tdEVs. Cyclic voltammograms were recorded at a scan rate of 50 mV/s with Ag/AgCl external reference electrode in 1 mM of pAPP in PBS solution. *Figure 5.3* **(b)** shows cyclic voltammograms obtained after the first three functionalization stages as described above. In all three cases, ALP was not present on the surface and hence, as expected, no significant change in current (redox current) was observed. pAPP is an electrochemically inactive and therefore ALP is required to convert it to pAP which is electrochemically active. However, these voltammograms were similar to the IV characteristics of an RC series circuit, showing a capacitive charging and discharging. Furthermore, the hysteresis of the CV curve changed with measurement after each surface functionalization step. This indicates an increase in the capacitance of the voltammograms, which corresponds to more charge accumulation on the surface as a result of the different surface functionalization steps. The current, $I$, is linearly proportional to the rate of change in voltage, $\frac{dV}{dt}$, through the capacitance C is described by the relationship $I = C \frac{dV}{dt}$. Hence, when the voltage scan rate is reversed, the direction of the current is reversed. The magnitude of that change in current depends on the surface capacitance. A considerable change in the capacitance is observed after the immobilization of the tdEVs. Although the capacitance change after the formation of sandwich assay with R-AE is discernible, it is relatively low compared to the preceding surface functionalization step with tdEVs. It might be an indication of capacitive charging through the vesicles, however, it is not conclusive at this moment. *Figure 5.3* **(c)** shows the cyclic voltammograms for 1 mM of pAPP in PBS (pH7.4) at a scan rate of 50 mV/s on nIDEs and µIDEs. It compares the response of (1) tdEV+R-AE (blue curve) but before the incubation with SA-ALP (as background current) on nIDEs, (2) pdEV + R-AE + SA-ALP functionalization (magenta curve) on nIDEs (3) tdEV on nIDEs (brown curve) and (4) tdEV on uIDEs (green curve), both with R-AE and SA-ALP functionalization. The capacitive current on tdEV + R-AE ($10^6$

particles/µl) immobilized electrodes was higher compared to the one incubated with pdEV ($\sim 10^8$ particles/µl). Again qualitatively, this suggests that tdEVs + R-AE are immobilized on the electrode surface, while the C-AE could not capture pdEV on the surface. ***Figure 5.3 (c)*** also compares the cyclic voltammograms after this SA-ALP incubation of the sample on nIDEs and µIDEs. It shows the characteristic sigmoid curve (brown and green curves) of diffusion-limited redox reaction current on closely spaced working electrodes. Here, the surface-bound ALP cleaves pAPP into pAP. Subsequently, as described earlier, on the anode pAP reduces into pQI, and the reduced pQI diffuses away from the anode to the nearby cathode to oxidize back into pAP. The electrochemical reaction can be denoted as: $pAP \Leftrightarrow pQI + 2e^-$. The limiting current is inversely dependent on the gap between the electrodes. Hence, although the surface areas of the nIDE and µIDE electrodes are the same, the relatively wider gap between the µIDE electrodes resulted in a lower current compared to the nIDE. Also, the collector efficiency (ratio of cathode to anode limiting current) of µIDEs is only 62.3% compared to 99.8% of nIDEs. This indicates that for µIDEs, the redox mediator molecules redox cycle fewer times between the anode and the cathode before diffusing into the bulk solution. The closer spacing of the nIDEs, aided the redox mediator molecules to redox cycle more times, as expected. Moreover, comparing the limiting currents at 0.6 V, we observed $\sim 60$ times amplification in signal compared to the background (brown curve) and control sample with pdEV for nIDE devices (magenta curve).
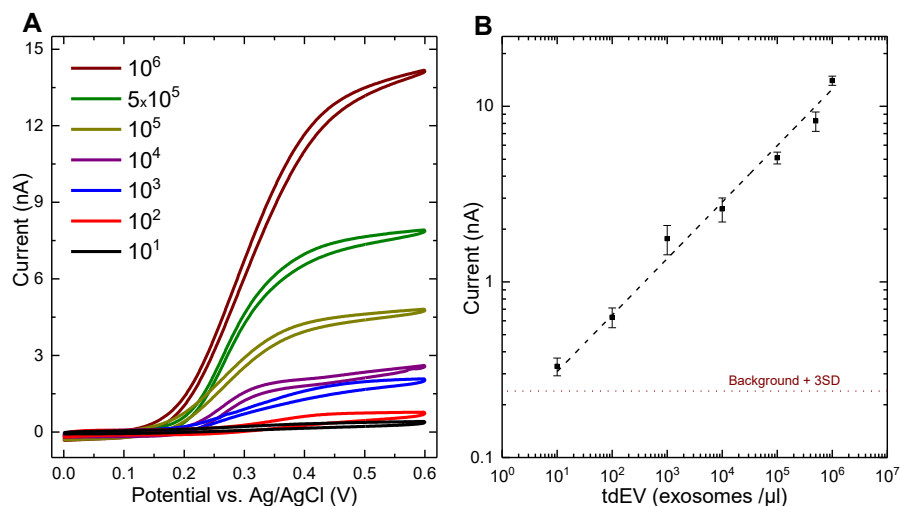
**Figure 5.4**: (**a**) Cyclic voltammograms for 1 mM of pAPP in PBS (pH7.4) at a scan rate of 50 mV/s for different concentrations of tdEVs (noted as the number of tdEVs per µL). Here, only the anodic current is presented. (**b**) calibration curve showing a dynamic range spanning 6 orders of magnitude (n=3). The horizontal dotted line corresponds to the background level plus 3 times the standard deviation of the redox current, indicating a theorectical LOD as low as 5 tdEVs/µl.

Subsequently the response of the nIDEs with varying tdEV concentration was tested. As shown in **Figure 5.4 (a)**, we established a calibration curve (number of nIDE devices, n = 3) and evaluated the LOD of our device and the EV analysis strategy. For each device and concentration, the measurements were performed three times after an interval of 5 minutes each to bolster the stability of the devices. The concentration of tdEVs was varied over 6 orders of magnitudes from 10 to $10^6$ per microliter. We could successfully measure down to 10 tdEVs/µl distinctively above the background signal. **Figure 5.4 (b)** shows the calibration curve demonstrating the dynamic range of our detection technique. The theoretical LOD of the technique as extrapolated from the slope is ~5 tdEVs/µl. To the best of our knowledge, such a low LOD is unprecedented for extracellular vesicles. **Table 1** compares the LOD in state-of-the-art EV detection techniques with the one presented in this chapter.

**Table 1:** Comparison of the different methods for EV detection, capture marker type and LOD.

| Reference | Detection Method | Marker | Lowest measured concentration (EVs per µl) |
|---|---|---|---|
| *Vaidyandan et al.*[27] | *Enzyme amplified colorimetric detection* | *Tumor- specific (various)* | *2760* |
| *Zhao et al.*[28] | *Fluorescent intensity* | *Tumor- specific (various markers)* | *750* |
| *Im et al.*[29] | *Surface plasmon resonance* | *Generic (CD63)* | *400* |
| *Reategui et al.*[10] | *Quantitative polymerase chain reaction* | *Tumor- specific (EGFR)* | *100* |
| *Xu et al.*[25] | *Enzyme amplified differential pulse voltammetry* | *Generic (Tim4)* | *76* |
| *Zhang et al.*[17] | *Enzyme amplified fluorescent signal* | *Generic (cocktail)* | *50* |
| *This work* | *Cyclic voltammetry* | *Tumor- specific (anti-EpCAM)* | *10* |

## 5.3 Conclusion

Here we reported a novel electrochemical sensor for tumor derived extracellular vesicle detection on nanoscale interdigitated electrodes using a sandwich immunoassay. We have proven the high sensitivity of our device combined with high selectivity. The high sensitivity is attained by the electrochemical amplification by redox cycling and the enzymatic conversion of the redox mediator molecules while the high selectivity is a result of the double specificity of the sandwich assay. We have established an unprecedented sensitivity of tdEVs as low as 10 tdEVs/µl (measured) with a detection range spanning about 6 orders of magnitude. Further optimization of the experimental conditions might lead to even better sensitivity. Consequently, this method can be used for prognosis, personalized medication and its efficacy, and the recurrence of the disease. This amperometric sensing method also gives the possibility to be developed as a portable point-of-care sensing device which can also be useful in population wide disease screening.

## 5.4 Materials and Methods

### 5.4.1 Materials

Dichloromethane and ethanol (VLSI grade) were purchased from VWR (Amsterdam, The Netherlands). Acetone (VLSI grade), Harris Uni-Core 1 mm I.D. biopsy punches, 11-Amino-1-undecanethiol hydrochloride (AUT), (Poly(ethylene glycol) diglycidyl ether (PEGDGE), PBS tablets, bovine serum albumin (BSA) and 4-Aminophenyl phosphate monosodium salt hydrate (pAPP) were obtained from Merck (Zwijndrecht, The Netherlands). Capturing anti-EpCAM (C-AE), Biotinylated reporter anti-EpCAM (R-AE), sodium phosphate buffer (pH 8.3) and extracellular vesicles were taken from laboratory stock. Streptavidin-conjugated alkaline phosphatase (SA-ALP) was purchased from Thermo Fisher (Eindhoven, The Netherlands). Sylgard 184 was obtained from Farnell (Utrecht, The Netherlands). Buffers were filtered through a 0.2 µm syringe filter before use.

## 5.4.2 *Device fabrication*

nIDEs were fabricated using a combination of optical and electron-beam lithography (EBL) and metal evaporation and lift-off process. 300 nm SiO2 was thermally grown on a 10 cm Si 100 wafer at 10000 C. First optical lithography step was carried out followed by Pt metal evaporation and lift-off for defining markers for EBL. CHF3 based plasma etching was performed afterwards to recess the adhesive metal layer into the substrate. Subsequently, nIDEs were patterned using EBL with metals (Ti, 5 nm- adhesive layer and Pt, 70 nm) were deposited and lifted-off. Later, the nIDEs were connected to contact pads via contact leads using second optical lithography followed by another metal evaporation (100 nm) and lift-off. 300 nm layer of parylene-C was evaporated (300 nm) as the first passivation layer. The third optical lithography step was used to pattern and later the contact leads were passivated and insulated using evaporated SiO2 (30 nm). This oxide layer covers everything except the contact pads and a rectangular window of 30 μm x 70 μm over the nIDEs.  The two passivation layers (parylene and SiO2) prevent current leakage through the contact leads and also enables the use of the nIDEs without fluidic systems if needed, by simply placing an analyte droplet on top of the IDEs. Bare Pt substrates for surface characterization and functionalization validation were prepared by sputtering 10 nm Ta as adhesive layer and 100 nm Pt on Mempax glass wafers. 10 x 10 mm² chips were diced.

## 5.4.3 *Surface modification*

The platinum nIDEs were first cleaned by rinsing sequentially in dichloromethane, acetone and ethanol (bare Pt substrates were ultrasonicated in said solvents for 7 minutes each). Platinum surfaces were finally cleaned in O2 plasma (Diener Pico, Diener Electronics, Ebhausen, Germany) for 30 s. After placing the PDMS device on the chip, the channel was filled with a solution of 1mM AUT in ethanol and left static at room temperature overnight to form a self-assembled thiol monolayer (SAM). Then the channels were washed with 1 ml of ethanol, blown dry with N2, filled with neat poly(ethylene glycol) diglycidyl ether (PEGDGE) and left overnight at 40 ºC. Afterwards, the channels were again rinsed with 1ml ethanol and blown dry with N2.  This yields an anti-biofouling layer, subsequently functionalized with capturing anti-EpCAM (C-AE). Capturing anti-EpCAM (C-AE) was diluted to a final concentration of 25 mg/ml in sodium phosphate buffer (pH 8.3) and injected in

the microchannel for overnight incubation. Prior to the EV capture, unreacted epoxide groups were blocked with filtered 1% BSA solution in PBS for 1 h at room temperature and rinsed with 1 ml PBS.

### 5.4.4 Extracellular vesicle capture and detection

In the following procedure, after every introduction of new components, unbound species were washed away by injecting 100 µl PBS. tdEVs with an initial concentration of $1 \times 10^9$ ml-1 were diluted 10n times in PBS (n = 0,1..5). As a negative control, pdEVs were used in their stock concentration of $8 \times 1000$ ml-1. 10 µl samples of EVs were injected in the channels and left to incubate for 20 minutes. Non-specifically bound species were washed away by injecting 100 µl PBS. After the successful capturing of tdEVs, a reporter anti-EpCAM with a biotin tag (R-AE) was used to complete the antibody-tdEV-antibody sandwich assay. 10 µl R-AE was diluted in PBS to 25 mg ml-1 and injected and left to incubate for 20 minutes. A reporter enzyme, alkaline phosphatase, conjugated with streptavidin (SA-ALP) was used to specifically tether it to the biotin-antibody complex, R-AE.. Channels were next incubated for 20 minutes with 10 µl (10 micro activity unit) SA-ALP for specific surface immobilization of this enzyme. 100 µl of 4-aminophenyl phosphate solution (pAPP, 10 mM in PBS) was finally injected in the channel and left in the inlet pipette tip to enable a fluidic connection to the reference electrode. The effect of the close spacing is demonstrated by comparison of our nIDE with an IDE with 3µm electrode spacing, limiting the amount of charged species that can reach the electrodes per unit time by increasing the diffusion length. As another negative control, platelet-derived extracellular vesicles (pdEVs) were also used. Due to the lack of specificity, C-AE failed to immobilize pdEVs on the electrode surface, and thus subsequently SA-ALP was also not tethered resulting in no enzymatic conversion of pAPP to pAP. Three devices were tested for the determination of the limit-of-detection; every device was tested with all concentrations, starting with the lowest concentration. For every concentration, three measurements were performed with an intermediate time of 10 minutes. For every measurement, three cycles were recorded. Before repeating measurements at higher concentrations, the surface was regenerated by flowing 100 µl PBS.

## 5.5 References

1. Alix-Panabières, C.; Pantel, K., Circulating tumor cells: liquid biopsy of cancer. *Clinical chemistry* **2013,** *59* (1), 110-118.

2. Nanou, A.; Coumans, F. A.; van Dalum, G.; Zeune, L. L.; Dolling, D.; Onstenk, W.; Crespo, M.; Fontes, M. S.; Rescigno, P.; Fowler, G., Circulating tumor cells, tumor-derived extracellular vesicles and plasma cytokeratins in castration-resistant prostate cancer patients. *Oncotarget* **2018,** *9* (27), 19283.

3. Coumans, F.; Dalum, G.; Terstappen, L. W. M. M., CTC Technologies and Tools. *Cytometry Part A* **2018,** *93* (12), 1197-1201.

4. Vaidyanathan, R.; Soon, R. H.; Zhang, P.; Jiang, K.; Lim, C. T., Cancer diagnosis: from tumor to liquid biopsy and beyond. *Lab on a Chip* **2019,** *19* (1), 11-34.

5. Poudineh, M.; Sargent, E. H.; Pantel, K.; Kelley, S. O., Profiling circulating tumour cells and other biomarkers of invasive cancers. *Nature Biomedical Engineering* **2018,** *2* (2), 72.

6. Yáñez-Mó, M.; Siljander, P. R.-M.; Andreu, Z.; Bedina Zavec, A.; Borràs, F. E.; Buzas, E. I.; Buzas, K.; Casal, E.; Cappello, F.; Carvalho, J., Biological properties of extracellular vesicles and their physiological functions. *Journal of extracellular vesicles* **2015,** *4* (1), 27066.

7. van Niel, G.; D'Angelo, G.; Raposo, G., Shedding light on the cell biology of extracellular vesicles. *Nature reviews Molecular cell biology* **2018,** *19* (4), 213.

8. Kanwar, S. S.; Dunlay, C. J.; Simeone, D. M.; Nagrath, S., Microfluidic device (ExoChip) for on-chip isolation, quantification and characterization of circulating exosomes. *Lab on a Chip* **2014,** *14* (11), 1891-1900.

9. Koliha, N.; Wiencek, Y.; Heider, U.; Jüngst, C.; Kladt, N.; Krauthäuser, S.; Johnston, I. C.; Bosio, A.; Schauss, A.; Wild, S., A novel multiplex bead-based platform highlights the diversity of extracellular vesicles. *Journal of extracellular vesicles* **2016,** *5* (1), 29975.

10. Reátegui, E.; Vos, K. E.; Lai, C. P.; Zeinali, M.; Atai, N. A.; Aldikacti, B.; Floyd, F. P.; Khankhel, A.; Thapar, V.; Hochberg, F. H., Engineered nanointerfaces for microfluidic isolation and molecular profiling of tumor-specific extracellular vesicles. *Nature communications* **2018,** *9* (1), 175.

11. Yadav, S.; Boriachek, K.; Islam, M. N.; Lobb, R.; Möller, A.; Hill, M. M.; Hossain, M. S. A.; Nguyen, N. T.; Shiddiky, M. J., An Electrochemical Method for the Detection of Disease-Specific Exosomes. *ChemElectroChem* **2017,** *4* (4), 967-971.

12. Julich, H.; Willms, A.; Lukacs-Kornek, V.; Kornek, M., Extracellular vesicle profiling and their use as potential disease specific biomarker. *Frontiers in immunology* **2014,** *5*, 413.

13. Lobb, R. J.; Lima, L. G.; Möller, A. In *Exosomes: key mediators of metastasis and pre-metastatic niche formation*, Seminars in cell & developmental biology, Elsevier: 2017; pp 3-10.

14. Galindo-Hernandez, O.; Villegas-Comonfort, S.; Candanedo, F.; González-Vázquez, M.-C.; Chavez-Ocaña, S.; Jimenez-Villanueva, X.; Sierra-Martinez, M.; Salazar, E. P., Elevated concentration of microvesicles isolated from peripheral blood in breast cancer patients. *Archives of medical research* **2013,** *44* (3), 208-214.

15. Coumans, F.; Doggen, C. J. M.; Attard, G.; De Bono, J.; Terstappen, L. W. M. M., All circulating EpCAM+ CK+ CD45– objects predict overall survival in castration-resistant prostate cancer. *Annals of oncology* **2010,** *21* (9), 1851-1857.

16. Shpacovitch, V.; Hergenroeder, R., Optical and surface plasmonic approaches to characterize extracellular vesicles. A review. *Analytica chimica acta* **2018,** *1005*, 1-15.

17. Zhang, P.; He, M.; Zeng, Y., Ultrasensitive microfluidic analysis of circulating exosomes using a nanostructured graphene oxide/polydopamine coating. *Lab on a Chip* **2016,** *16* (16), 3033-3042.

18. van der Pol, E.; Sturk, A.; van Leeuwen, T.; Nieuwland, R.; Coumans, F.; group, I. S. V. W.; Mobarrez, F.; Arkesteijn, G.; Wauben, M.; Siljander, P. M., Standardization of extracellular vesicle measurements by flow cytometry through vesicle diameter approximation. *Journal of Thrombosis and Haemostasis* **2018,** *16* (6), 1236-1245.

19. Nolan, J. P.; Duggan, E., Analysis of individual extracellular vesicles by flow cytometry. In *Flow Cytometry Protocols*, Springer: 2018; pp 79-92.

20.     Hisey, C. L.; Dorayappan, K. D. P.; Cohn, D. E.; Selvendiran, K.; Hansford, D. J., Microfluidic affinity separation chip for selective capture and release of label-free ovarian cancer exosomes. *Lab on a Chip* **2018,** *18* (20), 3144-3153.

21.     Contreras-Naranjo, J. C.; Wu, H.-J.; Ugaz, V. M., Microfluidics for exosome isolation and analysis: enabling liquid biopsy for personalized medicine. *Lab on a Chip* **2017,** *17* (21), 3558-3577.

22.     Im, H.; Lee, K.; Weissleder, R.; Lee, H.; Castro, C. M., Novel nanosensing technologies for exosome detection and profiling. *Lab on a Chip* **2017,** *17* (17), 2892-2898.

23.     Yuana, Y.; Oosterkamp, T.; Bahatyrova, S.; Ashcroft, B.; Garcia Rodriguez, P.; Bertina, R.; Osanto, S., Atomic force microscopy: a novel approach to the detection of nanosized blood microparticles. *Journal of thrombosis and haemostasis* **2010,** *8* (2), 315-323.

24.     Van Der Pol, E.; Hoekstra, A.; Sturk, A.; Otto, C.; Van Leeuwen, T.; Nieuwland, R., Optical and non-optical methods for detection and characterization of microparticles and exosomes. *Journal of Thrombosis and Haemostasis* **2010,** *8* (12), 2596-2607.

25.     Xu, H.; Liao, C.; Zuo, P.; Liu, Z.; Ye, B.-C., Magnetic-Based Microfluidic Device for On-Chip Isolation and Detection of Tumor-Derived Exosomes. *Analytical chemistry* **2018,** *90* (22), 13451-13458.

26.     Goluch, E. D.; Wolfrum, B.; Singh, P. S.; Zevenbergen, M. A.; Lemay, S. G., Redox cycling in nanofluidic channels using interdigitated electrodes. *Analytical and bioanalytical chemistry* **2009,** *394* (2), 447-456.

27.     Vaidyanathan, R.; Naghibosadat, M.; Rauf, S.; Korbie, D.; Carrascosa, L. G.; Shiddiky, M. J.; Trau, M., Detecting exosomes specifically: a multiplexed device based on alternating current electrohydrodynamic induced nanoshearing. *Analytical chemistry* **2014,** *86* (22), 11125-11132.

28.     Zhao, Z.; Yang, Y.; Zeng, Y.; He, M., A microfluidic ExoSearch chip for multiplexed exosome detection towards blood-based ovarian cancer diagnosis. *Lab on a Chip* **2016,** *16* (3), 489-496.

29.     Im, H.; Shao, H.; Park, Y. I.; Peterson, V. M.; Castro, C. M.; Weissleder, R.; Lee, H., Label-free detection and molecular profiling of exosomes with a nano-plasmonic sensor. *Nature biotechnology* **2014,** *32* (5), 490.

*"Every once in a while, a new technology, an old problem, and a big idea turn into an innovation."*

*Dean Kamen*

6

# Single-particle detection on nanodisc electrodes

**Abstract:** Particle impact electrochemistry has attracted a lot of interest recently for its ability to address individual particles together with incessant monitoring of the particle. This method can be used for detection of (bio)particles with a very rare occurrence. In this chapter, we investigate the possibility of using a nanodisc electrode for single-particle detection using particle impact electrochemistry. We simulate the performance of different geometries of the nanodisc electrodes, and observe that recessed nanodisc electrodes provide the highest signal-to-noise ratio for particle impact detection. We have fabricated recessed nanodisc electrodes of different sizes, and use them for single-particle detection of carboxylated latex nanoparticles, using a chronoamperometric method. Discrete *hit-and-stay* collision events are detected, and we also observe *hit-and-run* and *wobbling* events of latex particles. The AFM images underpin the adsorption of nanoparticles on the nanodisc electrodes after the current vs. time measurements. This proof-of-concept experiment reveals the potential of nanodisc electrodes for counting individual bioparticles.

## 6.1 Introduction

Label-free biosensing is an effective tool in diagnostics as it involves easy sample handling and continuous monitoring of analytes. Moreover, it also provides quantitative data with high throughput.[1] Detecting and analyzing an entity like a single cell, particle, vesicle or molecule using a label-free technique can provide useful information regarding the underlying science of the bulk response of these constituent entities.[2] Consequently, the past decade has seen the development of various label-free techniques to detect single objects using optical[3-8] and electrochemical methods[9-13]. The advantages of electrochemical methods over optical methods, like easy integration and direct signal acquisition without further transduction, makes them favorite biosensing techniques. Different methods have been used for single-entity electrochemistry[2], such as the resistive pulse technique (Coulter counter),[14-15] patch-clamp technique[16], single-molecule redox cycling[12, 17-18] etc. Consequently, nanoparticle impact studies recently gained a lot of interest among electrochemists. It involves the blocking of mass transfer of redox-active species towards the electrode surface by the impact of a nanoparticle on the electrode surface.[4] Conversely, a catalytic particle[19] can be used to amplify the signal when it hits the electrode surface or a particle that can undergo a transformative reaction[20] (e.g. oxidation) in order to amplify the signal. However, the current blocking method can be more useful for the detection of biological particles, since most of these particles are electrically insulating. Hence, this method can be developed as a key tool in biosensing. Nonetheless, in the current blocking method, in order to distinctively detect each event of particle blocking, the signal-to-noise ratio should be high. The current drop obtained when a particle blocks the electrode is dependent on the particle size and the electrode size. Thus, to detect sub-100 nm particles, the size of the electrode should also be in the same range in order to obtain a high signal-to-noise ratio. Although researchers have studied current blocking of nanoparticles on nanoelectrodes,[21-23] most of them used devices that are not compatible with industrial mass production, which is an important prerequisite for developing commercialized biosensors for point-of-care applications. However, here we report an array of nanodisc electrodes with different radii fabricated using a standard

semiconductor fabrication process that can be used for individual biomolecule detection.

### 6.1.1 Mass transfer on a nanodisc electrode

Micro- and nanoscale electrodes with different sizes and shapes were extensively investigated by electrochemists due to their high current density, thanks to the radial diffusion pattern of the redox molecules.[24] Due to this radial diffusion pattern, for an unperturbed system, well above the formal potential, the micro- and nanoscale electrodes generate a steady-state current. This steady-state current is determined by the diffusion-limited mass transfer of the redox molecules onto the electrode surface. The magnitude of this current varies with the geometry of the electrode. Moreover, for a similar shape and size, the steady-state current changes with the elevation of the electrode surface from the substrate level. The steady-state limiting current for a recessed disc electrode is given by[24-25]

$$I_{lim} = \frac{4\pi n_i F C_i D_i r^2}{4L + \pi r} \tag{6.1}$$

where $n_i$ is the number of electrons involved in the redox reaction, $F$ is the Faraday constant, $D_i$ is the diffusion constant and $C_i$ is the concentration of the redox mediator, respectively, $r$ is the radius of the electrode and $L$ is the recession of the electrode into the substrate. For particle blocking experiments, the mass transport of the particles is equally significant. Their mass transport towards an electrode surface is determined by diffusion, electromigration and convection. When the solution is kept undisturbed, the convection becomes irrelevant. Meanwhile, the diffusive flux of the particle depends on the diffusion coefficient and the concentration gradient of the particle in solution. Mass transfer of the particles due to electromigration can also be pivotal in certain experimental conditions. When a positive potential is applied on the electrode, it causes an electric field in the solution due to the oxidation current resulting in an electrophoretic force that attracts negatively charged particles onto the electrode surface. This electrophoretic force enhances the collision rate of

nanoparticles on the electrode. This electrophoretic collision rate can be approximated as[9]

$$J_{mig} \approx \frac{I_{ND} C_{NP}}{e C_e} \frac{U_{NP}}{U_{e+} + U_{e-}} \qquad (6.2)$$

where $I_{ND}$ is the anodic current at the nanodisc electrode, $e$ is the elementary charge, $C_{NP}$ and $C_e$ are the concentrations of the nanoparticles and the electrolyte, respectively, $U_{NP}$ is the mobility of the nanoparticles, while $U_{e+}$ and $U_{e-}$ are the mobilities of the cation and anion of the supporting electrolyte, respectively. It is evident from the equation that in a solution with low concentration of supporting electrolyte, the mass transfer of particles due to electromigration will be significant.

### 6.1.2 Biosensing using a nanodisc electrode

As mentioned earlier, nanoparticle blocking experiments on a nanodisc electrode can be used for highly sensitive biosensing applications. An electrically insulating bioparticle (e.g. a tumor-derived extracellular vesicle, tdEV) can block the current on the nanodisc electrode when it hits the electrode surface. A scheme for the detection of tdEVs is illustrated in **Figure 6.1**. Consider a nanodisc electrode, functionalized with antibodies that can recognize tdEVs. Upon addition of a droplet of solution, containing redox mediator molecules and tdEVs, tdEV start to approach the functionalized nanoelectrode surface, it interacts with the antibodies and gets immobilized, which blocks mass transfer of the redox mediator to the electrode, resulting in an abrupt drop in the measured current (OFF signal), as shown in **Figure 6.1 (b)**. If the dissociation rate, $k_{off}$, is smaller, the particle tends to stay longer on the electrode, resulting in longer current blockage. Thus, the OFF signal time duration gives valuable information about the interaction strength of the analyte and EV.
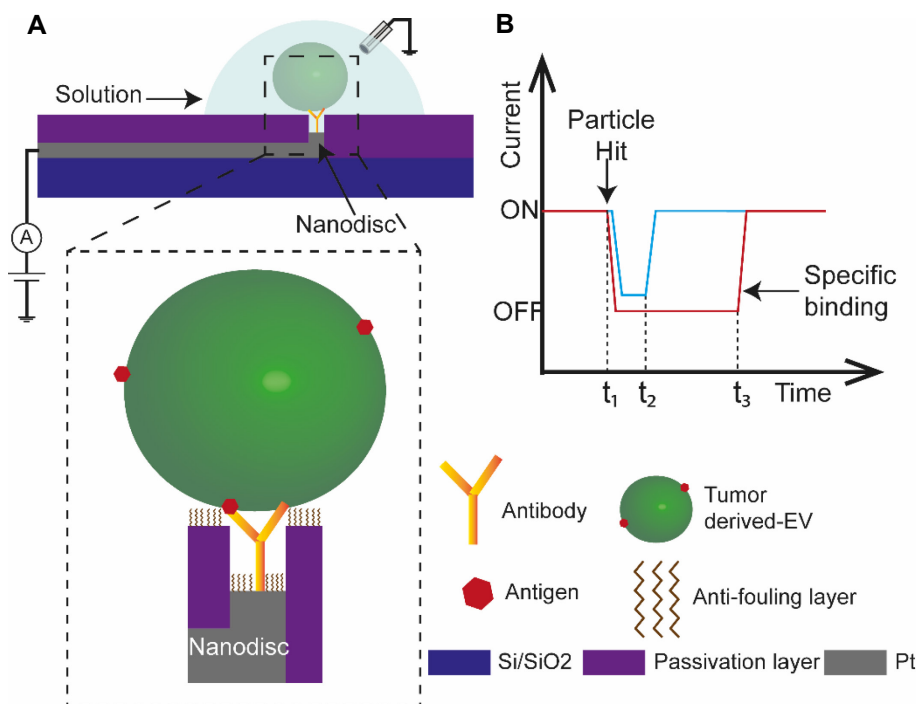
Figure 6.1:(a) Schematic diagram showing the method of tdEV detection by blocking current on a nanodisc electrode (not to scale). (b) Schematic of blocking current for specific and non-specific binding of particles on the electrode.

The amplitude of the current drop can also give information regarding the particle size. When the interaction is not specific, i.e. for non-tdEV, the particle will dissociate faster on average, resulting in a shorter OFF signal period compared to the longer period of tdEVs. This method is generic and a similar scheme of detection can be used for viruses, bacteria and other biomolecules. However, for nucleic acid detection, nanoparticles with nucleic acid decorated on them can be used in a similar sandwich assay scheme mentioned in **Chapter 4**, but with a non-conducting nanoparticle (for blocking experiments).

As mentioned in **Section 6.1.1**, in the presence of a low concentration of a supporting electrolyte, the oxidation of the redox mediator molecules on the nanodisc electrode generates an electrophoretic force pulling negatively charged particles towards the electrode, which is pivotal for low-concentration analyte detection. This is a crucial and unique feature of our device: qualitatively, with

diffusion alone, the particle will take much longer to reach the sensor surface due to its size, which would fundamentally hamper any detection at clinically relevant low concentration levels. However, this electrophoretic force applies to all charged entities in the solution and hence this force varies with the size and net charge of each particle. Consequently, a highly effective anti-fouling layer is crucial to minimize the *non-specific* binding of particles onto the electrode surface.[26] Detection of single tdEVs on nanodisc devices involves fabrication of the nanodiscs, electrochemical validation, surface functionalization with antibodies and anti-fouling molecules and time-resolved capture of tdEVs on the electrode surface. However, since this involves optimization of many process steps, we decided to first make a proof-of-concept of this detection method. Hence, here we report the simulation and fabrication of nanodisc electrodes, and the detection of carboxylated latex nanoparticles (negatively charged) in order to prove the concept of single-particle detection on nanodisc electrodes.

## 6.2 Results and discussion

### *6.2.1 Finite-element modelling*

**Table 6.1:** COMSOL model parameters

| $E_{appl}$ | -1 V | Applied potential on the nanoelectrode |
|---|---|---|
| $E_f$ | 0.18 V | Formal potential of the redox molecule (ferrocene dimethanol) |
| $C_{bulk}$ | 0.5 mol/L | Bulk concentration that exists outside of the particle |
| $R_e$ | 15 nm | Radius of the electrode |
| $R_p$ | 25 nm | Radius of the nanoparticle |
| $D_{ox}$ | $7^{-10}m^2/s$ | Diffusion coefficient of the oxidation species |
| $D_{red}$ | $7^{-10}m^2/s$ | Diffusion coefficient of the reduction species |
| $K_0$ | 4 n/ms | Reaction rate constant |

With the help of finite-element calculations (COMSOL Multiphysics® 5.3), we investigated the effect of the nanoelectrode geometry, the blocking particle size and its position (both lateral and vertical) on the electrode surface. Three different geometries of the nanoelectrode based on its elevation were examined: electrodes that are (1) raised from the substrate level, (2) same level as of the substrate and (3) recessed into the substrate. The model parameters used for the simulations were taken from the work of Kwon *et al.*[20] and is tabulated in **Table 6.1.**
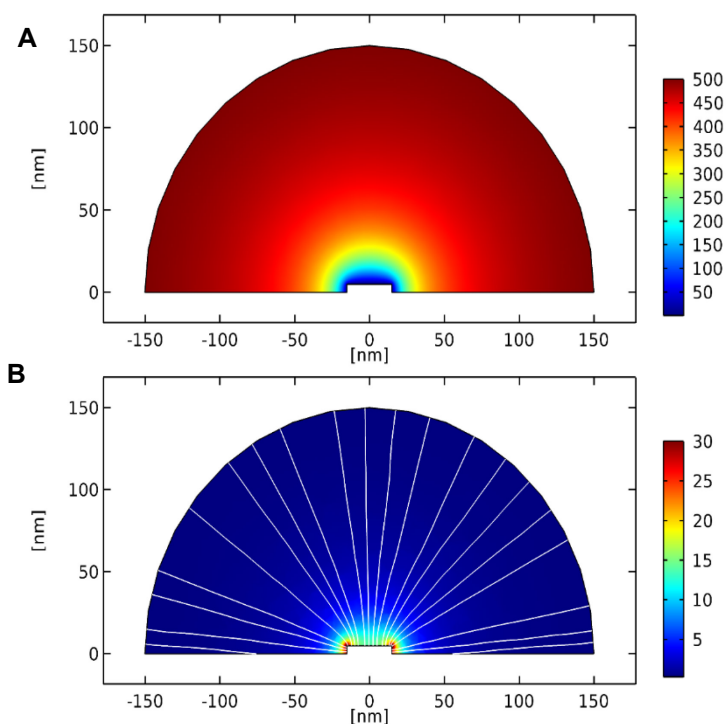


**Figure 6.2: (a)** 2-D concentration gradient of redox mediator around the nanodisc electrode. The false color scale represent concentration gradient in mol/m³. **(b)** 2-D diffusive flux of redox mediator towards raised nanodisc electrode The false color scale show diffusive flux in mol/ (m² s). The white solid lines (illustrative) show the flux of the redox mediator molecules onto the electrode surface.

**Figure 6.2: (b)** depicts the 2-D diffusive flux of the redox molecules towards the electrode with a raised geometry. Again, due to the radial diffusion pattern of the

redox molecules towards the electrode surface, the diffusive flux is higher along the edge of the electrode. This has a high impact on the current-blocking experiments. When the electrode is raised above the substrate, the highest current drop is obtained when the particle covers the area around the edge of the electrode. Hence, in order to obtain the highest signal to background ratio, the preferred geometry would be the recessed electrode geometry. That is, the edge effect is highest for the raised electrode geometry, and least for the recessed electrodes.

**Figure 6.3**: depicts the 2-D diffusive flux of the redox mediator towards the electrode surface in the presence (b-h) or absence (a) of a nanoparticle on the electrode surface. We studied seven different particle sizes (1, 3, 7, 9, 15, 21 and 23 nm) on an electrode of 15 nm radius recessed 5 nm into the substrate. Although the electrodes are recessed, as expected, the diffusive flux is highest at the edge due the radial diffusive pattern near the edge. It is also evident that with increasing particle size, the mass transfer of the redox molecules to the electrode surface is decreased. The presence of the particle prevents the free diffusion of the redox mediator molecules, and hence they have to diffuse around the particle to approach the electrode surface. This results in a smaller number of redox molecules reaching the electrode surface at any given time compared to when there is no nanoparticle on the electrode.

This effect is clearly evident in the images as a *shadow* of the particle (zero flux: blue shade) that is formed on the electrode surface below the particle. We repeated the simulation for all the three different geometries as described earlier with varying nanoparticle size and recorded the change in current due the presence of the nanoparticle and the results are summarized in **Figure 6. 4 (a)**.
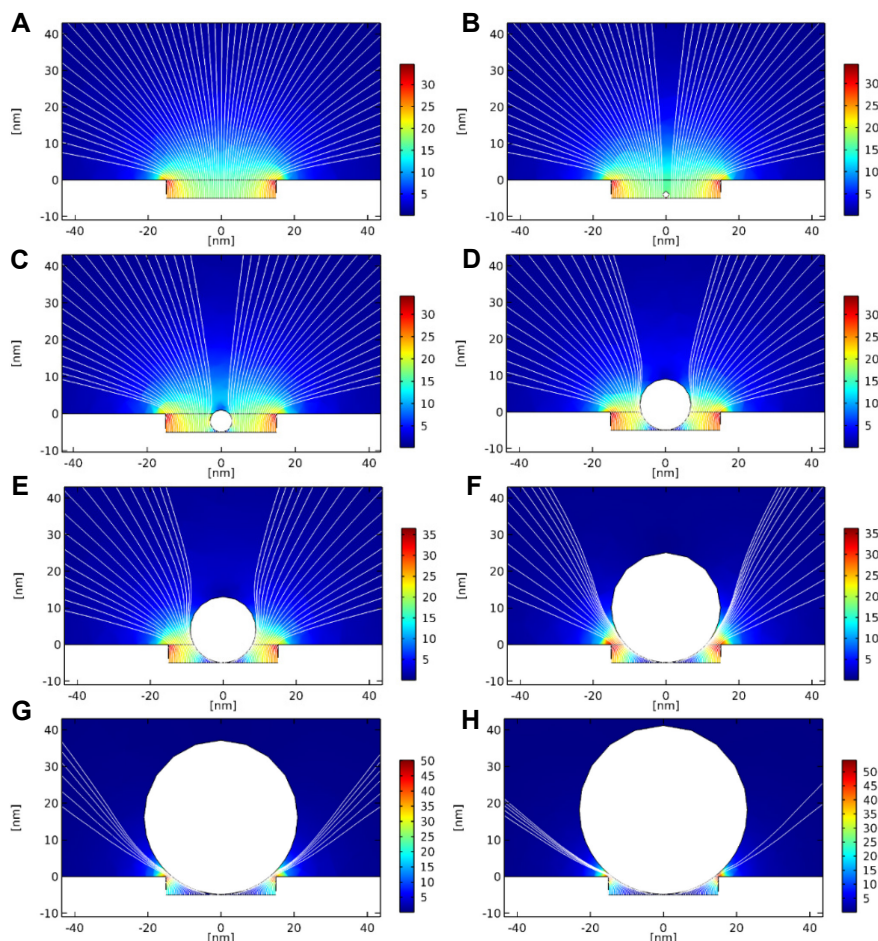
**Figure 6.3: (a)** 2-D diffusive flux of redox mediator towards recessed nanodisc electrode. Flux when blocked by **(b)** 1 nm **(c)** 3 nm **(d)** 7 nm **(e)** 9 nm **(f)** 15 nm **(g)** 21 nm and **(h)** 23 nm non-conductive particles, respectively. The false color scales represent diffusive flux in mol/ (m² s). The white solid lines (illustrative) show the flux of the redox mediator molecules onto the electrode surface. In order to emphasize the blocking by the particle and the circumvention of the mediator molecules around the particle to reach the electrode, the white solid lines representing the diffusive flux is not shown above the particle.

On the recessed electrodes, for particle radii more than half of the electrode radius, we observed that the drop in current is linearly proportional to the radius of the particle, as expected.[9] Simulation results also showed that on recessed

electrodes with radius 15 nm, the current is entirely blocked when a particle of radius 25 nm or more is adsorbed on the electrode, and hence the curve for the recessed electrode (yellow) in **Figure 6. 4 (a)** is not plotted beyond 25 nm particle radius. Furthermore, the recessed electrode showed the highest drop in current for any given particle size. For example, if a particle of radius 15 nm is adsorbed on the recessed electrode of radius 15 nm, the current drops 34%, while this will cause only 18% and 12% current drop for electrodes that are same level (geometry 2) and raised (geometry 1), respectively. Therefore, it can be easily deduced that the recessed electrode is the best design for the current blockage experiments, while the raised electrodes provide the worst result. Hence, throughout the rest of this chapter we use recessed electrodes for all the measurements. Until now, we discussed the cases where particles were adsorbed on top of the electrode. However, we also studied the current drop on the nanodisc electrode as a function of the particle position vertically above the electrode. **Figure 6. 4 (b)** shows the effect of a 25 nm particle above an electrode of 15 nm, from the state of being adsorbed (height = 0 nm) to the state where the particle is 60 nm above the electrode surface. As anticipated, an exponential relationship between the particle height and  the current drop was observed.[9]

Quinn *et al.*[9]  suggest that the lateral position of the particle with respect to the center of the electrode also has an effect on the magnitude of current drop. Since the current density is higher at the edge of the electrode, if a particle is adsorbed somewhere closer to the edge of the electrode, the current drop will be highest. Our simulation results also underpin this finding, as seen in **Figure 6. 4 (c)** and **(d)**. When the particle size is less than the size of the electrode (15 nm), we observe that the current drop is highest when the position of the particle is near the edge of the electrode. Meanwhile, when the particle is bigger than the electrode, the maximum drop in current is observed when the particle is in the middle of the electrode so that it covers the edge equally along the entire circumference.
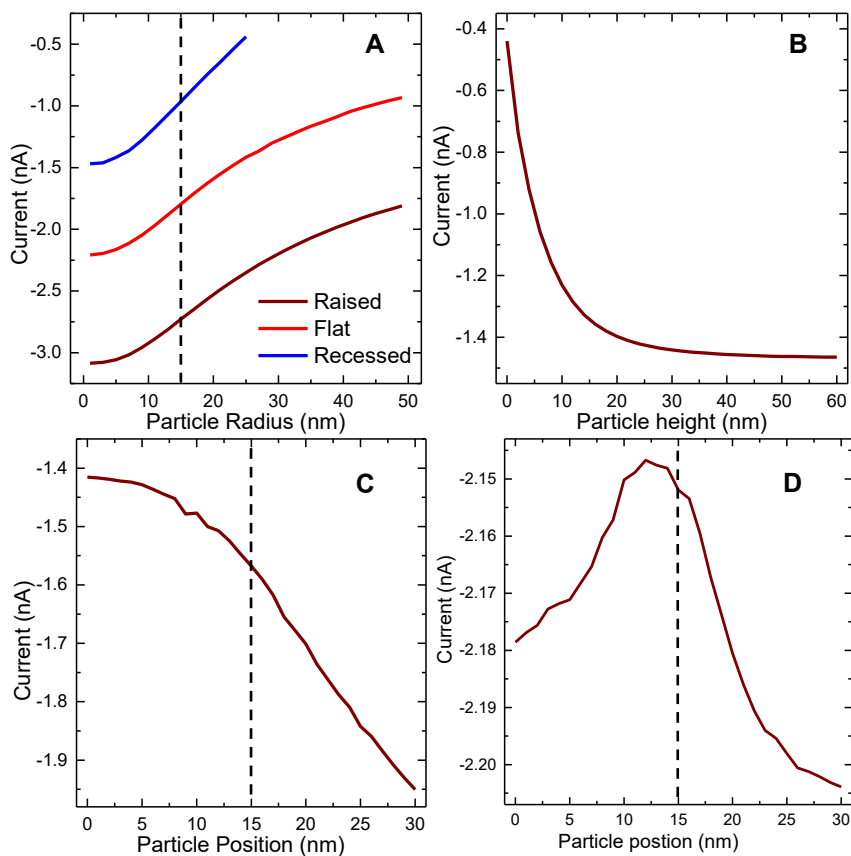
**Figure 6. 4**: **(a)** Current drop with respect to the particle radius on a nanodisc electrode of 15 nm radius that is raised (brown) 5 nm above the substrate, same level (red) with the substrate and 5 nm recessed (blue) into the substrate. **(b)** Current drop as a function of particle (25 nm radius) height above the electrode (15 nm radius) surface. Current drop as a function of lateral position of the particle from the center (at 0 nm) of the electrode (15 nm radius) **(c)** when the particle is smaller (radius 5 nm) than the electrode and **(d)** when the particle is larger than electrode (radius 25 nm). The dotted line indicates the radius of the electrode.

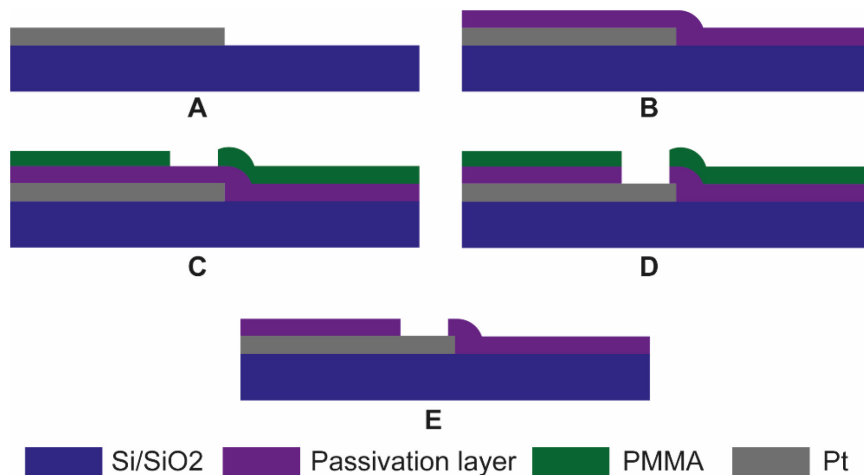## 6.2.2 Fabrication of the nanodisc electrode



**Figure 6.5**: Schematic diagram showing the fabrication process of recessed nanodisc electrode. **(a)** Contact pad and lead wires are pattered on thermally oxidized Si wafer using optical lithography and metal lift-off process. (b) A passivation layer ($Al_2O_3$, 20 nm) is grown using atomic layer deposition method. (ALD layer is conformal and for simplicity here it is shown as polarized) **(c)** PMMA resist is patterned to define the nanometer sized hole using the electron beam lithography. **(d)** Ion beam (Argon) etching is used to etch the passivation layer using PMMA as an etch mask. **(e)** PMMA is rinsed-off in acetone to obtain the recessed nanodisc electrode geometry.

Since the recessed electrode geometry favors the highest current drop, as observed from the simulation results, we fabricated only recessed nanodisc electrodes for the experimental studies. We used a rather simple method for nanodisc fabrication, as illustrated in **Figure 6.5**. The fabrication started with a thermally oxidized (300 nm) Si <100> wafer. Photoresist (Olin-17) was spin coated on the substrate and using an optical lithography mask, contact pads and leads were patterned onto it using a mask aligner (EVG 620). An electron-beam metal evaporator (DCA Metal-600) was used to evaporate Ti (adhesive layer, 5 nm) and Pt (50 nm) on the substrate followed by a lift-off process in acetone to remove photoresist and the unwanted metal from the substrate. Subsequently, the substrate was uniformly coated with $Al_2O_3$ (20 nm) using atomic layer deposition (Picosun). Later, the passivated substrate was spin coated with PMMA

photoresist and using electron beam lithography (Raith 150^TWO), dots were patterned on the PMMA at the tip of the lead wire. Successively, using PMMA as mask, the $Al_2O_3$ passivation layer was etched by an Ar ion beam etching (Oxford i300) process. This process opened up the recessed nanodisc electrodes by locally removing the $Al_2O_3$ passivation layer. An in-plane reference electrode (Pt) was also patterned and etched to avoid the usage of an external reference electrode. Later, the PMMA mask layer was rinsed-off in acetone. As the final step, the substrate was cleaned in oxygen plasma to get rid of any left-over organic residue. It also helped in removing oxygen vacancies in the passivation layer, and improved its insulating properties.
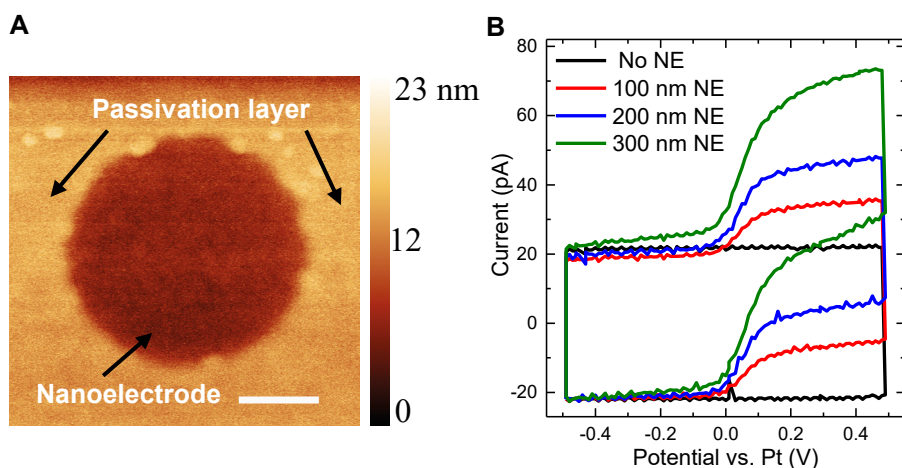
**A**



**B**



**Figure 6.6: (a)** Atomic force micrograph showing a recessed nanodisc electrode and the passivation layer around it. (Scale bar = 100 nm) The false color scale shows the height profile. **(b)** Cyclic voltammogram for 2 mM Fc(MeOH)$_2$ in 2 mM KCl at a scan rate of 50 mV/s on nanodisc electrodes with diameter 100 (red), 200 (blue) and 300 nm (green) and device without nanodisc electrode (black) versus a platinum reference electrode.

Nanodisc electrodes with different diameters were fabricated for a comparative study. Although we are interested in making nanodiscs with smaller diameters (30 - 50), for easiness in fabrication for the first generation of device, we made devices with 100, 200 and 300 nm diameters. The electrodes were characterized using atomic force microscopy (AFM). **Figure 6.6 (a)** shows the AFM image of the nanodisc electrode with a diameter of 300 nm. The recessed electrode (dark area)

and the passivation layer (lighter area) around it can be observed in the image. Cyclic voltammograms (CV) were obtained for 2 mM ferrocene dimethanol (Fc(MeOH)$_2$) in 2 mM KCl at scan rate of 50 mV/s on the nanodisc electrodes against an on-chip Pt reference electrode and presented in **Figure 6.6 (b)**. It can be observed that, well past the formal potential, the current approaches the steady-state current. The formal potential is shifted to 0.1 V due the on-chip Pt reference electrode. The control device without nanodisc electrodes, yielded no steady-state current as anticipated; it behaved like an ideal capacitor showing a *box*-like *IV* response based on the CV scan rate. Compared to the calculated limiting currents using **Equation (6.1)**, our devices showed lower currents. 100 nm and 300 nm devices showed 23% discrepancy, while 200 nm device yielded 35% less current. This discrepancy might due to the incompletely etched Al$_2$O$_3$ covering the electrode surface or some organic layer that has adsorbed onto the electrode during the fabrication process which effectively reduced the total electrode surface area.

### 6.2.3 Single-particle detection

Particle blocking experiments with insulating latex nanoparticles (40 nm) were performed on the nanodisc electrodes with 300 nm diameter. Chronoamperometry was used to record the current-time transient response on the electrode in the absence and presence of nanoparticles. According to **Equation (6.2)**, the collision frequency of the nanoparticle on the electrode can be increased by using a lower concentration of supporting electrolyte. Hence, here we used 2 mM Fc(MeOH)$_2$ as redox mediator, but without any supporting electrolyte in the solution. Collision events are mainly three types: (1) *hit and stay* (2) *hit and run* and (3) *wobbling*. For *hit and stay* events, the particle hits the electrode surface, adsorbs onto it and stays there, while for *hit and run*, the particle hits the electrode and moves away. On the other hand, if a particle comes near an electrode and wobbles over its vicinity and leaves afterwards, this is considered a *wobbling* event. **Figure 6.7** shows a few selected collision events on a 300 nm nanodisc electrode. The signal to noise ratio was ~6.5, which helped to clearly distinguish a collision event from the background noise.
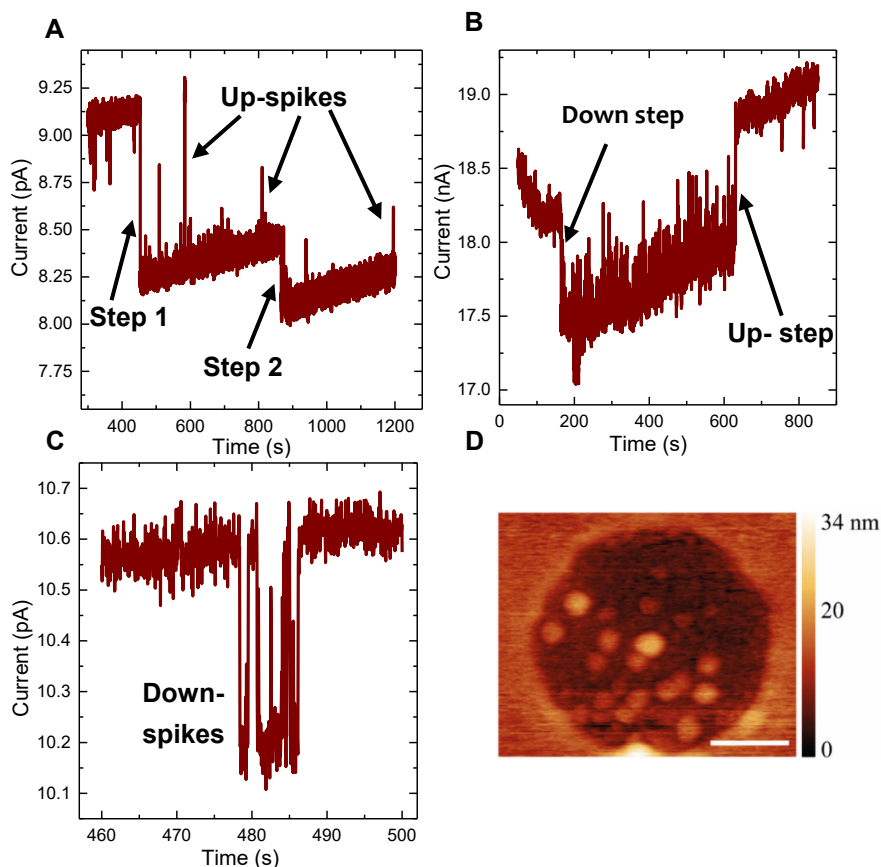
**Figure 6.7**: Current-time (I-t) transients of nanoparticles (40 nm) on nanodisc electrodes (300 nm). **(a)** Zoom-in of the part of the I-t curve showing discrete current blockage steps and up-spikes. **(b)** A part of the I-t curve showing adsorption and desorption of a nanoparticle. **(c)** A part of the I-t curve showing a wobbling particle in the vicinity of the electrode. **(d)** Atomic force micrograph of 300 nm electrode after nanoparticle detection experiment. The false color scale shows the height profile. (Scale bar = 100 nm)

**Figure 6.7 (a)** shows two *hit and stay* events and many *wobbling* events (up-spikes and down-spikes). The first *hit and stay* event (step 1) showed a ~10 % current drop while the second event showed ~5 % current drop. The first step has a relatively larger current drop, while the second step is around the estimated range. The current drop at the electrode, depends on the size and position of the particle. The latex nanoparticles are not homogenously distributed, hence a bigger particle

can cause a higher current drop. Moreover, as mentioned in **Section 6.2.1**, a particle hit at the edge of the electrode can also produce a higher current drop. Another reason could be the reduced surface area of the electrode to start with, which reduced the limiting steady-state current as mentioned earlier. Nonetheless, each *hit and stay* event can be individually resolved, underpinning the ability of single-particle detection using the nanodisc electrode geometry. It is also anticipated to have less current for later events since the background current is already reduced by the previous events. Most of the *hit and run* events (down-spikes), resulted in a current drop of 2 – 4% with a time duration less than 500 milliseconds. Some particles which were adsorbed on the surface stayed for a few seconds and then desorbed from the electrode surface. Adsorbed particles can also rearrange on the electrode surface, giving rise to extra steps or abrupt increases in the current. **Figure 6.7 (b)** shows such an event (both adsorption: down step and desorption: down step) where the particle stayed for several hundreds of seconds before being desorbed.

**Figure 6.7 (c)** shows a wobbling event where the particle wobbles over the electrode without being adsorbed on the electrode and leaves after a few seconds. **Figure 6.7 (d)** depicts the AFM image of the nanodisc electrode after chronoamperometric measurements. Compared to the AFM image in **Figure 6.6 (a),** one can easily notice that the nanoparticles are adsorbed on the electrode. It can also be observed that the sizes of adsorbed particles are not uniform, and the particles are absorbed in the middle as well as at the edge of the electrode, corroborating the difference in the current drop. Although we observed many collision events on the nanodisc electrodes with the latex nanoparticles, the collision rate was much lower than expected, for particles without any supporting electrolyte. This has to be investigated further in order to optimize the collision frequency of a biosensor involving nanodisc electrodes. Furthermore, there is trade-off between the gain of the amplifier and the measurement/data acquisition interval. For higher gains, the measurement interval becomes longer which prevents from measuring a few *hit and run* events. However, for a specific binding the particle stays longer and hence these *hit and stay* events is not affected from this trade-off.

## 6.3 Conclusion

In this chapter, the possibility of using a nanodisc electrode for single-particle detection was investigated. We have simulated the performance of different geometries of the nanodisc electrode and ascertained that the recessed nanodisc electrode provides the largest current drop for individual collision event. As a result, we fabricated recessed nanodisc electrodes of different sizes and validated their performance electrochemically. The cyclic voltammetry results were as expected, and the limiting currents were linearly proportional to the radius of the electrodes. Later, we used nanodisc electrodes for single-particle detection experiments using 40 nm carboxylated latex particles. Although the current drop was different than expected, individual collision events were easily discernable, thanks to high signal to noise ratio. Apart from *hit and stay* events, we also observed *hit and run* and *wobbling* events. The AFM images elucidated the adsorption of particles on the nanodisc electrodes after the I-t measurements. Although we have to optimize a few things like collision frequency and the amplitude of current drop in the future, this proof-of-concept experiment revealed the potential of using the nanodisc electrodes for counting individual particle for biosensing applications. This can be highly beneficial for the detection of very rare bioparticles individually.

## 6.4 Materials and Methods

### 6.4.1 Chemicals and Reagents

1, 1' –ferrocene dimethanol, $Fc(MeOH)_2$, as redoxactive mediator, potassium chloride, KCl, as supporting electrolyte were purchased from Sigma-Aldrich B.V, the Netherlands. Carboxylated latex nanoparticles (40 nm) were acquired from ThermoFisher Scientific, Netherlands. All solutions were prepared using Milli-Q water and experiments were carried out at room temperature.

### 6.4.2 Amperometric measurements

2 mM $Fc(MeOH)_2$ was prepared in Milli-Q water with 2 mM KCl as supporting electrolyte for the nanodisc electrode cyclic voltammetry validation experiments. On-chip Pt reference electrode were used throughout the experiments. For single

particle detection experiments, 2 mM $Fc(MeOH)_2$ was prepared in Milli-Q water without any supporting electrolyte. At first, the cleaned (oxygen plasma treated) nanodisc electrode (100 nm) chip was rinsed with MilliQ water and then a 10µL droplet of 2mM $Fc(MeOH)_2$ with carboxylated sulfate latex beads (16 µM of 40 nm) were pipetted onto the chip surface. The chronoamperometry experiments were then performed on the nanodisc electrode. The voltage on the electrode was kept at 0.3 V while Pt on-chip reference electrode was biased at -0.3 V.

## 6.5 References

1.  Colás, J. J., *Dual-Mode Electro-photonic Silicon Biosensors*. Springer International Publishing: 2017.

2.  Baker, L. A., Perspective and Prospectus on Single-Entity Electrochemistry. *Journal of the American Chemical Society* **2018,** *140* (46), 15549-15559.

3.  Vollmer, F.; Arnold, S.; Keng, D., Single virus detection from the reactive shift of a whispering-gallery mode. *Proceedings of the National Academy of Sciences* **2008,** *105* (52), 20701-20704.

4.  Quan, Q.; Floyd, D. L.; Burgess, I. B.; Deotare, P. B.; Frank, I. W.; Tang, S. K.; Ilic, R.; Loncar, M., Single particle detection in CMOS compatible photonic crystal nanobeam cavities. *Optics Express* **2013,** *21* (26), 32225-32233.

5.  Zhi, Y.; Yu, X. C.; Gong, Q.; Yang, L.; Xiao, Y. F., Single nanoparticle detection using optical microcavities. *Advanced Materials* **2017,** *29* (12), 1604920.

6.  He, L.; Özdemir, Ş. K.; Zhu, J.; Kim, W.; Yang, L., Detecting single viruses and nanoparticles using whispering gallery microlasers. *Nature nanotechnology* **2011,** *6* (7), 428.

7.  Dantham, V. R.; Holler, S.; Barbre, C.; Keng, D.; Kolchenko, V.; Arnold, S., Label-free detection of single protein using a nanoplasmonic-photonic hybrid microcavity. *Nano letters* **2013,** *13* (7), 3347-3351.

8.  Funke, S. A.; Birkmann, E.; Henke, F.; Görtz, P.; Lange-Asschenfeldt, C.; Riesner, D.; Willbold, D., Single particle detection of Aβ aggregates associated with Alzheimer's disease. *Biochemical and biophysical research communications* **2007,** *364* (4), 902-907.

9.   Quinn, B. M.; van't Hof, P. G.; Lemay, S. G., Time-resolved electrochemical detection of discrete adsorption events. *Journal of the American Chemical Society* **2004,** *126* (27), 8360-8361.

10.  Gooding, J. J., Single entity electrochemistry progresses to cell counting. *Angewandte Chemie International Edition* **2016,** *55* (42), 12956-12958.

11.  Steinbock, L. J.; Bulushev, R. D.; Krishnan, S.; Raillon, C.; Radenovic, A., DNA translocation through low-noise glass nanopores. *Acs Nano* **2013,** *7* (12), 11255-11262.

12.  Kang, S.; Nieuwenhuis, A. F.; Mathwig, K.; Mampallil, D.; Kostiuchenko, Z. A.; Lemay, S. G., Single-molecule electrochemistry in nanochannels: probing the time of first passage. *Faraday discussions* **2016,** *193*, 41-50.

13.  Dick, J. E.; Hilterbrand, A. T.; Boika, A.; Upton, J. W.; Bard, A. J., Electrochemical detection of a single cytomegalovirus at an ultramicroelectrode and its antibody anchoring. *Proceedings of the National Academy of Sciences* **2015,** *112* (17), 5303-5308.

14.  Clarke, J.; Wu, H.-C.; Jayasinghe, L.; Patel, A.; Reid, S.; Bayley, H., Continuous base identification for single-molecule nanopore DNA sequencing. *Nature nanotechnology* **2009,** *4* (4), 265.

15.  Bayley, H.; Martin, C. R., Resistive-pulse sensing from microbes to molecules. *Chemical Reviews* **2000,** *100* (7), 2575-2594.

16.  Obergrussberger, A.; Goetze, T. A.; Brinkwirth, N.; Becker, N.; Friis, S.; Rapedius, M.; Haarmann, C.; Rinke-Weiß, I.; Stölzle-Feix, S.; Brüggemann, A., An update on the advancing high-throughput screening techniques for patch clamp-based ion channel screens: implications for drug discovery. *Expert opinion on drug discovery* **2018,** *13* (3), 269-277.

17.  Lemay, S. G.; Kang, S.; Mathwig, K.; Singh, P. S., Single-molecule electrochemistry: present status and outlook. *Accounts of chemical research* **2012,** *46* (2), 369-377.

18.  Bard, A. J.; Fan, F.-R. F.; Pierce, D. T.; Unwin, P. R.; Wipf, D. O.; Zhou, F., Chemical imaging of surfaces with the scanning electrochemical microscope. *Science* **1991,** *254* (5028), 68-74.

19.  Xiao, X.; Bard, A. J., Observing single nanoparticle collisions at an ultramicroelectrode by electrocatalytic amplification. *Journal of the American Chemical Society* **2007,** *129* (31), 9610-9612.

20.     Kwon, S. J.; Fan, F.-R. F.; Bard, A. J., Observing iridium oxide (IrO x) single nanoparticle collisions at ultramicroelectrodes. *Journal of the American Chemical Society* **2010,** *132* (38), 13165-13167.

21.     Sekretaryova, A. N.; Vagin, M. Y.; Turner, A. P.; Eriksson, M., Electrocatalytic currents from single enzyme molecules. *Journal of the American Chemical Society* **2016,** *138* (8), 2504-2507.

22.     Lebègue, E.; Anderson, C. M.; Dick, J. E.; Webb, L. J.; Bard, A. J., Electrochemical detection of single phospholipid vesicle collisions at a Pt ultramicroelectrode. *Langmuir* **2015,** *31* (42), 11734-11739.

23.     Dick, J. E.; Renault, C.; Bard, A. J., Observation of single-protein and DNA macromolecule collisions on ultramicroelectrodes. *Journal of the American Chemical Society* **2015,** *137* (26), 8376-8379.

24.     Arrigan, D. W., Nanoelectrodes, nanoelectrode arrays and their applications. *Analyst* **2004,** *129* (12), 1157-1165.

25.     Bond, A. M.; Luscombe, D.; Oldham, K. B.; Zoski, C. G., A comparison of the chronoamperometric response at inlaid and recessed disc microelectrodes. *Journal of electroanalytical chemistry and interfacial electrochemistry* **1988,** *249* (1-2), 1-14.

26.     Van Andel, E.; De Bus, I.; Tijhaar, E. J.; Smulders, M. M.; Savelkoul, H. F.; Zuilhof, H., Highly specific binding on antifouling zwitterionic polymer-coated microbeads as measured by flow cytometry. *ACS applied materials & interfaces* **2017,** *9* (44), 38211-38221.

*"Opportunities don't happen. You create them."*

*Chris Grosser*

# 7

# *NanoDisc*: from research to business

**Abstract:** This chapter aims at the market feasibility study of the nanodisc particle impact technology under the company name *NanoDisc*, specifically for the cancer diagnosis market. A detailed proposal for the in-depth study of different aspects of the market feasibility study has been done here. We explain both the existing problem with the cancer diagnostics methods and market, and the nanodisc technology as a proposed solution. The main aim of this technology is the label-free electrochemical detection of individual tumor-derived EVs (tdEVs) in body fluids (e.g. blood) with unprecedented sensitivity and specificity. The long-term goal is to deliver an analytical sensing platform for (1) treatment efficacy assessment, (2) diagnosis of symptomatic patients, (3) remission monitoring, and (4) early-stage diagnosis of cancer. However, the technology is not limited to cancer diagnosis. It can be used for any particle analysis, making it suitable for sensing of other bioparticles like viruses, bacteria, enzymes, and in industries like pharmaceuticals and cosmetics, petroleum, food safety, water treatment, environmental pollution monitoring, biodefense, forensics etc.

## 7.1 The problem

According to the World Health Organization, a staggering 9.6 million deaths were reported across the globe in 2018 due to cancer, accounting for 17% of the total deaths. Also, about 18.1 million new cases were reported during the same year. Although the population of Europe accounts for only one tenth of the world, around one fourth of the cancer cases are reported in Europe. The situation is similar in the Americas as well. This implicates that one in five men and one in six women worldwide may acquire cancer at some point in their lifetime and one in eight men and one in eleven women might die due to cancer. The cancer diagnostics involve four main stages: (1) early-stage screening or prediction of cancer occurrence among high-risk populations, (2) diagnosis after tangible symptoms which helps in therapy selection, (3) diagnosis for treatment efficacy monitoring, and (4) follow-up diagnosis for recurrence monitoring.
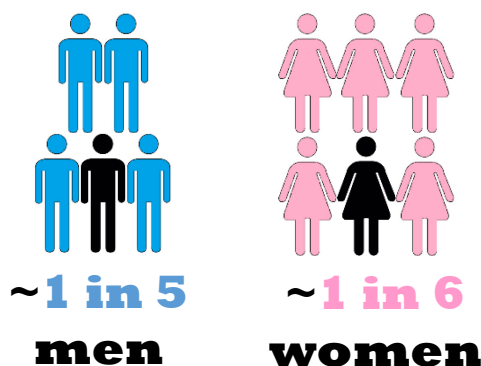


**Figure 7.1**: Illustration showing the risk of cancer among men and women during their lifetime.

The survival rate of patients varies with the type, size, stage and grade of cancer, and age, gender, and medical history of the patient. Globally at present, the five-year prevalence (patients who were able to live 5 years after the cancer diagnosis) amounts to 43.8 million people. Frequent patient monitoring tests are required to select the right treatment for each patient (personalized treatment), to monitor its efficacy and for prognosis of the disease. The existing cancer diagnostic facilities around the world have to cater to more than 65 million patients/

survivors each year. Hence, the importance of reliable, easy and inexpensive diagnostic tools is high for effective cancer patient management. Nowadays, for patient monitoring and prognostics, most of the established approaches use tissue staining, which implies their invasive collection through *e.g.*, biopsies of the tumor comprising surgery or incision. Endoscopic biopsy, another method, is done while the patient is under sedation or anesthesia. Moreover, these methods are time consuming procedures involving pain and posing health risks and the samples may not be easily obtained. Patient follow-up, therefore, requires serial biopsies making it very unpleasant for the patient. Alternatively, in vivo imaging approaches using Magnetic Resonance Imaging (MRI), Positron Emission Tomography–Computed Tomography (PET-CT) and X-ray based imaging (*e.g.* mammography) are used for cancer diagnosis although with a limitation that they cannot detect tumors smaller than ~1 cm. Nonetheless, high cost, radiation problems (for PET-CT and mammography), and the toxicity of required contrasting agents render these tests unsuitable for repeated use. Moreover, patients with bodily implants like pacemakers, defibrillators, coronary stents cannot undergo MRI scanning. Meanwhile, PET-CT demands stringent dietary restriction before undergoing the test. Furthermore, patients feel discomfort and claustrophobic while undertaking these tests and loud noise especially of MRI machines aggravates this uneasiness. Nonetheless, more frequent monitoring of the patient to study the treatment efficacy is crucial for making a more accurate prognosis and prescribing personalized treatment. This demands diagnostic tools with non/less- invasive methods, inexpensive, less patient discomfort, less side effects, high sensitivity and selectivity.

Another important aspect of cancer diagnosis is early-stage detection of the disease. In general, when diagnosed at stage 1 or earlier, when a tumor is small and not metastasized, the survival rate is ~90% for most type of cancers. However, if diagnosed at stage 4, the survival rate plummets to ~20%. Early diagnosis helps in providing effective treatment, resulting in high probability of survival, and less expensive treatment. When the patient is diagnosed with cancer at a later stage, curative treatment becomes challenging. This underscores the need for early diagnosis of cancer. The screening among a high-risk population can help in detecting cancer at early stages, which in turn facilitates in providing efficient and

personalized treatment. In order to conduct screening of a vast population with a relatively high risk-factor, an inexpensive and accurate diagnostic tool is essential. However, for most of the cancer types, early-stage screening tests are not available yet. Among those screening tests that are available, apart from a few like the Pap test or PSA test, most of them utilize imaging using MRI, PET-CT, X-ray or endoscopic procedures that bring about the aforementioned limitations. These conventional methods depend on the phenotypic properties of the tumor. Consequently, screening tools/devices that can test patients' samples taken by no-/less invasive methods are highly sought after.

Cancer markers that are available in body fluids are an alternative target. Although many detection schemes for sensing these markers were reported, hardly any techniques evolved into a clinical product. The frequent point of failure is the low concentration of these markers that demands diagnostic tools with high sensitivity. The major challenge, especially working with low concentrations, is to bring these markers to the sensor within practical time scales. Hence, without methods to actively direct markers to the sensor surface, highly sensitive detection is almost not feasible.

## 7.2 The proposed solution

As mentioned before, cancer markers that are available in body fluids are an alternative for the invasive sample collection by biopsy of a tumor tissue. Liquid biopsy is a simple and effective non-invasive sample collection method (compared to surgical biopsies) that provides enough information about a tumor through a simple body fluid sample. The body fluids can be blood, urine, saliva, seminal plasma, cerebrospinal fluid, lacrimal fluid etc. As described earlier, biomarkers like CTCs, ctDNA and tdEVs available in bodily fluids are highly promising targets for diagnostic, prognostic and predictive cancer detection. Since blood is the most common liquid biopsy sample, henceforth we consider blood or plasma as the sample of interest. The collection of blood samples from patients is a much quicker and convenient procedure for them involving minimal pain/ risk compared to the complex surgical or endoscopic biopsy. Thus using liquid biopsy, the diagnosis can be easily repeated periodically for disease progression and

treatment efficacy. Additionally, this helps in cancer detection long before it would trigger clinical symptoms or appear on imaging scans.

Each patient's cancer is different and it also changes over time requiring continuous monitoring of the patient for a personalized treatment regime. Hence, as a result of clinical propensity towards personalized precision therapy and advancement in selective and targeted therapeutics, the demand for accompanied diagnostic tools have increased a lot during the last decade. Considering tdEVs as the monitoring cancer biomarker, an effective therapy should result in a reduction or elimination of tdEVs in the blood, providing information about tumor regression in accordance with therapy. The value proposition of *NanoDisc* in treatment efficacy assessment is its ability to assess the number and type of tdEVs with a relatively simple test, using blood samples at more frequent intervals. It can be a very useful patient monitoring tool for frequent analysis of tdEV presence in bodily fluids. Moreover, after the treatment the survivors should undergo frequent follow-up care for remission monitoring and prognosis. Most of the times, this is done with imaging techniques to view the growth of new tumor at the primary location or a secondary location. However, due to the limitation in resolution of the imaging methods, small tumors are not detected and hence by the time a new growth can spot with imaging, the cancer might be progressed to a later stage making it difficult for curative treatment. Cancer can recur as late as 20 years e.g. in breast cancer survivors, after the treatment of the primary tumor. The presence of tdEV can provide an early indication of recurrence of cancer making it possible to prescribe the patient an early treatment to prevent or limit the relapse.

Occluded by billions of red blood cells and millions of white blood cells, only a few (typically <10) CTCs are present per milliliter of blood. The scarcity of CTCs hinders the statistical robustness of these measurements. The case of ctDNA is also similar since the it is vastly outnumbered by cell-free DNA circulating in the blood. The relatively high abundance of tdEVs compared to CTCs ($10^3$ fold higher) and ctDNA makes tdEVs much more appealing for cancer disease management. Their prognostic value was recently proven in breast, prostate, colon and lung cancer. If an accurate technique for the quantification of tdEVs in blood would exist, real-

time, personalized therapy adjustments could be based on statistically much more reliable liquid biopsy results. *NanoDisc* technology can be used for real-time quantification of individual tdEVs by screening minute volumes of patient sample. The selectivity required for this is provided by the chemical modification. The necessary sensitivity comes from the principle that the size of the electrodes corresponds to the size of the electrodes. Most importantly, the high throughput of the sensor is due to the electrophoretic transport of the analyte to the sensor array, which overcomes the analyte transport limitation. As a result, our device can detect cancer markers (tdEVs) individually from blood at a rate that gives useful results much faster.

As mentioned earlier, the detection of cancer at early stages increases the chance of patient survival. The early detection helps the oncologists to prescribe a curable therapy before the cancer is advanced. However, in order to detect the cancer at an early stage, a population-wide screening test should be organized at least among the high-risk population. Imaging the whole body searching for a small tumor (at early stage) with relatively low probability of occurrence is almost unachievable. Nonetheless, the presence of tdEVs in body fluids at early stages makes them an early-stage cancer biomarker. It can also provide information about the type and subtype of cancer, making it highly interesting. Our *NanoDisc* technology can thus be used as a non-invasive cancer sensing platform to monitor treatment efficacy, remission monitoring and prognosis and for early-stage diagnosis of cancer at the point of care.

## 7.3 NanoDisc technology

NanoDisc technology is based on nanoelectrodes that can be used as nanosensors for nanoparticle detection applications, especially in the LOC-based biosensing field. The initial focus of the technology is to detect tumor-derived extracellular vesicles (tdEVs) from body fluids (e.g. blood). These are submicron biological particles shed by (cancer) cells, that are recognized for their prognostic value in cancer diagnostics, being higher than that of MRI-scans. There are currently no other techniques commercially available, or even reported in literature, that can measure tdEVs from blood samples at physiologically relevant concentrations.

NanoDisc technology can useful in measuring these tdEVs one by one providing an ultra-high sensitivity.

The NanoDisc sensor consists of an array of chemically modified, disc-shaped nanoelectrodes functionalized with antibodies that can recognize tdEVs. The fabrication of the electrode involves standard micro-/nanofabrication techniques, making it highly scalable and suitable for integration. Electrolysis of a redox mediator on the nanoelectrodes produces a background current and simultaneously an electrophoretic force attracting the tdEVs onto the electrode. This latter is a crucial and unique feature of our technology that makes the measurement orders of magnitude faster (typically several minutes). With diffusion alone, mass transport of analytes (such as tdEVs) to the sensor surface is extremely slow and consequently, it is impossible to detect analytes at low concentration in practical time scales in passive systems. Since the electrophoretic force attracts all particles that are oppositely charged compared to the applied potential on the nanoelectrode, a highly effective anti-fouling layer is crucial to minimize the non-specific binding of particles onto the electrode surface. To this aim, the surface of the nanoelectrodes is chemically modified with an anti-fouling layer (zwitterionic polymers or poly(ethylene glycol) layers) functionalized with tdEV-specific antibodies (e.g. anti-EpCAM), to enhance specific binding and avoid non-specific binding. When an analyte with a size comparable to that of the electrode approaches, the redox current is obstructed, giving a detectable "off signal" (see Figure 1c). The interaction strength of a tdEV with the specific antibody on the electrode determines the duration of this signal: chance encounters based on non-specific binding (blue curve) will yield short dips after which the system returns to the "on signal", whereas specific binding will be more stable (red curve). Thus, statistic information of the current change duration helps to distinguish false positives and false negatives. This allows for highly selective detection of target analytes. In addition to this, it was also experimentally and theoretically identified that recessed nanoelectrodes produce higher SNR due to the shielding of the high electric field that is generated at the edge of the electrodes. Moreover, when the size of the nano electrode matches the size of the tdEVs, SNR increases further. This high SNR enables single tdEV detection. Figure 1 shows the schematic representation of the sensor and the

tdEV detection scheme. Since we measure the presence of tdEVs one by one, the sensitivity is extremely high.

## 7.4 Innovation aspects

The central point of this technology is developing a LOC diagnostic system for personalized treatment, prognostic diagnosis and early detection of cancer (and other diseases). Innovative aspects of *NanoDisc* technology are:

- Single-particle detection of tdEVs (reduces *false negatives*)
- Able to distinguish specific and non-specific particle detection (minimizes *false positives*).
- Edge protected nanoelectrode and compatible size of nanoelectrode (compared to size of tdEVs) provide *high signal to noise ratio*.
- *Particle size* (magnitude change of the current) and *concentration* (specific particle binding event per unit time) can be determined
- *Faster measurements* (in few minutes) even at low analyte concentration (thanks to particle attraction owing to electrophoretic force).
- Uses sample collected by less or non-invasive methods. (*reduces patient discomfort and helps frequent diagnostics*)
- Useful for (i) disease screening for *early-stage diagnosis*, (ii) *treatment efficacy* monitoring for personalized treatment and (iii) patient follow-up for *remission monitoring* and (iv) diagnosis of *patients with symptoms* (*four stage diagnostic applications*).
- Single-particle detection of other biological particles like virus, bacteria, particles with nucleic acids etc. as well as single particle analysis of non-biological particles (*diverse applications*).
- Individually accessible mass-producible array of nanoelectrodes for (i) enhanced sensing area and/or (ii) multiple analyte analysis (*scalable technology*)
- Cheap fabrication methods and easy integration into a *portable measurement setup.*

## 7.5 Commercial aspects

As of 2016, the global market for non-invasive cancer diagnostics is $110 billion which is highly dominated by imaging technologies like MRI, PET-CT and mammography. At the same time, according to a 2016 report by financial analysts

JP Morgan, by 2020 the liquid biopsy market is estimated to grow up to $22 billion including $14 billion for prognosis, treatment efficacy and symptomatic diagnosis. The liquid biopsy market has a staggering projected compound annual growth rate (CAGR) of 15 - 20% as summarized by various studies underscoring its high potential in the market. Based on the benefits of liquid biopsy one would expect the liquid biopsy market to take over the major share of the non-invasive diagnostics market.

In order to identify the right niche market where the *NanoDisc* devices can be introduced, the different segments of the cancer diagnostic market have to be recognized first. As discussed earlier, based on application the cancer diagnostics market is further segmented into four: (1) cancer screening among high-risk populations, (2) cancer diagnosis of symptomatic patients and treatment selection, (3) treatment efficacy assessment, and (4) recurrence monitoring. tdEVs are capable of being used in all the four segments. However, since the concentration of tdEVs is much higher in the treatment phase, it will be easier to initially focus on the 'treatment efficacy assessment segment'. In the treatment phase, the type, subtype, stage, location, size and extensiveness of the primary tumor is known. As a result, the treatment efficacy diagnosis helps to create an extensive database of tumors based on all these factors. This database can be highly beneficial when the technology is employed in other market segments, like recurrence monitoring, symptomatic diagnosis and early-stage screening. Thus, these markets can be targeted later. Furthermore, even before the technology can be used for cancer diagnosis, the *NanoDisc* devices can be sold to research laboratories focusing on different amplifications which demands no certification and clinical trials of the devices. This can generate both revenue and valuable feedback about the existing technology. Based on this feedback, we can address the problems quickly and the next generation of devices can be redesigned and optimized to improve the sensor performance. **Figure 7.2** shows the stages of potential market intervention for NanoDisc technology.
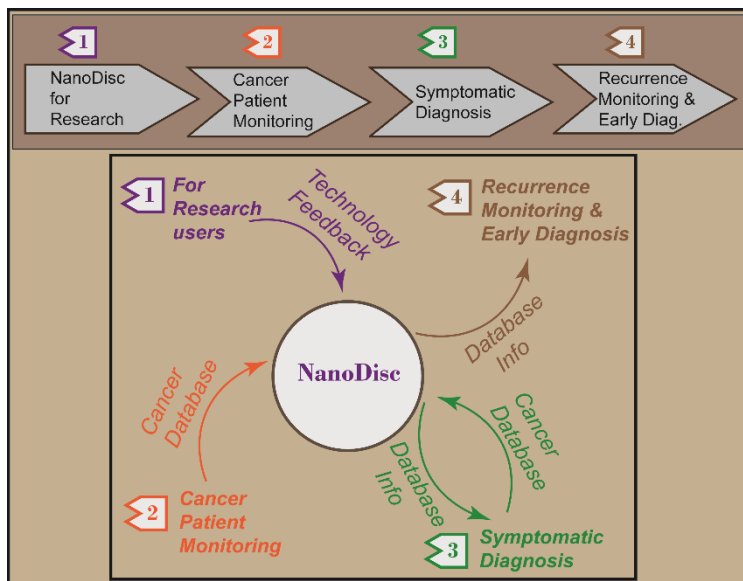
**Figure 7.2**: Product roadmap of *NanoDisc* for near-term: (1) the current generation of *NanoDisc* devices can be sold for research applications (2) After the clinical trial approvals and certifications *NanoDisc* can be sold for cancer patient monitoring  (3) later for cancer diagnosis of patients with tangible symptoms and (4) for recurrence monitoring and early diagnosis. Feedback and feedforward information available at each stages are also shown.

The NanoDisc based sensing platform will consist of three modules: (1) a sensor chip (disposable cartridge) with an array of nanodisc electrodes, (2) a portable sensor platform with electrochemical measurement and sample handling hardware and (3) a software to manage the real-time sensing and data analysis. **Figure 7.3** shows these marketable products that are necessary for the *NanoDisc* sensing technology. The costs per test is dependent on the subscription cost of the software, the cost of the portable sensing platform and the cost of the individual cartridge. In any case, the costs per test have to be low compared to conventional diagnostic methods in order for the test to be performed routinely resulting in a higher benefit-cost ratio. The production cost of *NanoDisc* systems are expected to be very competitive with other tests (e.g. CellSearch) since the nanofabrication is based on simple techniques and involves only a few steps, and the surface modification can be massively parallelized. To get a good estimate of

the actual production costs will be one of the goals of the feasibility study. NanoDisc will manufacture the disposable cartridge and sell them to hospitals, oncologists, general practitioners, laboratories, scientific research labs etc. The cartridge will consist of an array of nanodisc electrodes that can be used for (bio)particle analysis. The software development and the manufacturing of the portable sensing platform can be outsourced (at least in the initial stages).
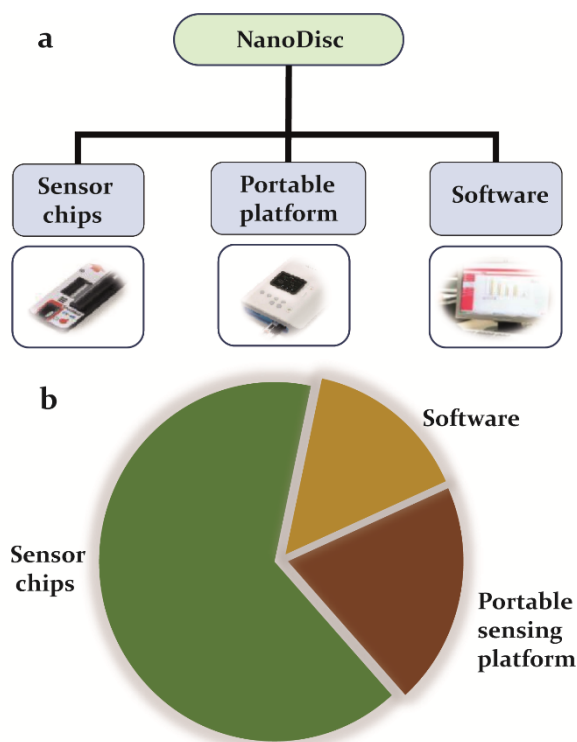


**Figure 7.3: (a)** Tree diagram showing the different marketable products based on NanoDisc technology. It consists of sensor chips (cartridge) with array of nanodisc electrodes, portable sensing platform which helps in electrochemical measurements and software which manages the sensing technique. *Pictures of the products are for illustrative purposes only.* **(b)** Pie chart showing the potential (estimated) cumulative annual revenue from each product.

Commercial tdEV detection methods are hardly available. This will give us a highly desirable first-mover advantage in the market. At the moment, there are a few companies that are active in general EV (*not tumor derived*) characterization from concentrated samples are Systems Biosciences, Hansa Biomed, Biovision. Similarly, only a very few commercial quantification methods of alternative targets like CTCs and ctDNA are available. In Table 1, a comparison is made between different available cancer sensing platforms with our proposed *NanoDisc* technology. We believe that the main advantage of *NanoDisc* will be its highly selective and sensitive detection resulting in less false positives and negatives and the analyte enrichment on sensor surface due to electrophoretic force. Moreover, the diagnostic and prognostic value of *NanoDisc* is also very high compared to other techniques.

**Table 7.1:** Comparison of different available cancer sensing platforms with *NanoDisc*

| Technology | Technological Readiness | Diagnostic Value | Prognostic Value | Invasiveness | Cost |
|---|---|---|---|---|---|
| Solid biopsy | ***** | **** | *** | ***** | ***** |
| MRI | ***** | *** | *** | *** | **** |
| PET-CT | ***** | **** | *** | **** | **** |
| Circulating Tumor Cell quantification | **** | **** | **** | * | *** |
| Circulating nucleic acid screening | *** | **** | *** | * | *** |
| NanoDisc | ** | ***** | ***** | * | ** |

In addition to cancer diagnosis *NanoDisc* can be applied for other different applications. Basically, it can be used as a particle analyzer platform particularly for small particle (nanometer sized) analysis. Consequently, other potential commercial sectors for *NanoDisc* technology are:

- Biosensing: Virus, bacteria, insulin, other enzymes etc.
  - Food safety: pathogen detection
  - Water treatment
  - Biodefense
  - Forensics
- Pharmaceuticals & cosmetics
- Analysis of opaque liquids: Petroleum Industry
- Plastic and ceramic manufacturing
- Small particle analysis

## 7.6 IP Position

A patent with the title "Sensor for particle detection" (*EP19160822.3*) has been filled on 5 March 2019 (priority date) with 15 claims. An international application will be filed within the priority period and a continuation of the patent will be applied in Europe, USA, Australia, Canada, Japan, India, China and South Korea. We expect that the innovative aspects of this detection method are unique and novel enough to produce a positive outcome for the patent application. The cost of patent application will be covered by the patent fund of the University of Twente, which demonstrates their enthusiasm about our technology and business development team. Furthermore, we will aim to produce more patents in course of time related to core device technology, different applications, system integration etc.

As an early revenue stream, *NanoDisc* devices can be sold to research laboratories and centers for different research activities. This does not require any certification or stringent clinical approval from authorities like FDA. In addition to revenue generation, this will also provide valuable research user feedback about the device and technology which can be used later to improve the sensor performance. Apart from the patent, we hope to develop a cancer marker

database from our product which focuses on patient monitoring and prognosis. This will provide vast amount of accurate data regarding the about different types and subtypes of cancer and types of specific markers associated with them. These data help further for launching the *NanoDisc* sensor for prognostic and early-stage cancer screening tests. Furthermore, copyright of the sensor software and astute branding strategy can be useful for a unique IP position.

## 7.7 Project plan for feasibility study

The purpose of this project is to conduct a detailed feasibility study of the business idea. We intend to scout different success-determining aspects and components of our business idea through a systematic, organized and comprehensive feasibility study. A detailed feasibility analysis can further deepen our knowledge beyond the preliminary peripheral estimation to a greater understanding about the viability of our business idea and which can be useful in attracting prospective business investors. Some of the aspects that this feasibility study will focus are as follows:

*Market feasibility:*
A feasibility study here will include a thorough market analysis of the current and future market potential, relevant competitors, prospective sales opportunity and potential customers and end-users. A detailed market analysis has to be done in order to strategize and optimize financial goals, production and business operations. It also helps to assess the market size and the potential growth the company can aspire for. An opportunity assessment facilitates the appraisal and understanding of market opportunities as well as risks involved. A detailed opportunity assessment should also include user requirement analysis that identifies the potential customers and end-users and exploring their actual requirements, unmet needs and priorities. Market analysis can also examine whether cancer diagnosis is the right market to focus and can also identify the other possible market beyond cancer diagnosis. The market analysis will also include a competition assessment. This gives insight into the competitors, their strengths and weaknesses that can be utilized to formulate the strategy of our company.

*Financial feasibility:*

A financial feasibility assessment allows us to estimate the cumulative funding needed to run the company for a first few years especially before we obtain the necessary regulatory approvals to step into the cancer diagnostics market. Meanwhile it can also provide us valuable information regarding different revenue streams which can be used to develop a five/ten year financial projections and also provide information about the breakeven point and profitable stage in the business. This assessment will also study the financial performance of similar businesses and assimilate their strategies to improve ours. Moreover, a financial feasibility study helps in identifying and mitigating the financial issues that can occur in the first few years of the company. Furthermore, the various strategical and financial scenarios can be examined and their implications, strengths and weaknesses can be assessed. It helps in providing interesting information about the financial prospects of the company for potential business investors, bankers and other monetary sources. The most influencing factor regarding the financial viability of the project depends on the marketability of our device which in turn depends on the price and volume of the products sold. Thus a correlated study of the market and financial analyses can reveal the different aspects of marketability. Our proposed method of project implementation will also be evaluated in terms of financial feasibility (Current method analysis). This will help to further understand the strengths and weaknesses of our current approach. These pros and cons identification can help save both money and time in the future and restructure the implementation strategy of the business.

*Organizational feasibility:*

We have already identified the roles of our available organizational resources based on their skills and experiences. However, during the feasibility study, we will perform an analysis to recognize the approaches to further improve the organizational resources by formulating the future organizational structure of the company to optimize human resource in order to maximize the operational and financial performance of the company. This helps in identifying and attracting people with relevant expertise (*e.g.* as advisory members or direct employees) to get the company off the ground and keep it operational. Furthermore, with organizational feasibility analysis we can identify the possibilities of establishing

favorable strategic partnerships with potential collaborators, suppliers as well as prospective customers. Organizational resources assessment will also identify the potential business investors who are specifically interested in cancer biosensing field. We may also contact bigger biosensing companies to understand their interest in collaborating, investing or acquiring our company in future.

***Technical feasibility:***

A technical feasibility study will focus on identifying the technological challenges of *NanoDisc* devices. It will also focus on critically analyzing similar and/or competitive technologies and assess their strengths and weaknesses. At present we have a technical team working on completing the second level proof-of-concept of the *NanoDisc* technology with tdEVs. After the concept test, a device prototype development is essential for demonstration of the technology to potential customers and business investors. Moreover, these prototypes can be used for beta tests, pilot tests and clinical trials leading to more comprehensive feedback for future improvements of the device. Consequently, as part of the technical feasibility we will also focus on developing a prototype system. Experts from the different fields (like oncologists and sensor experts) will be contacted to get some valuable advice and feedback about our technology and business plan. Furthermore, technical feasibility will also explore the possibility of obtaining intellectual property protection in other key areas. It will also seek alternative technologies for our company.

## 7.7.1 Planned activities for feasibility studies

Different activities will be arranged in order to perform different aspects of feasibility study as identified above. Some of the activates are mentioned as follows:

- The team (as described below) will conduct an internal market analysis
- A detailed search to asses latest trends and development in the market
- Hire services of startup analysts especially for the market analysis in particularly competition analysis and assessment of investor readiness and to prepare financial projects
- Costing of products based on competitor product cost and analysis of anticipated volume of sales

- Seek business investors interested in biosensing field through networking
- Meeting business investors, bankers and other monetary sources for possible investments
- Corresponding with (or assessing by other means) relevant competitors to identify their strengths, weaknesses and strategies
- Contacting bigger biosensing companies to understand their interest in collaborating, investing or acquiring our company
- Meeting potential users (for cancer diagnosis) like oncologist, cancer patients, clinical laboratories for user requirement analysis
- Discussion with potential users at research laboratories for first product sales
- Communicate with particle analyzer companies to identify other possible market opportunities and possible collaboration
- Identifying and attracting people with relevant expertise for the company through networking and assessments
- Communicating with key partners like electrical instrumentation companies for developing a prototype of portable platform and management software
- Making prototype of *NanoDisc* devices for demonstration to potential users, collaborators and investors
- Meeting experts to seek alternative technologies for our company

## 7.8 Milestones and time scheme

**Figure 7.4** shows the major milestones of the company for the next 8 years until the completion of certification and approval of tdEV sensor. The feasibility study will run for six months during Q3 and Q4 of 2019. The main milestones during this feasibility study are as follows:

a) Detailed market analysis
b) Competition analysis
c) Finding and connecting with research collaborators and experts
d) Seeking key partners and developing prototype in collaboration with them for demonstration to potential users, collaborators and investors
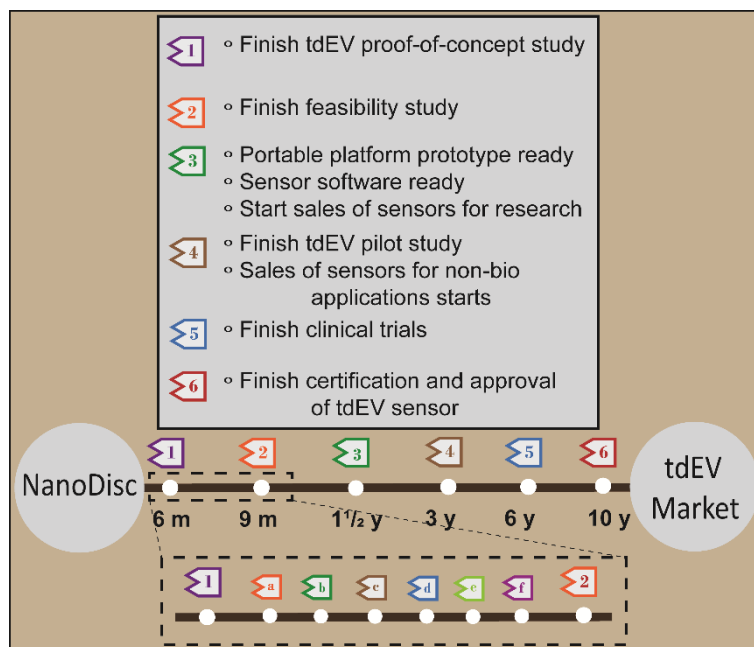e) Communicating with potential users
f) Seeking business investors

**Figure 7.4**: Roadmap showing the milestones with the time plan for *NanoDisc* technology to *hit* the tdEV market. A zoom in of the milestones during the feasibility study is also shown. (*See text below for the legends of feasibility study milestones*)

## 7.9 Project team

In order to be a successful start-up company there should be clear focus on both technological and business aspects of the company. For this reason, we have people working on developing the business as well as maturing the technology. Company's co-founder Mr. Dilu Mathew, MSc will perform the role of the chief executive officer giving emphasis on developing the business idea to a successful start-up. He will coordinate the feasibility study and work towards bringing more funding both for business and for research. The *Metrohm Young Chemist's Award 2018* that he received underscores his ability to foster this project further. Other co-founder Mr. Pepijn Beekman, MSc, Chief Technology Officer, will manage scientific and technological development and work towards the necessary actions for acquiring certifications and approvals based on clinical trials. Both the co-

founders are PhD researchers expecting to graduate in 2019 who has immense experience in electrochemical detection of tdEVs. As the scientific members of board of advisors Prof. W. G. van der Wiel and Prof. S. J. G. Lemay will render their highly valuable scientific knowledge and project managerial experience for the development of the company.

Furthermore, NovelT, Enschede, help us in providing useful information to lead a new successful innovative business. They also provide help in patent application, knowledge and technology transfer advice, legal advice, networking with prospective business investors etc. Dr. Roy Kolkman (Manager Knowledge & Technology Transfer) and Mr. Semme Moolenaar (Business Developer) have been connected with us since the inception of the idea of the company.

## 7.10 Conclusion

The *NanoDisc* technology is an extremely promising method for a highly sensitive and selective detection of single particles. By the valorization of this technology, millions of people across the globe can potentially benefit by increasing their quality of life. Nonetheless, the potential of this technology to scale up and be useful for other industrial applications, helps to make it stand out in a business plan. A team of highly motivated young entrepreneurial talents (as mentioned in previous section) has dedicated to maximize *NanoDisc*'s impact on society by founding a research start-up (currently ongoing). A feasibility study as mentioned here will help the company to steer their interest based on the actual market requirement.

*"The solution often turns out more beautiful than the puzzle (itself)."*

*Richard Dawkins*

8

# Conclusion and Outlook

We have fabricated three types of nanoscale electrodes and explored their potential use in the biosensing field. The **Nanogap electrodes** described in **Chapter 2** were fabricated with conventional optical lithography without using nanolithography techniques like electron-beam lithography (EBL) or nanoimprint lithography. Fabricating nanoscale devices with conventional optical lithography alone is highly appealing since it enables batch processing of devices and also avoids the usage of expensive equipment like EBL. Using this method, we were able to make nanogaps as small as 10 nm. Later we used these nanogaps for the electrical detection of DNA by performing a conduction enhancement for trapped DNA strands. We could detect the presence of metallized DNA strands trapped across the nanogaps in sub-micromolar concentration. The metallization procedure for DNA conduction enhancement proved to be the challenging part of this detection method. It had to be controlled in such a way that false positives and false negatives are minimized. However, the trade-off between the false positive and false negative detection hampered the sensitivity of this method. Furthermore, the high ratio of "*dead*" to active sensing area was another concern for the nanogap devices, which prompted us to search for alternative device designs. Nevertheless, these nanogaps might be useful for biosensing using electrochemical methods provided that the *dead* sensing area is passivated. It can also be used for other applications, like molecular nanoelectronics.

In order to lower the ratio of *dead* to active sensing area, we designed and fabricated a **nanoscale interdigitated electrodes** (nIDE) array. Furthermore, to

minimize false positives, we also discarded conduction enhancement by DNA metallization. Instead, we employed more widely used electrochemical sensing method. In **Chapter 3**, we electrochemically validated our nIDE devices. The devices proved to produce an amplification of ~36 fold when operated in generator-collector dual mode compared to single mode and also with a high collection efficiency (98.6%). Working without supporting electrolyte, provided an additional 2-fold amplification. Taking advantage of this, we developed an electrochemical DNA sensor using a nanoparticle (NP) DNA sandwich assay, as described in **Chapter 4**. An electrically floating metal nanoparticle in solution can act as a bipolar electrode when it experiences a steep concentration gradient across it. In the presence of NPs, nIDEs produced a 4-fold amplification compared to nIDEs without any surface functionalization, owing to the bipolar effect on NPs and ion enrichment of the ferrocenium ions. With this detection strategy, we were able to detect DNA at 10 pM concentration. Although, it vary a lot under different conditions, the concentration of circulating tumor DNA (ctDNA) in blood, range from a few picomolar to a few nanomolar as mentioned in **section 1.2**. For that reason, our sensor is competent enough to sense ctDNA. However, further optimization has to be done in order to make it suitable for sensing directly in blood or serum. Also, the device design has to be optimized further in order to have an improved sensitivity (sub-picomolar range) of DNA for applications other than ctDNA detection.

Tumor derived extracellular vesicles (tdEVs) are promising cancer markers, which can be used for both early-stage diagnosis and to study the progression of a tumor. Hence, it can be used for both cancer screening and patient management. **Chapter 5** described the capturing of tdEVs on nIDEs, and its quantification. We used a *sandwich* immunosorbent assay on nIDEs, using anti-EpCAM antibodies (capture and reporter) that *sandwich* tdEVs between them. Alkaline phosphatase enzyme tagged to the reporter anti-EpCAM antibody, converted the electrochemically inactive p-aminophenol phosphatase to p-aminophenol, and consequently provided an enzymatic amplification. Meanwhile, the redox cycling of electrochemically active p-aminophenol on nIDEs also offered another amplification. As a result, we were able to quantify tdEVs with a dynamic range of 6 orders of magnitude and a limit of detection (measured) of 10 tdEVs/µl. Our

method is 5 times better in terms of limit of detection and 2 orders better in dynamic range compared to next best reported as discussed in **section 5.2.2**. This unprecedented limit of detection makes our technique applicable for EV detection in a regime of physiologically relevant concentrations (1 to $10^7$ tdEVs/µl). However, further investigation has to be done to quantify tdEVs in blood or serum which contains numerous other particles demanding high selectivity for detection.

Although a plethora of detection schemes, including labelled and label-free techniques with different transduction methods like optical, electrochemical, electrical or mechanical were reported by research laboratories across the globe for many decades, only a handful of those techniques were made available for clinical applications like blood glucose or cholesterol testing kits. One of the main reasons behind this is the reproducibility of the results of these methods/devices with high reliability in analyte quantification. Moreover, many of these sensing systems are not capable of easy integration, not mass producible, or require stringent measurement conditions. Furthermore, the sensitivity of these methods ought to be high enough to detect biomolecules/particles in physiologically relevant concentrations. Consequently, another major challenge, working with low concentrations, is to *bring* the analyte molecules/particles to the sensing area in a limited time. If not addressed properly, this can be the bottle neck in improving the sensitivity of the detection method. However, this can be solved to a certain extent by the flow through of analyte near/over the sensing area. An alternative and very promising method is to benefit from additional forces that actuate the movement of analytes towards the sensing surface, rather than relying on diffusion alone. **Chapter 6** described the usage of the electrophoretic force, in actuating charged particles/molecules, to improve their impact rate on the sensing area. In this chapter, we proposed a method of detection of tdEVs and DNA with NPs with high sensitivity and selectivity using particle impact electrochemistry on **nanodisc electrodes**. This method can be used for time-resolved counting of tdEVs or particles individually, thus providing a very high sensitivity. As a proof of concept, we also demonstrated the detection of individual nanoparticles on the nanodisc electrode. These results indicate that the way to proceed with biosensing is to measure individual, specific binding events of analyte particles/molecules to the sensor, rather than using a collective

binding sensing technique. Hence, sensors like nanodisc electrodes that can measure individual binding events will be the future of biosensing!

# Samenvatting

Kanker is wereldwijd de tweede doodsoorzaak. In 2018 alleen al zijn er wereldwijd 10 miljoen mensen overleden aan kanker en zijn er 18 miljoen nieuwe patiënten bijgekomen. Kanker wordt over het algemeen in een laat stadium gedetecteerd, waardoor genezing vaak niet meer mogelijk is. Het detecteren van kanker in een vroeg stadium draagt bij aan het opstellen en uitvoeren van persoonlijke behandeltrajecten welke de kans op overleven vergroten. Dit benadrukt de urgentie van kankerdetectie in een vroeg stadium. Daarbij komend, worden detectiemethoden waarbij minder tot geen invasieve methoden worden toegepast, steeds belangrijker. Gebaseerd op deze motivaties hebben wij een diagnostisch laboratorium op een chip ontwikkeld welke gebruikt kan worden voor vroegtijdige detectie van kanker. Er zijn verschillende kankerindicatoren bekend die gebruikt kunnen worden voor deze vroegtijdige detectie, bijvoorbeeld circulerende tumorcellen. Geïnspireerd door de betere prognostische en diagnostische eigenschappen van door tumorcellen afgescheiden extracellulaire blaasjes (tumor-derived extra cellular vesicles, tdEVs) en circulerend tumor DNA (ctDNA), worden beide gebruikt voor de vroegtijdige detectie.

Drie verschillende types nanoschaal elektroden zijn gefabriceerd: (i) nanogap elektroden (ii) in elkaar grijpende nanokam elektroden en (iii) nanoschijf elektroden. Het potentieel gebruik van deze elektroden in biologische detectie werd ook onderzocht. Daarnaast is een onconventionele elektronische methode en een meer conventionele elektrochemische methode voor de transductie van signalen door de eerdergenoemde elektroden onderzocht. Hoofdstuk 2 beschrijft het fabricageproces op basis van conventionele optische fotolithografie van het nanogap systeem dat de elektrische transductiemethode gebruikt. Met deze techniek konden wij nanogaps ter grootte van 10 nm maken. Deze nanogaps zijn gebruikt voor DNA-detectie door middel van geleidingsverbetering van de gevangen DNA-ketens over de nanogap. We konden de aanwezigheid van

gevangen en gemetalliseerde DNA-ketens over deze nanogaps in sub-micromolaire concentraties meten. Hoofdstuk 3 beschrijft het fabricageproces van de in elkaar grijpende nanokam elektrodes (nano interdigitated electrodes, nIDEs) en hun elektrochemische validatie. De systemen produceren een 36-voudige amplificatie wanneer ze in de generator-collector duale modus bediend worden ten opzichte van de enkele modus bediening, en ze hebben een hoog opvangrendement (98.6%). Zowel de amplificatie als het opvangrendement zijn hoger dan bij andere gerapporteerde open-systeem alternerende redox systemen. Daarnaast hebben we gedemonstreerd dat de amplificatie met twee keer verhoogd kan worden wanneer het gebruik van een ondersteunend elektrolyt achterwege wordt gelaten. Hoofdstuk 4 beschrijft de biologische detectie van DNA-moleculen met de nIDEs en een alternerende nanodeeltjes assay. Een viervoudige amplificatie wordt verkregen wanneer nanodeeltjes worden gebruikt in combinatie met de nIDEs ten opzichte van nIDEs zonder enkele oppervlakte functionalisatie. Deze amplificatie is het resultaat van het bipolaire effect van nanodeeltjes (drijvend metaal) en ion verrijking van de ferroceniumionen in een oplossing zonder ondersteunend elektrolyt. Door middel van deze methode konden wij DNA in concentraties van 10 pM detecteren. Dit maakt de techniek bruikbaar als ctDNA-detectiemethode voor fysiologische relevante concentraties.

Hoofdstuk 5 beschrijft het vangen van tdEVs op nIDEs en de kwantificatie hiervan door middel van een alternerende immuno sorbent assay op de nIDEs. Anti-EpCAM antilichamen zijn gebruikt voor het immobiliseren en detecteren van tdEVs. Het detectie antilichaam was gefunctionaliseerd met het alkalische fosfatase (alkaline phosphatase, ALP) enzym, welke in staat is om de fosfatasegroep van een substraatmolecuul te splitsen. Dit maakt het anders elektrochemisch inerte molecuul, elektrochemisch actief. Dit biedt een enzymatische amplificatie voor de detectie van tdEV. Naast deze enzymatische amplificatie is een alternerende redoxreactie van de redox-actieve moleculen tussen de nIDEs uitgevoerd als tweede amplificatie. Het resultaat is dat we tdEVs konden kwantificeren in een dynamisch gebied van zes ordegrootes met een (gemeten) ondergrens van 10 tdEVs/µl. In vergelijking met de best gerapporteerde methode is de detectielimiet van onze methode vijf keer beter en

het dynamische gebied is met twee ordegroottes vergroot. Deze ongeëvenaarde detectielimiet maakt onze techniek toepasbaar voor EV detectie in het gebied van fysiologisch relevante concentraties. Hoofdstuk 6 stelt een nieuw type nanoschaal elektrodes voor, de nanoschijf elektroden. We hebben deze elektroden gebruikt voor de detectie van enkele deeltjes op basis van elektrochemie. De unieke eigenschap van deze methode is dat de blootstelling van het analyt (bijvoorbeeld de tdEVs) aan het sensoroppervlak op basis van elektroforetische krachten gebeurt. Dit helpt om de meetsnelheid te verhogen, zelfs bij lage concentraties van het analyt. Deze methode kan vanwege zijn hoge gevoeligheid gebruikt worden voor continue telling van individuele deeltjes. Het kan ook onderscheid maken tussen specifieke en niet-specifieke binding van deeltjes aan het sensoroppervlak, wat ten goede komt aan de selectiviteit. Als demonstratie hebben wij individuele nanodeeltjes op de nanoschijf elektrode gedetecteerd. Het potentieel van de nanoschijf technologie is groot vanwege zijn geschiktheid voor snelle analyses en verminderde kans op foutnegatieve of foutpositieve resultaten. Daarbij komend is het een schaalbare technologie, die de fabricage makkelijker en goedkoper maakt. Dit wordt daarom in Hoofdstuk 7 verder uitgewerkt in de vorm van een commercieel idee. Er is ook patent aangevraagd op deze vinding. Hierbij wordt in de vorm van een marktonderzoek ingegaan op het probleem dat de huidige methoden hebben en de oplossing die onze methode kan bieden. Om samen te vatten: dit proefschrift probeert de verschillende mogelijkheden in de ontwikkeling van een nanosensor voor kankerdetectie te beschrijven.

# Summary

Cancer is globally the second most common cause of death. Cancer burden rises to about 10 million deaths and more than 18 million new cases in 2018. Cancers are often diagnosed at a later stage preventing curative treatment instead leading to only a palliative care. Early stage diagnosis helps in planning and executing a personalized curative regimen which improves patient's survival chance. When a patient is diagnosed with cancer at a later stage, the curative treatment becomes challenging. This underscores the need for early stage diagnosis of cancer. Consequently, screening methods that can test patients' samples taken by no-/less invasive methods capable of early stage diagnosis is highly sought for. Based on this motivation here we developed lab-on-a-chip diagnostic systems for early detection of cancer. Different cancer markers for diagnosis are known including circulating tumor cells. However, inspired by the better prognostic and diagnostic values of tumor-derived extra cellular vesicles (tdEVs) and circulating tumor DNA (ctDNA), here we focused on developing sensing methods for both of them.

Three different types of nanoscale electrodes were fabricated: (i) nanogap electrodes (ii) nano interdigitated electrodes and (iii) nanodisc electrodes. Their potential use in the biosensing field were also explored. We also investigated the possibility of an unconventional electrical method and a more conventional electrochemical method for transduction using the above mentioned electrodes. **Chapter 2** describes the fabrication of nanogap device using conventional optical lithography and DNA detection across it using the electrical method. Using this method, we were able to make nanogaps as small as 10 nm. Later, these nanogaps were used for DNA detection by performing a conduction enhancement for trapped DNA strands across the nanogap. We could detect the presence of metallized DNA strands trapped across the nanogaps in sub-micromolar concentration. **Chapter 3** details the fabrication of nano interdigitated electrodes (nIDEs) and their electrochemical validation. The devices proved to produce an

amplification of ~36 fold when operated in generator-collector dual mode compared to single mode and also with a high collection efficiency (98.6%). Both the amplification and the collection efficiency are higher than other reported open-system redox cycling devices. Moreover, we demonstrated that the amplification can be increased (2 times) further by working without a supporting electrolyte. **Chapter 4** describes the biosensing application of nIDEs using nanoparticle *sandwich* assay for the detection of DNA molecules. In the presence of NPs, nIDEs produced a 4-fold amplification compared to nIDEs without any surface functionalization. This amplification is a result of bipolar effect on NPs (floating metals) and ion enrichment of the ferrocenium ions in a solution without a supporting electrolyte. This method helped us to detect DNA at 10 pM concentration making it competent enough to measure ctDNA in physiologically relevant concentration.

**Chapter 5** describes the capturing of tdEVs on nIDEs, and its quantification using a *sandwich* immunosorbent assay on nIDEs. Anti-EpCAM antibodies, both for capturing and reporting, were used to immobilize tdEVs. The reporter antibody was tagged with alkaline phosphatase (ALP) enzyme that are capable of cleaving phosphatase group of a substrate molecule, thus making the molecule electrochemically active which are otherwise electrochemically inert. This provides and enzymatic amplification for detection of tdEV. On top of enzymatic amplification, redox cycling of the redox active molecules between the nIDEs provides a second amplification. As a result, we were able to quantify tdEVs with a dynamic range of 6 orders of magnitude and a limit of detection (measured) of 10 tdEVs/µl. Our method is 5 times better in terms of limit of detection and 2 orders better in dynamic range compared to next best reported methods. This unprecedented limit of detection makes our technique applicable for EV detection in a regime of physiologically relevant concentrations. **Chapter 6** proposes a new type of nanoscale electrodes which are termed as nanodisc electrodes. We used these electrodes for single particle impact electrochemistry. The unique feature of this method is the active delivery of analyte particles (*e.g.* tdEVs) onto the sensor surface using electrophoretic force. This helps to improve the measurement speed even in a low concentration of the analyte. This method can be used for time-resolved counting of particles individually, thus providing a very

high sensitivity. It also allows to distinguish between specific and non-specific binding of particles on the sensor surface improving the selectivity. As a proof of concept, we also demonstrated the detection of individual nanoparticles on the nanodisc electrode. The potential of nanodisc technology is huge due to its capability of faster measurement, reduced false negatives and false positives. Additionally, it is a scalable technology with easy and cheaper fabrication methods. Thus, **chapter 7** explores the possibility of developing the nanodisc technology to a business idea. A patent has also been applied based on this finding. The chapter tries to look at the problem and the solution for the business idea and it also opens up the need of a market feasibility study based on its different aspects, specifically for the cancer diagnosis market. In short, the whole thesis tries to explore the different possibilities in developing a sensor that can be useful for cancer diagnosis.

# Acknowledgements

Whenever I get a thesis from a colleague or a friend, the first thing I read is the acknowledgements. So I reckon how important this part of the thesis is! ☺ When I look back at my PhD journey, it puts a big grin on my face. There are a lot of people who have not only influenced, helped, supported and encouraged me but also who have criticized and disagreed with my opinions and decisions, throughout this period which proved to be rewarding at the end.

First and foremost, I would like to thank my promotor, **Wilfred** for giving me this opportunity and also for his incredible supervision and motivation throughout the project.  More than a supervisor, I like to call him a visionary whose scientific and diplomatic traits, astuteness and aspiration bewildered me most of the time. I greatly admire those things and I definitely have imbibed at least a few of those skills as well! You gave me absolute freedom to work on this project the way I wanted to, nonetheless, you steered me in the right direction whenever needed. Thanks a lot Wilfred! **Serge**, I met you only in the third year of my PhD. That was the time when I was switching from electrical transduction to electrochemical transduction. My knowledge in electrochemistry was feeble. Initially I was dumbfound as well as intimidated with the profoundness of your knowledge in this field. You always found time to discuss my results and guide me to a fruitful direction. You allowed me to use your lab facilities without which this thesis wouldn't have been possible. Without your help, I couldn't have developed the nanodisc idea to a patent and a highly potential track of research. I immensely thank you for the all the help you have extended.

When I first saw the promotion video of Nanopil project, I felt it as a sci-fi propaganda movie and nothing close to reality. Later, when I became a part of the Nanopil, I realized that you have to dream certain things before it would ever become a reality. The Nanopil project meetings were exceedingly informative and

helpful in designing my experiments and rectifying my shortcomings and strengthening my weaknesses. It gave me lot of multi-disciplinary exposure which was absolutely necessary for my PhD research. I would like to immensely thank all the current and previous members of Nanopil especially **Rick, Loes, Alejandro, Roberto, Raquel, Tina** and **Lisette** and **Martina. Jurriaan** and **David,** you are extremely good at chemistry where my knowledge was very little when I started this project. Thanks a lot for all your fruitful discussions and valuable suggestions which helped to improve my chemistry knowledge and succeed experimentally. **Almudena,** it was so fun to work with you. Your joyous words, loud laughs and beautiful songs filled the chemical lab with full of good vibes. I was so happy to collaborate with you and hopefully we will publish the article soon based on chapter 4. I would also like to thank **Ab** for all the assistance and useful tips you gave while working at the BioElectronics lab. Being at the lab, more than science we also discussed many other topics without which my lab work would have been monotonous and banal experience. **Guy,** thanks for helping me with the simulations described in chapter 4. Good luck with your MSc. thesis completion!

When I first came to the Netherlands, I was all alone, far away from my beloved ones. However, within no time I made friends with a bunch of Dutch students: **Henk-Willem, Peter, Pepijn, Haye** and **Ton**. When I entered the room, you immediately switched from Dutch to English, to make sure that I don't feel odd one out and still now you do that hoping one day I'll be fluent in Dutch. ☺ The parties we organized, tons of fun we shared, myriad of serious and silly talks we made, the scientific knowledge we conquered together; everything was extremely amusing and satiating. Being and electrical engineer, without you guys I wouldn't have gone "this far" into life sciences. **Henk-Willem,** you are the first Dutch person I became friend with! Even now you are still one of my best friends ever. You have been so kind and extremely pleasing to me all these while. You helped whenever, I was in need. Thank you so much! **Pepijn** you are a special person: you are always willing to help whatever the matter is. I still remember you helping me with French to English translation. *French Description: "Douche Sèche-cheveux" and your translation : "Dry horses in the shower". And the Google Translate says: "Hair dryer". Pepie, I would at least expect the horses to be wet in the shower.* ☺ We laughed a lot all these days for many reasons. More than

friends, we also collaborated further for science's sake. It was a very fruitful collaboration with excellent results described in chapter 5 and we could already submit the paper based on our research. Now, we are collaborating further more in business. I hope we continue to be friends forever and our (soon to be real) company will be a big success. Thank you so much for everything and also being my paranymph on my big day.

NanoElectronics (NE) is a pleasant group to work at and I thoroughly enjoyed every moment being at NE. Doing science at NE was fantastic with people around to help you. Apart from science, we also did many other activities during these years: hot air ballooning, exploration of Giethoorn (by foot and by boat), archery, laser shooting, carting, buggy ride, solex ride, escape room, bubble football, exploration of Hulsbeek, climbing, kayaking, camping, borels, BBQs, Christmas dinners etc. I'm always happy and thankful to be at this group.

Talking about NE members, first I should mention **Karen,** the audacious lady among a pride of male scientists. I came to your office many times with a question or asking for a help and in no time you answered me or assisted me with what as to be done. You fixed things for me even when you were on holidays.  Thanks a lot for the supporting hand you have extended to me whenever required! I would like to thank **Martin** for his assistance with AFM, **Thijs** for probe-station support and ordering chemicals, **Michel** for his scientific advice during hybrid-electronics meetings and non-scientific discussions at our coffee corner, and **Floris** for his intricate impromptu jokes that made me laugh each time and tips for parenting. I would also like to thank **Peter** and **Hao** for interesting chats once in a while which I thoroughly enjoyed. **Johnny,** I would like to extend my special thanks to you for your help both scientifically and non-scientifically. You were there with assistance whether in the lab or in the clean-room or at the office or with Dutch translation. Thank  you! **Susan,** although you left our group soon after I joined, you were always ready to help me each time when I approached you. You were always competing with Thijs to see who can laugh louder. I think you always won and even these days your innocent laughs reverberates loud and clear through the corridor from MCS/IDS coffee corner to NE corner. ☺

During my PhD, I had an opportunity to supervise nine students for their thesis assignments. **Francesca** and **Loek,** your master thesis work helped me to wrap up the chapter 2. Thank you both for the help! **Tom,** for me, you were the right student at the right time. You stayed slightly more than a year with the project for your double master degrees. You explored a lot of things during your work and almost everything was helpful especially your work on nanodisc technology described in chapter 6. It was extremely pleasant to work with you and thank you for the fruitful contribution! Hope you are enjoying your long get away deep into the *soul* of Asia. Good luck in all your future endeavors. **Thjis O.H.,** hope you can extend Tom's work to a greater success. Thanks for choosing this project and good luck with that. I also thank other students who worked with me during my PhD. **Karolina, Edith, Alex** (for both BSc. and MSc. theses), **Jordi,** and **Laduona.**

**Yuki,** you came to the group when I was almost finishing my project. It was nice to have you in our group and I also enjoyed your lessons about Japan and helping you with the humidity controlled measurements at the probe-station. **Pavel,** although you joined the group very late in my PhD days, you came at the right time. You took a lot of stress away from me during my thesis writing period with your jokes, Russian and American stories, shooting chronicles with Kalashnikovs and *complaints* about everything under the sky. It is indeed an extreme pleasure to be with you at the office and hope to continue that longer. Thanks **Oguzhan** for helping us, the organizers, with burger making at the NEvent-2017. Good luck with your thesis writing and PhD defense. **Alejandro,** it was a great pleasure to work with you. You added the word "calisthenics" to my English vocabulary. Your carefree attitude towards life was inspiring. Wish you all the best for your future endeavors! And good luck **Michal,** the new Frank, with completion of your PhD! Hope to see you when you are back from Singapore. **Yigitcan,** thanks for the nice discussions and a memorable NEvent in 2018. **Antonio,** you always allured me with your variety of lunch dishes; lekker! Waiting for the day you are gonna invite me at your place. ;) **Hans,** together with **Miha,** we had some interesting discussions about many interesting topics during lunch. I miss those talks a bit these days, I think we should invite Miha over more often for lunch so that we catch up. **Tao,** you were extremely nice with me at many times when I was in need. Thanks! Hope we meet more often with the families so that our kids play together while we talk,

eat and enjoy. **Bram vd V.,** although we work at completely different projects, at times we had similar interest. We organized Inascon-2016 together and also helped Yuki with his measurements during his internship here. Hope we work together more often in future! I would also like to thank **Pim** for his enthusiastic words about my research most of the time after my presentation at the group seminars. I also take this opportunity to thank all the current NE students: **Mark, Lennart, Enzo, Steven** and **Bram d W**. I always like to deal and talk with students, since they motivate me to be young at mind. These days, the NE guys are throwing parties almost every week and I'm missing most of these fun filled parties that they enjoy because of being a responsible family man living in Hengelo. But I'll try to join more often after my defense. My work involved a lot of fabrication work including several processes in the cleanroom. I thank all the cleanroom staff for the technical assistance you provided and especially to **Marion, Hans, Ton, Robert, Peter, Gerard, Rene,** and **Christiaan.**

Life in Enschede/Hengelo would have been banal without my friends outside work. **Mini** family, **Dhanya** family, **Bindhu** family, **Kamalamma** family, **Lekshmi** family, **Bisni** family, **Fiji** family and **Nitha** family, I thank you all for sharing fun, being motivating and encouraging throughout my PhD career and being good to Ajin whenever I was away or busy. I would like to also take this opportunity to thank all my good old friends who talked or skyped or texted me during my busy PhD days and to name a few: **Akku, Alen** (& **Nimmy**), **Rijo, Renjith, Sujith, Manesh, Roobin, Noble, Santhosh, Garvin,** and **Kevin** (Adoor boys), **Harishanker, Ajay, Jake, Ajit, Greeshma,** (B.Tech friends), **Reji, Suraj, Philip** (SB friends). Thank you guys for being there always!

Family has been my stronghold throughout my life. When I was distressed you inspired me and when I was blissful you cheered me further. I whole heartedly thank my aunties and uncles of the Kuttiyil family and the Chakkalayil family. I also would like to thank all my beloved cousins and to name a few who intermittently kept in touch with me during my PhD days: **Aggie, Philby, Viji, Saji, Roshan, Suja, Saju** and **Joel. Aldin, Jebin,** and **Appu,** you guys were extremely encouraging to me throughout my *adventure* in the Netherlands. We chatted for hours about tons of different things. Also you visited us and we visited you during this time; it was

so much fun. Thank you for keeping me cheerful throughout my stressful days. **Daddy** and **mummy** (parents-in-law), you always eagerly listened to what I talked, you were curious to know what I'm working on, then you proudly shared them to others, and you motivated me to go higher. I know you are happy for me and I wish you could be here to see me graduating!  Thank you for everything! **Divya**, my dearest sister, growing up with you was both fun and "challenging". ☺ You helped me foster most of my skills, which paid off well during my challenging days as a PhD researcher. **Mummy** and **Papa**, without your support I wouldn't have accomplished this much. You never said no to me, you always agreed to my wishes. You gave me the best you could. You loved me and supported me always. Thank you so much for being there for me. I sincerely hope you could join my defense and be delighted about it. Finally, **Ajin** and **Naomi**, you deserve my abundant love and extreme indebtedness. Thank you for all your love and care. The fun we shared, movies and series we watched together, mouthwatering food we cooked, games we played and stories we enjoyed after a tiring day at the lab, helped me to rejuvenate my body and mind for the endless work day after day in my PhD life. You almost never complained when I failed to put my contribution to the family and household affairs, during this time. On the other hand, at times when I was feeling low you lifted me up; you divided my sorrows and you multiplied my joys. Thank you so much!

Dilu Mathew, March 2019

# Metrohm Young Chemist Award-2018

Metrohm AG is an internationally active producer of precision instruments for chemical analysis, in particular ion analysis, based in Herisau, Switzerland. 2018 is a very special year for Metrohm – this is our 75 year jubilee! Metrohm values the spirit of innovation and believes in the value of novel research performed by pioneering young scientists. Hence as the part of their jubilee celebration, they organized Metrohm young chemist award (MYCA) for different regions worldwide. Undergraduates to doctorate students were encouraged to apply and submit abstracts of their original work in order to have a chance at winning a cash prize.



The ceremony for the MYCA Benelux winners was held on Wednesday, October 3 at the World of Technology and Science exhibition (WOTS) in Utrecht, NL, and was hosted by the Royal Netherlands Chemical Society (KNCV). The winners were introduced by Metrohm Applikon CEO Timoer Frelink, and each of them gave a brief presentation about their research to the audience. The first prize award (€2500) was given to PhD student Dilu George Mathew from the University of

Twente in the Netherlands. His research focuses on label free electrochemical DNA sensing (Highly selective and sensitive DNA detection on nanoscale interdigitated electrodes using gold nanoparticle amplification).

WE WANT
YOUR TOUCH

UNIVERSITEIT TWENTE.

HIGH TECH HUMAN TOUCH

Dilu George Mathew

# DETECTING CANCER FROM URINE

**His aspiration was to save lives, and so he decided to switch from engineering to nanotechnology. Dilu George Mathew now works on 'Early Stage Cancer Detection Sensor', a device able to detect cancer from patients' urine. 'This technique could not only save lives, but also a lot of money.'**

PhD candidate from the NanoElectronics group Dilu G. Mathew, who originally comes from India, first moved to England, where he acquired a Master's degree in engineering and worked for several years. However, he soon realized that wasn't his true calling. He says: 'I knew I wanted to do something to save lives; develop something that could be a crucial diagnostic device. For me, bionanotechnology was the way to do that, so I pursued with my studies and research at the UT.'

### Nanogap device

'If you detect cancer at an early stage, you can save the person's life, but today most cancers are diagnosed too late which reduces the survival rate. I'd like to change that. We have developed nanogap devices using easy microfabrication techniques at MESA+ cleanroom. These nanogaps can be used to detect certain cancer modified DNA – also called hypermethylated DNA - and therefore determine if the person has cancer', explains Mathew.
'We are aiming to develop a device that can detect cancer from the patient's urine. Therefore we could avoid painful invasive tests and the testing would become very cheap and fast and could be done directly in the doctor's office, without involving a big lab to analyze the results', Mathew lists all the possible advantages of the sensor he is working on.

'For example, 150 000 cystoscopy tests are being carried out every year in the Netherlands for bladder cancer screening and each one of those costs about 1000 Euros. We are aiming to create devices with the cost of under 50 Euros. Then more people can get tested, thus we can save a lot of lives and money', adds Mathew. The research is currently focused on detecting bladder cancer, cervical cancer and prostate cancer, but the hope is to use such devices for detecting also other types of cancer and diseases.

### Researcher-entrepreneur

Dilu G. Mathew is not only a dedicated researcher, but he might also contribute to the list of UT spin-offs. 'After I'm finished with my PhD research, I'd like to start a company that produces such devices, able to detect cancer early on', he says. It's too soon to tell if this company will succeed, but Mathew's research project surely has the potential to change many people's lives.

**PhDs are the backbone of our university. But who are they? Every month, we introduce another PhD candidate to you. This month: Dilu George Mathew, PhD candidate in the NanoElectronics Group (MESA+).**

Scan me

FSC